AEROSOL CHARACTERIZATION IN THE SOUTHEASTERN U. S. USING SATELLITE DATA FOR APPLICATIONS TO AIR QUALITY AND CLIMATE

A Dissertation
Presented to
The Academic Faculty

By

Erica J. Alston

In Partial Fulfillment
Of the Requirements for the Degree
Doctor of Philosophy in the
School of Earth and Atmospheric Sciences

Georgia Institute of Technology
May 2012

AEROSOL CHARACTERIZATION IN THE SOUTHEASTERN U. S. USING SATELLITE DATA FOR APPLICATIONS TO AIR QUALITY AND CLIMATE

Approved by:

Dr. Irina N. Sokolik, Advisor
School of Earth and Atmospheric Sciences
Georgia Institute of Technology

Dr. Judith A. Curry
School of Earth and Atmospheric Sciences
Georgia Institute of Technology

Dr. Micheal H. Bergin
School of Earth and Atmospheric Sciences
Georgia Institute of Technology

Dr. Viatcheslav V. Tatarskii
School of Earth and Atmospheric Sciences
Georgia Institute of Technology

Dr. Bruce G. Doddridge
Chemistry and Dynamics Branch
NASA/LaRC/Science Directorate

Date Approved:

To all who have come before and those who will come after…never stop pushing towards your goals.

ACKNOWLEDGEMENTS

I would first like to thank Dr. Irina Sokolik. Her belief in my abilities and me has been steadfast throughout. Without her caring, determination and urging this would not have happened. Second, I would like to thank Dr. Judith Curry. Her advice and advocacy has been greatly appreciated. Third, I thank Bruce Doddridge for his time and efforts. I appreciate the opportunity to further my education thanks to NASA Langley Research Center, the Science Directorate at LaRC and my co-workers who have served as sounding boards. Last, I want to express my thanks to the other members of my committee Dr. Micheal Bergin and Dr. Viatcheslav Tatarskii for their time and feedback.

I thank my family for their uplifting and encouraging words, but let me give a special thanks to my mother. Mama, you have seen me through so many of life's milestones, and nothing makes me prouder than to be your daughter. So this work is a testament to the strength of character and drive you have ensteeled within me.

I also want to acknowledge the special friends who have helped me along the way with hugs, food, positive energy and sympathetic ears: Akia, L'Erin, Lauren, Dana, Jessica, Alisa, Rosalyn, Audrey, and Michelle F. I would be remiss if I did not acknowledge my furry companions, Scamp (deceased) and Sasha, whose company has soothed and consoled my overworked mind. I also appreciate all the assistance my group members (Xin, Anton, Zheng and Prashant) have given me over the years. Finally, I want to give praise to God for seeing me through.

TABLE OF CONTENTS

LIST OF TABLES

LIST OF FIGURES

LIST OF ABBREVIATIONS

AOD	Aerosol Optical Depth
AERONET	Aerosol Robotic Network
CALIPSO	Cloud-Aerosol Lidar and Infrared Pathfinder Satellite Observations
EPA	Environmental Protection Agency
MSA	Metropolitan Statistical Area
MODIS	Moderate Resolution Imaging Spectroradiometer
MISR	Multi-angle Imaging Spectroradiometer
NASA	National Aeronautics and Space Administration
NOAA	National Oceanic and Atmospheric Administration
NPOES	National Polar Orbiting Environmental Satellite
NPP	NPOES Preparatory Project
OMI	Ozone Monitoring Instrument
$PM_{2.5}$	Particulate Matter of an aerodynamic diameter < 2.5 μm
RFE	Radiative Forcing Efficiency
RH	Relative Humidity
SBDART	Santa Barbara Disort Atmospheric Radiative Transfer model
SSA	Single Scattering Albedo
SZA	Solar Zenith Angle

LIST OF SYMBOLS

τ	AOD (Aerosol Optical Depth)
g	Asymmetry parameter
T_{atm}	Atmospheric transmission
R^2	Coefficient of determination
r	Correlation coefficient
ρ	Density
$F^{\downarrow}$	Downward flux
k_{ext}	Extinction coefficient
A_c	Fractional cloud amount
D	Fractional day length
R	Geometric radius
σ	Geometric standard deviation of the size distribution
Δz	Layer depth
M*	Mass concentration ($\mu g/m^3$) valid for N=1 cm^{-3}
N	Number concentration
f_j	Number fraction
ΔF	Radiative forcing
k_{sca}	Scattering coefficient
S_0	Solar Constant
ω_0	SSA (Single Scattering Albedo)
R_s	Surface albedo (Surface reflectance)

β	Up-scatter fraction
$F^{\uparrow}$	Upward flux
λ	Wavelength

SUMMMARY

Tropospheric aerosol information from NASA satellites in space has reached the milestone of ten years of continuous measurements. These higher resolution satellite aerosol records allow for a broader regional perspective than can be gained using only sparsely located ground based monitoring sites. Decadal satellite aerosol data have the potential to advance knowledge of the climatic impacts of aerosols through better understanding of solar dimming/brightening and radiative forcings on regional scales, as well as aid in air quality applications. The goal of this thesis is to develop and implement methodologies for using satellite remotely sensed data in conjunction with ground based observations and modeling for characterization of regional aerosol variations with applications to air quality and climate studies in the Southeastern U. S. This region is of special interest because of distinct aerosol types, less warming climate trends compared to the rest of U.S., and growing population.

To support this primary goal, a technique is developed that exploits the statistical relationship between $PM_{2.5}$ (particulate matter that has an aerodynamic radius of 2.5 μm or less) and satellite AOD (Aerosol Optical Depth) from MODIS (Moderate resolution Imaging Spectroradiometer) where a probabilistic approach is used for air quality assessments in the metropolitan Atlanta area. The metropolitan Atlanta area experiences the poorest air quality during the warmer seasons. We found that satellite AODs capture a significant portion of $PM_{2.5}$ concentration variability during the warmer months of the year with correlation values above 0.5 for a majority of co-located (in time and space) ground based $PM_{2.5}$ monitors, which is significant at the 95% confidence interval. The developed probabilistic approach uses five years of satellite AOD, $PM_{2.5}$ and their related

AQI (Air Quality Index) to predict future AQI based solely on AOD retrievals through the use of AOD thresholds, e.g., 80% of Code Green AQI days have AOD below 0.3. This approach has broad applicability for concerned stakeholders in that it allows for quick dissemination of pertinent air quality data in near-real time around a satellite overpass.

Examination of the use of multiple satellite sensors to aid in investigating the impacts of biomass burning in the region is performed. The utility of data fusion is evaluated in understanding the effects of the large wildfire that burned in May 2007.

This wildfire caused $PM_{2.5}$ in the metropolitan Atlanta area to exceed healthy levels with some measurements surpassing 150 $\mu g/m^3$ during the month. OMI (Ozone Monitoring Instrument) AI (Aerosol Index), which qualitatively measures absorbing aerosols, have high values of more than 1.5 during May 26 – 31, 2007. CALIPSO (Cloud-Aerosol Lidar and Infrared Pathfinder Satellite Observations) a space based lidar was used to determine the vertical structure of the atmosphere across the region during the active fire period. CALIPSO was able to identify wildfire aerosols both within the planetary boundary layer (likely affects local air quality) and aloft where aerosol transport occurs. This has important implications for climatic studies specifically aerosol radiative effects.

In-depth analysis of the satellite and ground based aerosol data records over the past decade (2000 – 2009) are performed from a climatic perspective. The long temporal scale allowed for better characterization of seasonality, interannual variability, and trends. Spatial analysis of ten years of AOD from both MODIS and MISR (Multi-angle Imaging Spectroradiometer) showed little variability of AOD during the winter with

mean AOD below 0.1 for the entire region, while the summer had decidedly more variability with mean AOD around 0.33 for MODIS and 0.3 for MISR. Seasonal analysis of the $PM_{2.5}$ revealed that summer means are twice as high as winter means for $PM_{2.5}$. All of the datasets show interannual variability that suggests with time AOD and $PM_{2.5}$ are decreasing, but seasonal variability obscured the detection of any appreciable trends in AOD; however, once the seasonal influence was removed through the creation of monthly anomalies there were decreasing trends in AOD, but only MODIS had a trend of -0.00434 (per month) that statistically significant at the 95% confidence level.

Satellite and ground-based data are used to assess the radiative impacts of aerosols in the region. The regional TOA (Top Of the Atmosphere) direct radiative forcing is estimated by utilizing satellite AOD from MODIS and MISR both on Terra, along with satellite derived cloud fraction, surface albedo (both from MODIS), and single scattering albedo (SSA) from MISR data from 2000 – 2009. Estimated TOA forcing varied from between -6 to -3 W/m^2 during the winter, and during the warmer months there is more variation with ΔF varying between -28 to -12.6 W/m^2 for MODIS and -26 to -11 W/m^2 for MISR. The results suggest that when AOD, cloud fraction and surface albedo are all consider they add an additional 6 W/m^2 of TOA forcing compared to TOA forcing due to aerosol effects only. Varying SSA can create changes in TOA forcing of about 5 W/m^2. With removal of the seasonal variability timeseries anomaly trend analysis revealed that estimated TOA forcing is decreasing (becoming less negative) with MODIS based estimates statistically significant at the 95% confidence level.

Optical and radiative 1-D radiative transfer modeling is performed to assess the daily mean TOA forcing and forcing at the surface for representative urban and

background aerosol mixtures for summer and winter. During the winter, modeled TOA forcing is -2.8 and -5 W/m^2 for the WB (Winter Background) and WU (Winter Urban) cases, and the modeled summer TOA forcings e.g., SB = -13.3 W/m^2 (Summer Background) also generally agree with earlier estimates. While surface forcings varied from -3 to -210 W/m^2. The radiative forcing efficiency at the TOA (amount of forcing per unit of AOD at 550 nm) varied from -9 to -72 $W/m^2\ \tau^{-1}$, and RFE at the surface varied from -50 to -410 $W/m^2\ \tau^{-1}$. It was found that the forcing efficiency for biomass burning aerosols are similar to the forcing efficiency of background aerosols during the summer that highlights the importance of possible increased biomass burning activity. Ultimately, the methodologies developed in this work can be implemented by the remote sensing community and have direct applicability for society as a whole.

CHAPTER 1

INTRODUCTION

1.1 Motivation and Goals

With the launch of the first U. S. earth mission satellite, Explorer 1 in January 1958, the age of mining remotely sensed data was thrust upon us. We now use satellites for not only communications, defense strategies, but for weather and climate. We use satellites to provide us information about natural disasters, often in real-time. In the future, satellites will provide understanding on how human activity has changed our home planet in a myriad of ways.

In the U. S. the National Aeronautics and Space Administration (NASA) designs, operates and manages a number of satellites that focus upon different aspects of Earth's system, e.g., aerosols, clouds, oceans. Aerosols are highly dynamic in their properties, spatiotemporal distributions, and impacts. Aerosols play a role in air quality, but are an equally important part of the climate system. There has been recent interest in the climatic phenomena of solar dimming/brightening, which basically is trying understand how much incident solar radiation makes it to the surface in the context of light extinction due to atmospheric aerosols. The intersection of air quality and climate is another interesting perspective as recent research suggests that policies that have improved air quality for a majority of developed countries, might have masked the true extent of climate change [*Andreae*, 2009; *Jacob and Winner*, 2009; *Jimenez et al*., 2009].

Satellites can provide a broad regional perspective. Satellite data have been thought of as a means to address the lack of spatial coverage by ground based monitoring

sites. Satellite observations can be used to characterize aerosols, identify aerosol transport, and identify cases of biomass burning [*Wu et al.*, 2006; *Ahn et al.*, 2008; *Dirksen et al.*, 2009; *Fairlie et al.*, 2009] that can result in air quality degradation. Studies that relate satellite measurements to $PM_{2.5}$ (particulate matter with an aerodynamic diameter of 2.5 μm or less) generally use AOD retrieved from the NASA MODIS (Moderate Resolution Imaging Spectroradiometer) instrument. The Terra satellite, which houses both the MODIS and MISR (Multi-angle Imaging Spectroradiometer) instruments has provided over a decade of data, while the satellite Aqua, which also has a MODIS sensor on board has been providing data since 2002. AOD (aerosol optical depth) is a measure of light extinction through the atmosphere for a given wavelength.

Engel-Cox et al. [2004] completed one of the first nationwide studies that presented results of the relationship between $PM_{2.5}$ and AOD, and they demonstrated that the relationship varied by region. Further highlighting this regional perspective is the work of *Al-Saadi et al.* [2005], which developed a methodology for applying AOD maps over maps of $PM_{2.5}$ concentrations for the entire U.S. to improve air quality forecasts through the IDEA (Infusing satellite Data into Environmental Applications) website (http://www.star.nesdis.noaa.gov/smcd/spb/aq/).

Hoff and Christopher [2009] provided an in-depth critical review of satellite applications to air quality. Their overview outlines issues that can prohibit wider applicability of satellite data for air quality studies. One issue is the spatial mismatch between satellite data and the ground-based air quality monitoring sites that provide point measurements. When stations are located closely together, it is likely that those sites will occur in the same satellite pixel, which reduces the number of independent observations

per station. Another issue lies in the assumptions used for satellite retrievals. The satellite science teams are constantly making updates to their retrieval algorithms to better represent the regionality of aerosol composition. AOD does not provide information about the location of aerosols within the atmospheric column. Aerosols that are transported into an area can be located higher in the atmosphere, where ground based monitors do not detect it, but satellites do. Instances such as this can cause a mismatch between what the satellite and ground-based monitors observe.

Any person flying into Atlanta, Georgia's Hartsfield-Jackson Atlanta International Airport during the summer will see first-hand the visible effects of poor air quality in Atlanta. Atlanta has the highest population density in the southeastern U.S. making it one of the larger urban areas in the contiguous U.S. (http://www.census.gov/popest/metro/metro.html). The metropolitan area is comprised of 31 counties, with the city boundary contained mostly within Fulton County. High population density and large amounts of environmental toxins have placed Atlanta at the top of Forbes's Most Toxic City List for 2009 (http://www.forbes.com/2009/11/02/toxic-cities-pollution-lifestyle-real-estate-toxic-cities.html). The American Lung Association declares Atlanta as the 17th worst city for year-round particle pollution (http://www.lungusa2.org/sota/2009/).

By penetrating deep into the human body, $PM_{2.5}$ (particulate matter with aerodynamic diameters less than 2.5 μm) can cause not only adverse respiratory complications such as asthma and emphysema but also could contribute to stroke, lung cancer, and heart disease [*Slaughter et al.*, 2003; *Metzger et al.*, 2004]. Epidemiological studies in Atlanta have linked increases in particle pollution to increased asthmatic

pediatric emergency room visits [*Tolbert et al.*, 2000], while *Peel et al.* [2007] found that the risk of death increased for hypertensive people in cases of elevated PM_{10} (particulate matter with aerodynamic diameters less than 10 μm).

According to the EPA Our Nation's Air publication in 2008 (http://www.epa.gov/airtrends/2010/index.html), $PM_{2.5}$ concentrations nationwide have decreased by 19% since 2000, with the Southeastern U.S. showing a decrease in annual $PM_{2.5}$ concentrations. There have been, for instance, large scale ground based measurement studies in the region consisting of a U.S. Environmental Protection Agency (EPA) Supersite Study [*Solomon et al.*, 2003], and ongoing work through the Southeastern Aerosol Research and Characterization Study (SEARCH) (http://www.atmospheric-research.com/studies/SEARCH/index.html). This region is of interest because of the distinct aerosol mixtures associated with this geographic region that has been studied from the ground, yet little research has been done incorporating satellite data. The primary sources of $PM_{2.5}$ in this region are from secondary processes driven primarily through photochemical reactions [*Lee et al.*, 2007]. Sulfate and organic carbon primarily comprise particulate aerosols in this region [*Edgerton et al.*, 2005; *Weber et al.*, 2007]. Measurements and modeling studies have shown that significant portions of organic aerosols are formed through secondary processes, which are biogenic in origin [*Weber et al.*, 2007; *Lee et al.*, 2010]. This forms the basic premise behind the research of *Goldstein et al.* [2009], which summarily states that the Southeastern U. S. is experiencing radiative cooling at the TOA due to a layer of biogenic organic aerosols aloft from the surface. More details will be discussed further in Chapters 4 and 5.

Air quality policies focus upon controlling emissions of pollution from local and regional sources (such as transportation and industries), which have led to the introduction of national health standards such as the 24-hour $PM_{2.5}$ National Ambient Air Quality Standards (NAAQS) [*U.S. Environmental Protection Agency*, 2006]. At the same time, there has been a growing recognition of the role of wildfires on urban air quality that cannot be regulated or controlled easily [*Spracklen et al.*, 2009; *Tian et al.*, 2009]. Given the most likely increase in the frequency of wildfires in a warming climate [*Confalonieri et al.*, 2007] and growing urbanization, a better understanding of the extent to which fires can degrade the air quality of large metropolitan areas is needed. Additionally wildfire impacts can be large in spatial extent, and using a sporadic network of ground-based monitors can limit the amount of information needed to address these events. However, satellite data can provide a broad overview of entire regions that lends itself useful for these types of investigations.

Air quality analyses are generally done for short time scales, but satellites can aid in understanding aerosols over longer time periods, providing insight into the air quality - climate linkages. Over the past fifty or so years global ground-based measurements of solar radiation reaching the surface have shown first a decrease (i.e., dimming) and in the last fifteen years have shown an increase (i.e., brightening) [*Alpert and Kishcha*, 2008; *Gilgen et al.*, 2009; *Wild et al.*, 2009]. During the 1980s, many industrialized countries enacted policies for controlling emissions of aerosols and their precursors. In the 1990s, a shift from dimming to brightening was reported at some locations [*Streets et al.*, 2009]. It is hypothesized that the magnitude of global warming has been masked due to solar

dimming [*Wild*, 2009; *Schwartz et al.*, 2010], thus linking this phenomenon to current climate.

Solar dimming/brightening is more nuanced when observed from a smaller regional perspective, e.g., regions of the U.S. For example, some studies found that solar dimming/brightening is likely dominated by emissions from large urban areas [*Alpert et al.*, 2005; *Alpert and Kishcha*, 2008]. Recent work by *Wild* [2009] further substantiates this point by investigation of trends of solar dimming/brightening at multiple locations. The locations from the U.S. all show a similar behavior, but each site's trend slope is different owing to the influence of differing aerosol mixtures and loading associated with each site's respective region. *Long et al.* [2009] investigated brightening of downwelling shortwave radiation at multiple U.S. locations and found that collectively the brightening is significant, but that the varying degrees of brightening amongst the different sites suggested that research into dimming/brightening should address local to regional scales. Ultimately, understanding of dimming/brightening variations requires knowledge of spatiotemporal changes in aerosols on a regional basis. Each satellite sensor uniquely positioned to provide a continuous timeseries of AOD that can be directly related to the dimming/brightening phenomena [*Mishchenko et al.*, 2007; *Hinkelman et al.*, 2009].

Atmospheric aerosols are an important climate-forcing agent. Some aerosols such as dust and black carbon can heat the atmosphere by absorbing solar radiation, while others (e.g., sulfates, and secondary organic aerosols, SOA) can have a cooling effect [*Forster et al.*, 2007]. In climate studies, the concept of the Top-of-the-Atmosphere (TOA) forcing is a commonly used metric for quantifying the radiative impact of aerosol on climate. The Intergovernmental Panel on Climate Change (IPCC) (www.ipcc.ch) asses

changes to the climate system by using the metric of top-of-the-atmosphere (TOA) forcing, which is usually used in reference to global scale forcing. The IPCC (2007) report states that greenhouse gases produce a net warming, while aerosols are generally shown as having a cooling effect; however, the uncertainty associated with the magnitude of the aerosol forcing is less constrained than the uncertainty associated with greenhouse gases. *Carrico et al.* [2003] estimated TOA forcings ($\Delta F = -11 W/m^2$) for Atlanta based on a six weeks of optical measurements during 1999. While Goldstein et al. [2009] used satellite AOD for their estimate of TOA forcing caused by organic aerosols of -3.9 W/m^2 over the Southeastern U. S. The complex nature of aerosols, in particular, their inhomogeneous distribution and variability in time and space, is one of the major factors that cause significant uncertainties in assessments of TOA direct radiative forcing exerted by aerosols on climate. The effects of aerosols on climate need more study to increase confidence in the understanding of these controlling processes.

The main goal of this research is to develop and implement methodologies for using satellite remotely sensed data in conjunction with ground based observations and modeling for characterization of regional aerosol variations with applications to air quality and climate studies in the Southeastern U. S. To address this goal, the research featured in this dissertation will focus upon:

(1) Development of a technique that exploits the relationship between $PM_{2.5}$ and satellite AOD from MODIS (Moderate resolution Imaging Spectroradiometer) where a probabilistic approach is used for air quality assessments in the metropolitan Atlanta area.

(2) Investigate the use of multi-sensor satellite data to aid in understanding the impacts of biomass burning in the region through a case study analysis.

(3) Determination of the decadal behavior of aerosols in the region from both satellite and ground measurements.

(4) Explore the radiative impacts of aerosols in the region through the use of a first-order approximation and 1-D radiative transfer modeling.

Figure 1.1 provides a schematic of the major goals and themes contained within this dissertation.

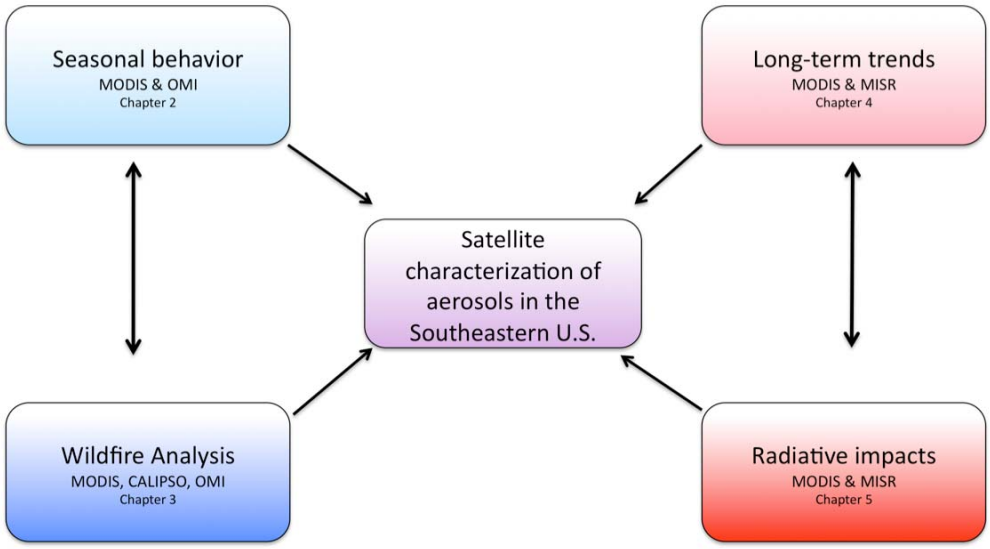

Figure 1.1: Schematic of thesis structure and goals

1.2 Outline of Dissertation

Chapter 2 presents an assessment of the use of satellite data in air quality in the metropolitan Atlanta, GA based on five years (2004-2008) of statistical analyses of $PM_{2.5}$, satellite AOD, and air quality designations during the spring and summer seasons.

We will explore the utility of aerosol speciation from the OMI (Ozone Monitoring Instrument) for defining background levels of scattering and absorbing aerosols to help identify cases of aerosol transport. Additionally we explore the specific goals of the robustness of the $PM_{2.5}$-AOD relationship through linear regressions, which establishes and motivates the probabilistic approach developed in this chapter.

The main focus of Chapter 3 is to examine multi-satellite data as a tool for characterizing wildfire impacts on a large urban area. Our specific goals are to (1) examine the dynamics of $PM_{2.5}$ and AOD retrieved from MODIS aboard Terra and Aqua satellites and the $PM_{2.5}$-AOD relationship in the case of high smoke loadings (exceedance days); (2) examine the capability of CALIPSO lidar to detect and identify smoke and quantify the vertical structure of AODs; (3) identify the wildfire signatures through the analysis of OMI data; (4) perform an in-depth analysis of smoke events that caused the largest impact on air quality across the Atlanta metro area in May of 2007 through a combination of multi-satellite data.

Chapter 4 presents a characterization of aerosols in the U.S. Southeast through analysis of ground and space based measurements from 2000 – 2009, with the emphasis on seasonal and interannual aerosol variations, and trends. The specific objectives are to (1) examine the temporal changes of ground based $PM_{2.5}$ and AODs from MODIS and MISR over the past ten years; (2) determine common features and differences between these data records; and (3) determine if there is a discernible trend.

Chapter 5 presents the results of an assessment of the regional TOA aerosol direct radiative forcing and its dynamics along with forcing at the surface. . We use satellite data from over the past decade in the U. S. Southeast, including cloud cover, surface

albedo, and aerosol optical depth and single scattering albedo. We use a Mie model to determine optical properties of representative aerosol mixtures based on EPA aerosol speciation data. These optical properties are then used in a 1-D radiative transfer model that predicts TOA and surface forcings, and their efficiencies. Finally, this thesis concludes with a summary of key findings and their implications in Chapter 6. This concluding chapter 6 also outlines the direction of future work.

CHAPTER 2

INVESTIGATION INTO THE USE OF SATELLITE DATA IN AIDING CHARACTERIZATION OF PARTICULATE AIR QUALITY IN THE ATLANTA, GA METROPOLITAN AREA

The work presented in this chapter is published in the Journal of the Air & Waste Management [Alston et al., 2011a]

2.1 Introduction

Many studies have focused on ozone pollution in Atlanta [*Chameides et al.*, 1992; *Cardelino et al.*, 2001; *Diem et al.*, 2010] to name a few, but just as important is particulate matter pollution. Specifically, particle pollution of particles that are less than 2.5 microns in diameter is known as $PM_{2.5}$. Until 2008, Atlanta was designated as being in nonattainment of the National Ambient Air Quality Standard (NAAQS) for $PM_{2.5}$ as determined by the U. S. Environmental Protection Agency (EPA) [*U.S. EPA*, 2009]. Like other cities on the U. S. east coast, Atlanta $PM_{2.5}$ is impacted by local and regional sources [*Engel-Cox et al.*, 2005; *Fairlie et al.*, 2009].

In the U.S. assessment of air quality is currently based on averages of 24-hour data from ground-based measurements of $PM_{2.5}$ performed at dedicated monitoring sites. The use of 24-hour average $PM_{2.5}$ data is to relate concentrations to the air quality index (AQI), which relates the level of air pollution to possible health effects, and for compliance with the $PM_{2.5}$ NAAQS. The AQI is used to disseminate information about

air quality to the public via different methods of media, e.g., local television news, radio or newspaper. The AQI is scaled to relate the $PM_{2.5}$ concentrations to NAAQS [*U.S. Environmental Protection Agency*, 2006]. Through the Clean Air Act of 1990, the U.S. EPA has the authority to set national air quality standards to protect the public health. In 2006, the U.S. EPA strengthened the NAAQS by reducing the 24-hour standard from 65 $\mu g/m^3$ to 35 $\mu g/m^3$. In doing so, the AQI must now be revised to reflect the changes in the NAAQS, and this action by the EPA is currently under review. Table 2.1 gives the current AQI and the proposed AQI revisions. These changes will certainly affect a city's proportion of good, moderate, and unhealthy days. The $PM_{2.5}$ measurements that are used for AQI forecasts provide high temporal resolution, but lack spatial resolution and coverage. In a large metropolitan area like Atlanta with only seven monitoring sites for forecast purposes, the lack of spatial resolution has implications for air quality forecasts.

Table 2.1: Current and proposed AQI designations. Source: U.S. EPA (http://www.epa.gov/pm/pdfs/20090115fs.pdf)

AQI Category	Color	Index Values	PM2.5 24-hour ($\mu g/m^3$)	
			Current	Proposed
Good	Green	0 - 50	0.0 - 15.4	No change
Moderate	Yellow	51 - 100	15.5 - 40.4	15.5 - 35.4
Unhealthy for Sensitive Groups	Orange	101 - 150	40.5 - 65.4	35.5 - 55.4
Unhealthy	Red	151 - 200	65.5 - 150.4	55.5 - 150.4
Very Unhealthy	Purple	201 - 300	150.5 - 250.4	No change
Hazardous	Maroon	301 - 400	250.5 - 350.4	No change
		401 - 500 (this level used for emergency episode planning only.)	350.5 - 500	No change

States in the eastern U.S. have to consider air quality in a regional perspective especially under the onus of the U.S. EPA.'s Clean Air Interstate Rule. Satellites

provide a snap-shot picture of atmospheric conditions, and in some cases can provide information about aerosol loading and composition. Past studies defined a methodology for determining the relationship between $PM_{2.5}$ and AOD through linear regressions [*Wang and Christopher*, 2003]. *Engel-Cox et al.* [2005] highlight the use and applicability of satellite data in observing aerosol transport over the entire state of Texas. *Gupta et al.*, [2006] state that ground-based measurements cannot capture the synoptic transport of aerosols from region to region, and source identification of transported aerosols cannot be addressed necessarily by ground-based measurements alone. In areas where ground-based measurements are limited satellites could be useful tool for air quality stakeholders. One conclusion from *Hoff and Christopher* [2009] is that reducing the uncertainty of the $PM_{2.5}$-AOD through statistical regressions is unlikely, which is why here we propose an alternative method that uses a statistical analysis of AOD values to directly relate them to AQI bypassing the $PM_{2.5}$-AOD regression.

In this study, hourly and 24-hour averaged $PM_{2.5}$ measurements from seven $PM_{2.5}$ stations across the metro Atlanta area are analyzed along with MODIS AOD from March 1- August 31, 2004 – 2008 (spring and summer seasons only). From the $PM_{2.5}$ hourly data, subsets are created to coincide with Terra and Aqua satellite overpasses. In addition, we analyze data from the Ozone Monitoring Instrument (OMI) that provides measurements in the UV-region of the electromagnetic spectrum. OMI performs many functions; however, of most interest to this study is its ability to detect light absorbing aerosols, especially over land [*Torres et al.*, 2007].

In this chapter we present an assessment of the use of satellite data in air quality air quality in the metropolitan Atlanta, GA based on five years (2004-2008) of statistical analyses of $PM_{2.5}$, satellite AOD, and air quality designations during the spring and summer seasons. We will explore the utility of aerosol speciation from the OMI (Ozone Monitoring Instrument) for defining background levels of scattering and absorbing aerosols to help identify cases of aerosol transport. Additionally we explore the specific goals of the robustness of the $PM_{2.5}$-AOD relationship through linear regressions, which establishes and motivates the probabilistic approach outlined in this chapter.

2.2 Data and Methodology

2.2.1 $PM_{2.5}$ Monitoring Stations

The EPA makes determinations of whether states meet the NAAQS for particulate matter. That standard states that in order to receive attainment for daily $PM_{2.5}$, the 98^{th} percentile of the three-year average at each pollution monitor cannot exceed 35.5 $\mu g/m^3$ [*U.S. Environmental Protection Agency*, 2006]. We use surface $PM_{2.5}$ measurements from two different networks: continuous $PM_{2.5}$ measurements ($PM_{2.5,TEOM}$) provided by the Georgia Dept. of Natural Resources, and the filter-based $PM_{2.5}$ measurements courtesy of the EPA ($PM_{2.5,FRM}$), which will be discussed in Chapter 4. The location of the sites is shown in Figure 2.1. The network operated by the Georgia Dept. of Natural Resources Ambient Monitoring Program (AMP) (http://www.air.dnr.state.ga.us/amp/) performs continuous hourly measurements using TEOMs (Tapered Element Oscillating Microbalance). The TEOM measurements are not used for determination of NAAQS compliance; however, AMP assigns an exceedance whenever their 24-hour averaged TEOM-based $PM_{2.5}$ measurements exceed

the current NAAQS daily standard of 35.5 $\mu g/m^3$. Across Georgia, there are eighteen network sites located primarily within or near a city. For our study we use twelve sites. Seven of those sites are within the large metro Atlanta area and the remaining sites are smaller sized cities and towns. Most of the stations have seven years of data; however, sites without at least five years of data were excluded from this analysis. The time coverage of this is 2003 – 2009.

For this chapter, we obtained one-hour and 24-hour measurements of $PM_{2.5,TEOM}$ from all seven metro Atlanta stations from March 1 – August 31, 2004 – 2008. Five out the seven stations have data for the entire period, while two stations (Confederate Ave. and Walton) only have data for 66% of 2005. These stations cover three types of locations: urban – Confederate Ave., suburban – Gwinnett, S. DeKalb, McDonough, and rural – Newnan, Walton, Yorkville. For easier identification, for this chapter and Chapter 3 we will drop the TEOM subscript notation, since in these chapters we only use data from TEOM monitors. The $PM_{2.5,24}$ dataset is a moving average that uses the current hour's concentrations and the past 23 hours' concentrations. Two more data sets were created for pairing with Terra and Aqua satellite observations, which have different equatorial crossing times. To match MODIS aboard Terra observations, hourly $PM_{2.5}$ measurements from 10 and 11 am were averaged together to create the dataset $PM_{2.5,T}$. Similarly for MODIS aboard Aqua, hourly measurements from 1 and 2 pm were averaged together to create the dataset $PM_{2.5,A}$. Analyses are performed using all three $PM_{2.5}$ datasets ($PM_{2.5,24}$, $PM_{2.5,T}$ and $PM_{2.5,A}$). $PM_{2.5,24}$ refers to the 24-hr averaged data, whereas $PM_{2.5,T}$ and $PM_{2.5,A}$ are averaged concentrations centered around the satellite overpass times for Terra and Aqua, respectively.

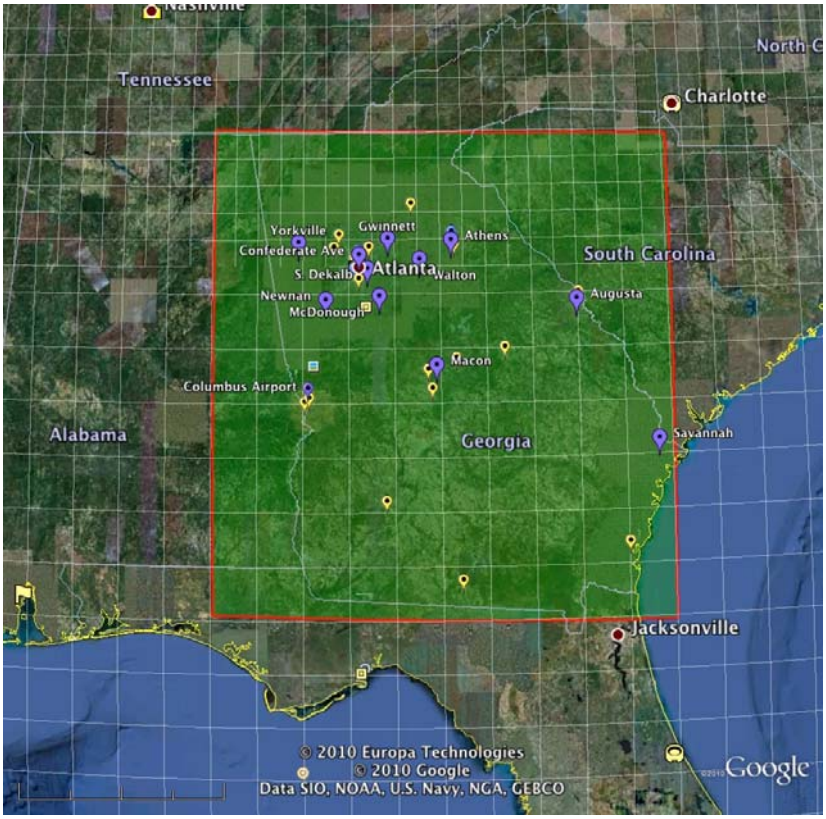

Figure 2.1: Map of the U.S. Southeast. Green box with red outline denotes study spatial domain for satellites 5° x 5°. Yellow markers represent EPA active $PM_{2.5}$ monitors ($PM_{2.5,FRM}$). Blue markers represent EPA inactive $PM_{2.5}$ monitors. Purple markers represent TEOM $PM_{2.5}$ monitors ($PM_{2.5,TEOM}$).

2.2.2 MODIS Data

The MODerate resolution Imaging Spectroradiometer (MODIS) instrument flies onboard two of NASA's Earth Observing System (EOS) satellites: Terra and Aqua. Terra flies in the descending polar orbit with an equatorial crossing time of approximately 10:30 am, while Aqua flies in the ascending polar orbit with an equatorial crossing time of approximately 1:30 pm. Generally, the satellites have overpass times over Georgia 5 -15 minutes after their equatorial crossing times. Both

satellites orbit 700 km above the Earth in low earth orbit, and they have near global coverage daily.

MODIS passively measures reflected radiances from Earth across a broad wavelength spectrum. It primarily uses three channels (0.47, 0.66 and 2.12 μm) to measure atmospheric aerosols over land [*Levy et al.*, 2007]. We use over five GB and 3,700 files of Collection 5 data from NASA's LAADS (Level 1 and Atmosphere Archive and Distribution System). Collection 5 is the most recent release of the data products from the MODIS science team. The analysis is performed with MODIS Level 2 data, which have a nominal resolution of 10x10 km^2 at nadir. Level 2 products are processed from the Level 1B geo-located 5-minute granules, which contain reflected radiance measurements at spatial resolutions of 250 m (660 nm channel) and 500 m (470 and 2120 nm channels). There can be resolution degradation at the swath edges. The variable of most importance to this study is "Optical_Depth_Land_and_Ocean" at the 500 nm wavelength. AOD is an unitless measure of the amount of light attenuation over a set distance, i.e., path. In general, AOD varies between 0 and 5 with values greater than 1 being associated with heavy haze, biomass burning, or dust events [*Engel-Cox et al.*, 2004].

Following similar methodologies from *Gupta and Christopher* [2008b] and *Engel-Cox et al.* [2004], satellite data were matched with station data using a 0.5° degree box around each ground station. The Atlanta metropolitan area consists of 31 counties, with 5 counties comprising the actual city of Atlanta. The metro area covers over 8,000 sq. miles and at its widest covers seven counties. The spatial distribution of $PM_{2.5}$ stations minimizes overlap in satellite pixels by using the 0.5° search radius. Only

days where both data types were available are considered for additional correlation analysis. The time period of March 1 – August 31, 2004 – 2008 (spring and summer seasons only), is considered for this research. Thus, we created and analyzed seven different datasets that correspond to the AOD measurements from each MODIS instrument over the seven ground-based $PM_{2.5}$ measurement stations. Another dataset was created for comparisons with the OMI sensor, i.e., city-scale averaged AOD. This dataset is considered to be Atlanta AOD and covers a lat/lon box of 33 – 34.5° N and 83.5 – 85.3°W. Additionally, the time period for this dataset matches the OMI dataset.

2.2.3 OMI Data

The Ozone Monitoring Instrument (OMI) takes measurements in the near-ultraviolet (UV) for retrievals of gases and aerosols [*Torres et al.*, 2007]. OMI flies onboard the NASA satellite Aura. Aura and Aqua (MODIS) fly together in a satellite constellation called A-Train. A great advantage of the satellite constellation is multiple measurements made from different sensors within 15 minutes of each other.

In this study, we consider the OMI aerosol products only that are cloud screened, primarily the UV Aerosol Index (AI). The time period of March 1- August 31, 2005 – 2008, is considered, which is one year shorter than the $PM_{2.5}$ and MODIS data because Aura did not launch until July 2004. OMI data were obtained from the NASA GES DISC (Goddard Earth Sciences Data and Information Services Center). The most recent release of data is in Collection 3. The OMI instrument has a swath of 2,600 km and provides mostly global coverage daily. Aerosol products are retrieved at a spatial resolution of 13 x 24 km at nadir; however, the spatial resolution increases at the extremes of the satellite swath [*Torres et al.*, 2007]. In the presence of UV-absorbing

aerosols, AI has positive values between 0 and 5 [*Ahn et al.*, 2008], where the highest values of AI occur during episodes of dust storms and/or biomass burning [*Herman et al.*, 1997; *Ahn et al.*, 2008]. In the presence of UV-scattering aerosols, AI has negative values that can vary between 0 and -2 [*Langmann et al.*, 2009; *Penning de Vries et al.*, 2009]. Due to OMI's larger footprints, it is difficult to match OMI measurements with specific station locations. Thus, OMI measurements are taken for a lat/lon box of 33 – 34.5° N and 83.5 – 85.3°W covering the metropolitan Atlanta area. Although AI is a qualitative measure, it does provide valuable information about the spatial pattern of UV-absorbing aerosols over land and their transport [*de Graaf et al.*, 2005; *Fromm et al.*, 2005; *Torres et al.*, 2007; *Dirksen et al.*, 2009]. Past studies have attempted to establish the quantitative relationship between OMI AI and MODIS AOD [*Torres et al.*, 2007; *Ahn et al.*, 2008]. However, that is not the focus of this research. The purpose of our analysis is to determine the specific signal of UV-absorbing aerosols over Georgia in terms of OMI AI values and their dynamics over the spring and summer seasons. Although we report here correlations between MODIS AOD and OMI AI, this analysis is only done to facilitate the characterizations of seasonal dynamics of urban aerosols across the state of Georgia.

2.3 Results

2.3.1 Characterization of urban aerosols through $PM_{2.5}$

We first want to determine the variability of $PM_{2.5}$ on a yearly (spring and summer) and seasonal basis. The analysis of yearly means reveals that there is year-to-year variability within all three $PM_{2.5}$ datasets ($PM_{2.5,T}$, $PM_{2.5,A}$, and $PM_{2.5,24}$). Barplots

of the five years of selected months (1 March – 31 August) of the $PM_{2.5,A}$, $PM_{2.5,T,}$ and $PM_{2.5,24}$ datasets for Gwinnett (33.96°, -84.07°) and Newnan (33.40°, -84.74°) sites are shown in Figure 2.2(a and b). Gwinnett and Newnan are used to contrast differences between urban/suburban vs. rural stations. These barplots display how $PM_{2.5}$ averages varied over the study period. The years of 2006 and 2007 have the highest means for all seven sites. The means for each year for all the stations are summarized in Table 2.2.

Though we only consider spring and summer, our $PM_{2.5}$ averages agree well other published work of $PM_{2.5}$ in Atlanta [*Edgerton et al.*, 2006]. The years 2004 and 2008 are below the five-year average (shown by dashed lines in Figure 2.2), while 2006 and 2007 are the highest above the five-year average for Gwinnett, and 2005–2007 are the highest above the five-year average for Newnan. $PM_{2.5,24}$ for all stations has values in between $PM_{2.5,T}$ and $PM_{2.5,A}$, but it behaves similarly to the other $PM_{2.5}$ datasets. Both Table 2.1 and Figure 2.2(a and b) show that the differences between minima and maxima of the $PM_{2.5,T}$ and $PM_{2.5,A}$ means are about 5 – 8 $\mu g/m^3$. To determine if the observed differences are statistically significant, we used a T-test to determine that for $\alpha = 0.05$ the two means are in fact statistically different from each other, and those instances are bolded in Table 2.2.

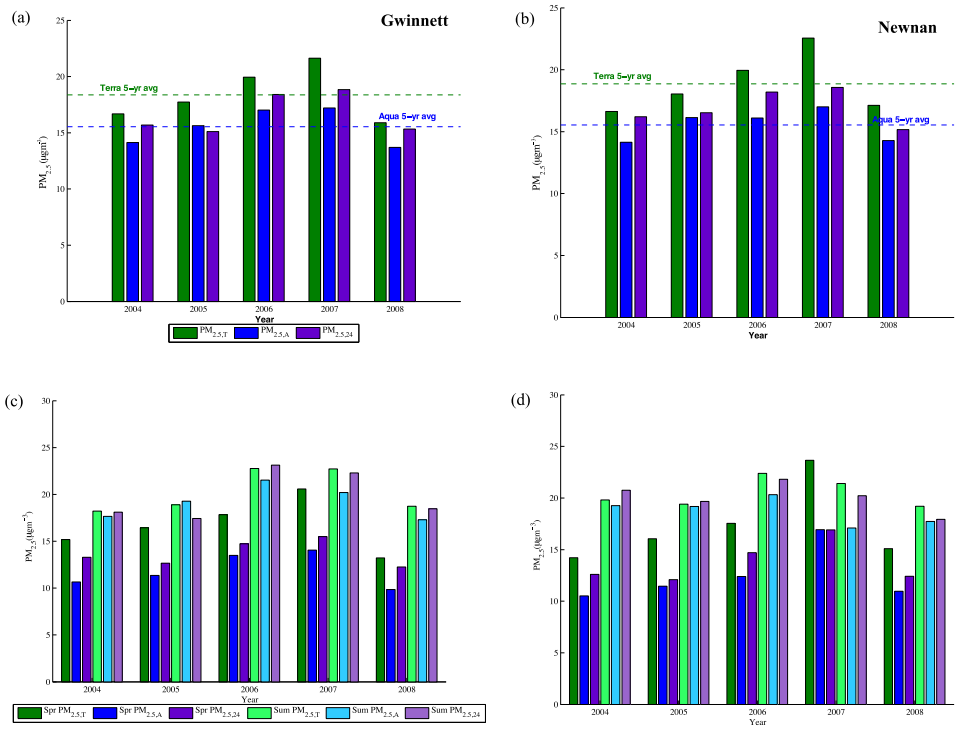

Figure 2.2: Bar plots of yearly averaged $PM_{2.5}$ at Gwinnett (a) and Newnan (b). Green dashed line represents $PM_{2.5,T}$ five-year average, and blue dashed line represents $PM_{2.5,A}$ five-year average. Bar plots of seasonally averaged $PM_{2.5}$ at Gwinnett (c) and Newnan (d).

Table 2.2: Means of $PM_{2.5,T}$ and $PM_{2.5,A}$ concentrations (μgm^{-3}) for considered stations. Bold numbers are significantly different from each other for $\alpha = 0.05$.

Location	2004		2005		2006		2007		2008	
	Terra	Aqua	Terra	Aqua	Terra	Aqua	Terra	Aqua	Terra	Aqua
Con. Ave.	-	-	18.61	18.87	**23.63**	**21.25**	23.42	21.31	**20.68**	**17.89**
Gwinnett	**16.69**	**14.12**	17.72	15.63	**19.94**	**17.02**	**21.64**	**17.22**	**15.90**	**13.70**
McDonough	**17.26**	**14.74**	18.41	16.59	**21.13**	**17.32**	**21.54**	**16.63**	**17.29**	**13.51**
Newnan	**16.63**	**14.14**	18.05	16.14	**19.94**	**16.10**	**22.55**	**17.01**	**17.13**	**14.29**
S. Dekalb	**17.24**	**14.33**	**18.54**	**15.50**	**19.20**	**16.96**	23.04	21.42	**18.22**	**15.42**
Walton	-	-	16.80	15.23	**18.81**	**16.48**	**19.70**	**15.79**	**15.84**	**13.17**
Yorkville	14.86	14.64	16.30	16.24	18.60	16.87	19.45	19.33	14.30	13.58

Edgerton et al. [2006] found that during the day, hourly mean measurements can vary by as much as 50 μg/m^3 in the Atlanta area comparable to observations in this study.

The $PM_{2.5}$ data show a distinct seasonality having higher values in the summer compared to spring. Figure 2.2(c and d) shows seasonal averages of the three $PM_{2.5}$ datasets for Gwinnett and Newnan. During the spring at Gwinnett, $PM_{2.5,T}$ varies from around 15 – 21 μg/m^3, $PM_{2.5,A}$ varies between 10 -14 μg/m^3, and $PM_{2.5,24}$ varies between 13 – 16 μg/m^3. Summer averages show increases of 30 – 45% over spring averages. All stations show similar values. The similarity between stations is established through timeseries analysis of $PM_{2.5}$ (not shown), and the analysis also indicates that summer has more variability than spring. Our seasonal results are similar to the works by *Butler et al.* [2003] and *Edgerton et al.* [2005] even though they considered different sites and different years. It should be noted that the reduced seasonality in 2007 is likely a product of the late spring wildfire, which produced the additional influx of smoke aerosols to the metro area [*Christopher et al.*, 2009].

We have discussed the yearly and seasonal trends within the $PM_{2.5}$ data; however, we also want to understand how each of the satellite-overpass datasets relate to each other and to $PM_{2.5,24}$. To assess the similarity between $PM_{2.5,T}$ and $PM_{2.5,A}$, we created scatterplots of the two datasets and calculated linear regression statistics. Scatterplots of $PM_{2.5,A}$ vs. $PM_{2.5,T}$ for 2004 - 2008 and all years combined are shown in Figure 2.3. Correlation coefficients (r or r-values) between $PM_{2.5,T}$ and $PM_{2.5,A}$ vary around 0.78 – 0.85. The coefficient of determination (R^2), which is a measure of variance, varies between 0.61 – 0.72. When seasonality was examined between these

two datasets, the summertime showed higher r-values than spring. Our results are consistent with *Butler et al.* [2003],

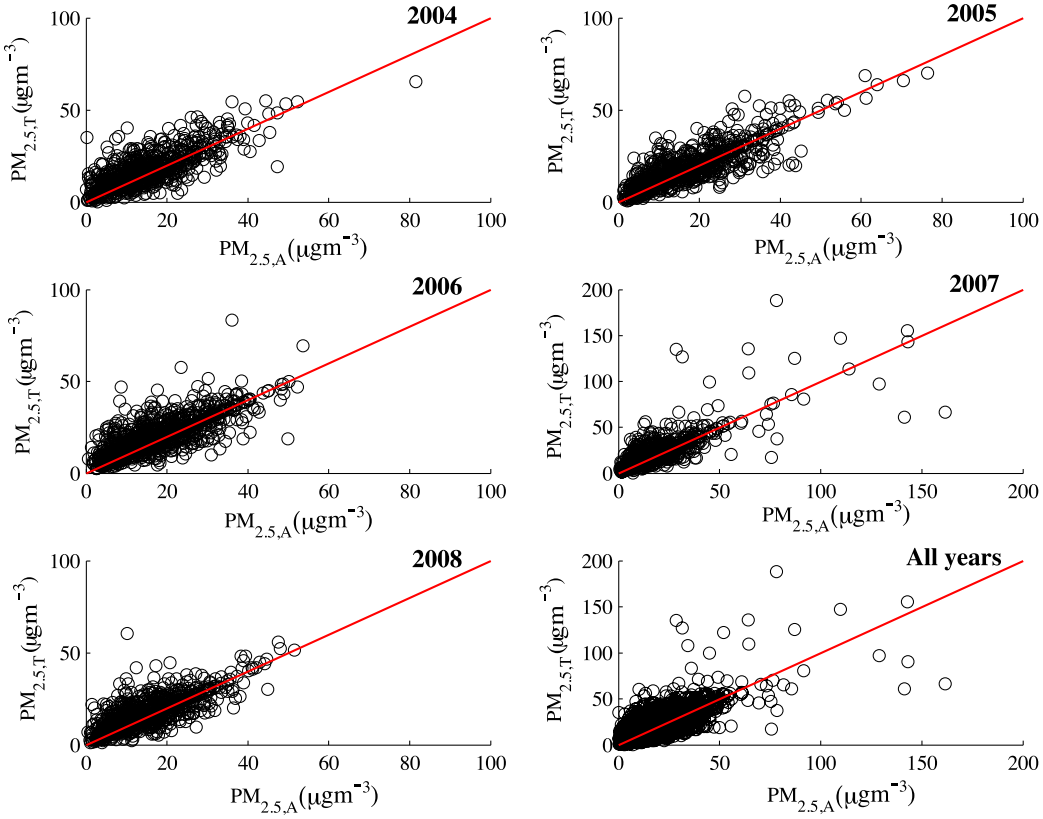

Figure 2.3: Scatterplots of $PM_{2.5,T}$ vs. $PM_{2.5,A}$ for all considered stations. Dashed line represents 1:1 correspondence

which shows diurnal variation of $PM_{2.5}$ in Atlanta as a function of season, and during the summer the diurnal variation is less pronounced than during other seasons. When the $PM_{2.5,24}$ dataset is compared to the $PM_{2.5,A}$ and $PM_{2.5,T}$ datasets, statistics show that they are well correlated with r-values between 0.65 – 0.83. $PM_{2.5,24}$ captures 70% (R^2 = 0.7) of the variability within the satellite-overpass $PM_{2.5}$ datasets ($PM_{2.5,T}$ and $PM_{2.5,A}$). This could have implications for studies that relate MODIS AOD to the 24-hour average of $PM_{2.5}$.

We have shown that during our study period the $PM_{2.5}$ concentrations across metro Atlanta are similar but have differences due to location. A majority of stations have their highest means during 2006 and 2007, with 2004 and 2008 as local minima. The year 2007 was dominated by a wildfire that changed the nature of $PM_{2.5}$ in Atlanta by lessening the difference between spring and summer seasons. Across all stations summer months have increased $PM_{2.5}$ concentrations as shown by increased means and variances. Additionally, we have shown that $PM_{2.5,T}$ correlates slightly better than $PM_{2.5,A}$, but 30% ($1-R^2 = 0.3$) of the variance shown by the satellite-overpass datasets is not represented in the 24-hour average; this could impact the strength of the AOD and $PM_{2.5}$ correlations. For instance, during short (hours) duration exceedance events, the $PM_{2.5}$-AOD correlation will be lower if $PM_{2.5,24}$ is considered rather than hourly data centered around the satellite overpass. In the following section we will compare satellite measurements to the $PM_{2.5}$ measurements to determine how well the satellites capture the $PM_{2.5}$ behavior spatiotemporally.

2.3.2 Characterization of urban aerosols with satellite products (MODIS AOD and OMI AI)

In this section, we focus upon comparing the variability of MODIS AOD to $PM_{2.5}$, as well as assessing the variability of OMI Aerosol Index and its linkages with MODIS AOD. In comparing yearly AOD averages of MODIS Terra to MODIS Aqua, the latter has higher AOD at all stations for 2004-2006 and 2008. However, in 2007 Terra is markedly higher than Aqua. This finding is different from the $PM_{2.5}$ yearly averages where $PM_{2.5,T} > PM_{2.5,A}$,which might imply that Terra should record higher values of AOD, yet this is not the case. Yearly averages of MODIS AOD at Gwinnett

and Newnan are presented in Figure 2.4(a and b). Like the feature shown in Figure 2.2(a and b), MODIS AODs have their highest averages in 2006 and 2007 and minima in 2004 and 2008.

From a seasonal perspective, MODIS AOD has higher summer averages than spring averages, which is in agreement with $PM_{2.5}$ (see Figure 2.2(c and d)). In fact, for many cases the summertime AOD as shown in Figure 2.4(c and d) is almost double that of the springtime, yet this doubling is not found in the $PM_{2.5}$ record. During the years of 2005-2007, MODIS summertime AOD averages were almost double the springtime averages, whereas in 2004 and 2008 average summertime AOD was almost 50% higher than average springtime AOD. Barplots of seasonally averaged AOD from MODIS at Gwinnett and Newnan are shown in Figure 2.4(c and d). Our results indicate that the difference between Aqua and Terra spring AOD is smaller than the difference between the two during the summer. However, examination of the $PM_{2.5}$ record yields that the largest difference between the datasets occurs during the spring rather than the summer. *Goldstein et al.* [2009] hypothesize that the high summertime AOD values are driven by secondary organic aerosols (SOA) from biogenic volatile organic compounds (BVOC) that occur aloft in the lower troposphere thus not impacting surface mass measurements of $PM_{2.5}$. Other studies, however, pointed out that $PM_{2.5}$ might be biased low due to significant losses of semi-volatile organics from particles collected on the filter during sampling [*Eatough et al.*, 2003]. Further analysis is needed to determine, where in the atmospheric column SOA formation is most influential and implications to air quality assessments.

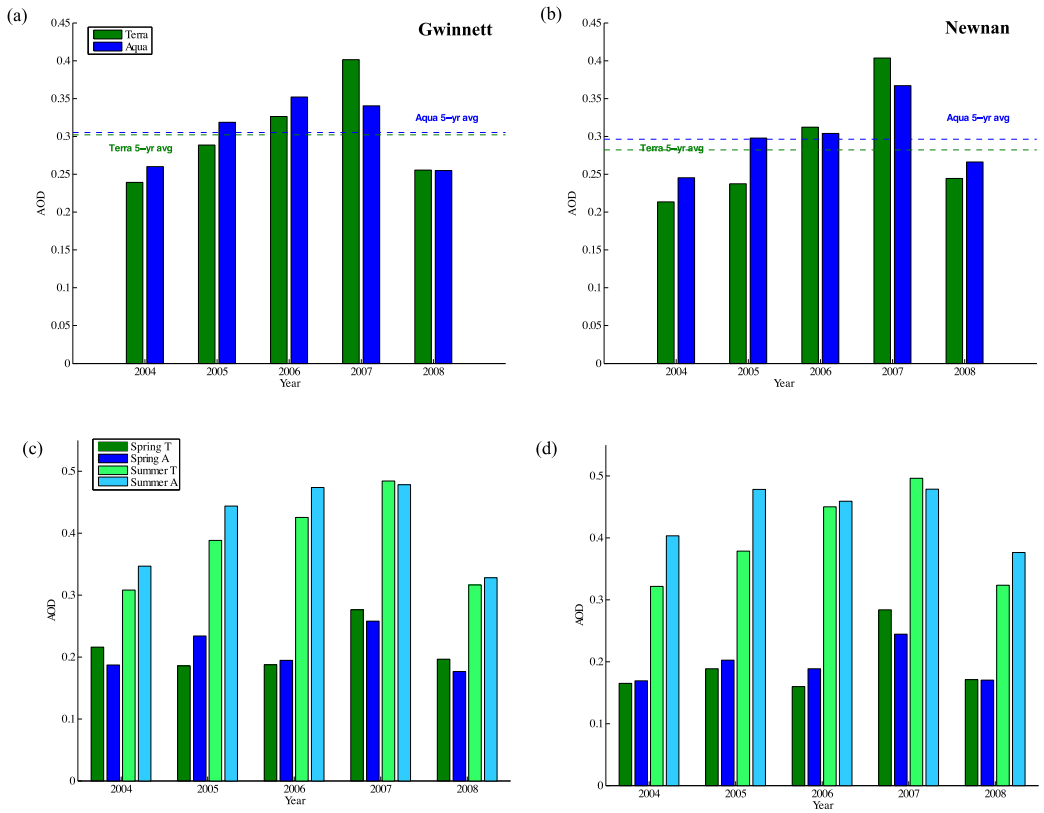

Figure 2.4: Bar plots of yearly averaged MODIS AOD at Gwinnett (a) and Newnan (b). Green dashed line represents MODIS Terra five-year average, and blue dashed line represents MODIS Aqua five-year average. Bar plots of seasonally averaged MODIS AOD at Gwinnett (c) and Newnan (d).

Further, we examine the variability of UV-absorbing aerosols in Atlanta as seen in OMI AI data and linkages with MODIS AOD. For this analysis we use the city-scale datasets (see MODIS and OMI Data Sections for explanation) considering positive (larger than zero) values of OMI AI, which are indicative of the presence of UV-absorbing aerosols. We found that positive values of OMI AI show little variability from year to year, with a slight maximum occurring in 2007. As viewed from space, the carbonaceous aerosol signal in terms of positive AI values is fairly constant in the Atlanta metro area, with a multi-annual (2005-2008) mean of around AI = 0.3. Also, across all years a majority (80%) of AI values are below AI = 0.5. Using the yearly

average or 80% cutoff to establish background conditions of Atlanta implies that if AI rises above these values it could be indicative of UV-absorbing aerosol transport such as cases of wildfires smoke. Given the robustness of AI retrievals over land compared to MODIS AOD, establishing a threshold AI for a certain location provides a useful tool for assessing the area affected by smoke or dust transport with possible degradation of air quality.

OMI AI does not appear to have the same seasonality as MODIS AOD. The mean and median values of AI vary little between spring and summer. *Penning de Vries* [2009] found that in the southeastern U.S. AI is at a minimum during the summer which is in agreement with our analysis of AI during the considered time period. Scatterplots between OMI AI vs. MODIS AOD Terra/Aqua are shown in Figure 2.5. It is apparent that there is not a discernable linear relationship between the AI and AOD, also evidenced by the low r-values shown in Table 2.3. Possible reasons for the low correlations include differences between retrieval algorithms' assumptions of aerosol height, different spatial resolutions, and the vertical distribution of aerosols. Differences in the relative roles of factors affecting remote sensing at UV vs. visible wavelength [*Ahn et al.*, 2008] show that comparisons between OMI measurements at 388 nm and MODIS measurements at 500 nm do not have a 1:1 relationship. This is an expected result, given that UV-absorbing aerosols (such as black carbon) comprise a relatively small mass fraction compared to other aerosol types that dominate AOD at 500 nm. This might not be the case, however, in the locations affected by the transport of dust aerosols.

Table 2.3**:** Correlation coefficient and number of observations for OMI AI vs. MODIS AOD

Year	Season	r		#	
		Terra	Aqua	Terra	Aqua
2005	Spring	-0.13	-0.05	57	53
	Summer	0.06	0.23	46	48
2006	Spring	-0.12	-0.09	65	64
	Summer	0.30	0.42	66	67
2007	Spring	0.03	-0.13	65	69
	Summer	0.08	0.10	58	61
2008	Spring	-0.35	-0.31	60	62
	Summer	0.18	0.15	60	59

Having shown that AI and AOD are not related further substantiates the effectiveness of AI as an indicator for transport events of UV-absorbing aerosols. For instance, the small box in Figure 2.5 for 2005 shows that AI is almost 1.4, but AOD is around 0.3 on April 13, 2005. There are no $PM_{2.5}$ exceedances on this day; this suggests that increased concentrations of aerosols were aloft in the lower atmosphere. We believe this is an example of smoke remnants being transported into the area from the central U.S. Another example occurs in 2007 (see box in Figure 2.5 for 2007), where smoke aerosols were transported into the area. There were large active wildfires in Idaho and Montana during the time period August 2007. Those wildfires caused a large haze event across the eastern U.S. During this event there were $PM_{2.5}$ exceedances in Atlanta on August 13 and 15-18, 2007. The carbonaceous aerosols detected by OMI on August 14 are aloft and most likely become entrained in the PBL on the following days. *Jacob and Winner* [2009] conclude that wildfires could become an important and more frequent contributor to $PM_{2.5}$. The aerosols associated with this additional particulate matter burden will most likely be carbonaceous in nature, and the baseline of AI established from multi-year OMI data would help to better assess the impact these

potential wildfires will have on air quality over a certain region and its dynamics with time.

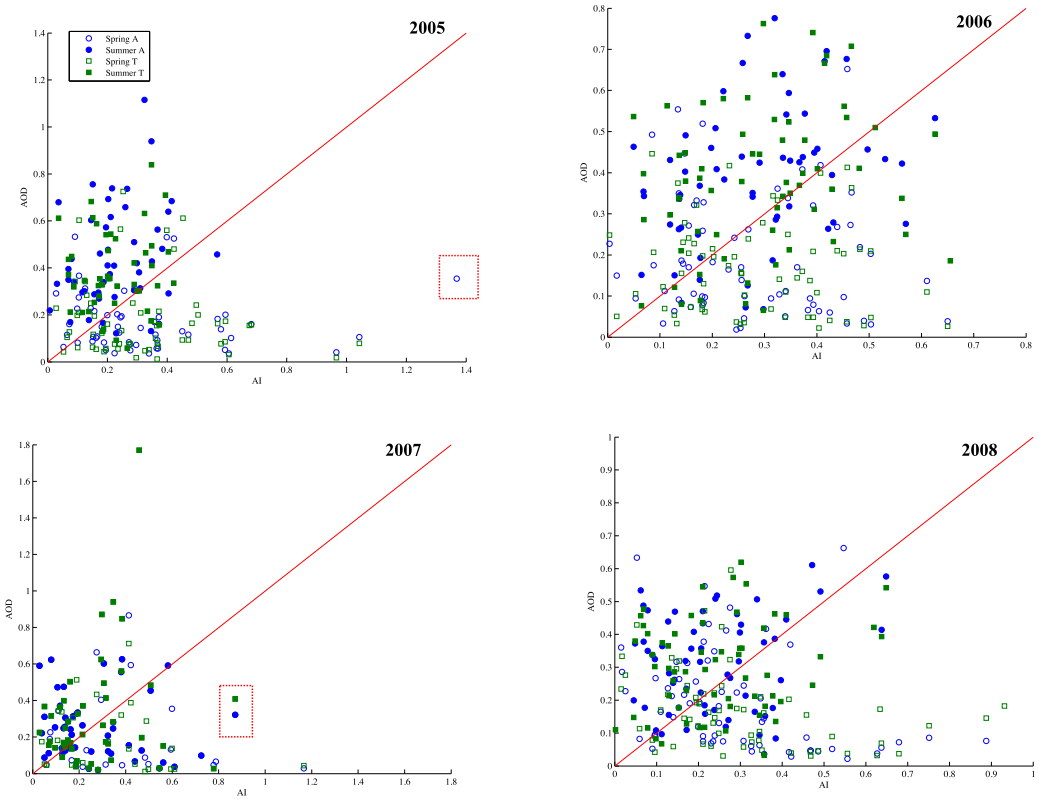

Figure 2.5: Scatterplots of MODIS Terra/Aqua AOD vs. OMI AI. Dashed line represents 1:1 correspondence. Data highlighted by inclusion in rectangular boxes are discussed in text.

The above analysis demonstrates that satellites adequately capture the general nature of urban aerosols in the metro Atlanta area. Though there are some differences between what times of day results in the highest values, the overall patterns of MODIS AOD match well with the $PM_{2.5}$ observed patterns on a yearly and seasonal basis. OMI AI allowed us to identify specific cases of aerosol transport into the metro area by detecting the UV-absorbing signature associated with these events.

2.3.3 $PM_{2.5}$ and AOD Analysis

One of the goals of this research is to investigate the $PM_{2.5}$-AOD relationship, and to statistically determine AOD thresholds that correspond to the AQI for the Atlanta metropolitan area. First, we investigate the $PM_{2.5}$-AOD relationship through linear regression analysis and calculate statistics to quantify that relationship. Second, we use frequency distributions to determine statistical thresholds of AOD that relate directly to AQI.

We begin by assessing the strength of the linear relationship between the two MODIS sensors, see Figure 2.6. Linear regression analysis on a per year basis shows that the two sensors are well correlated. Excluding 2005, r-values between MODIS Terra AOD and MODIS Aqua AOD are above 0.8 ($R^2 > 0.66$), which are statistically significant correlations for $\alpha = 0.05$. The year 2005 had instances where MODIS Terra and MODIS Aqua observed the same event, but MODIS Aqua AOD is higher than MODIS Terra AOD. Some of these instances are associated with afternoon increases in aerosol concentration as measured by surface monitors and a few others are associated with haze events being advected into the area in the afternoon. Combining all years results in a statistically significant r-value of 0.78 for $\alpha= 0.05$. We expect the two sensors to be well correlated because they are calibrated to be consistent with each other and use the same aerosol retrieval algorithm, yet as our analysis reveals persistent variability between morning and afternoon aerosols could results in differences, e.g., year 2005 (See above). Over the period of our study, MODIS Aqua has fewer observations than MODIS Terra. During the summer in Georgia, the timing of convective systems growth often occurs in the early afternoon, which coincides with

Aqua's overpass. This might explain why MODIS aboard Aqua has fewer observations than MODIS aboard Terra, but both satellites have between 50 – 65% data available. Other U.S. locations have shown similar satellite data loss [*Gupta and Christopher*, 2008a; *Christopher and Gupta*, 2010].

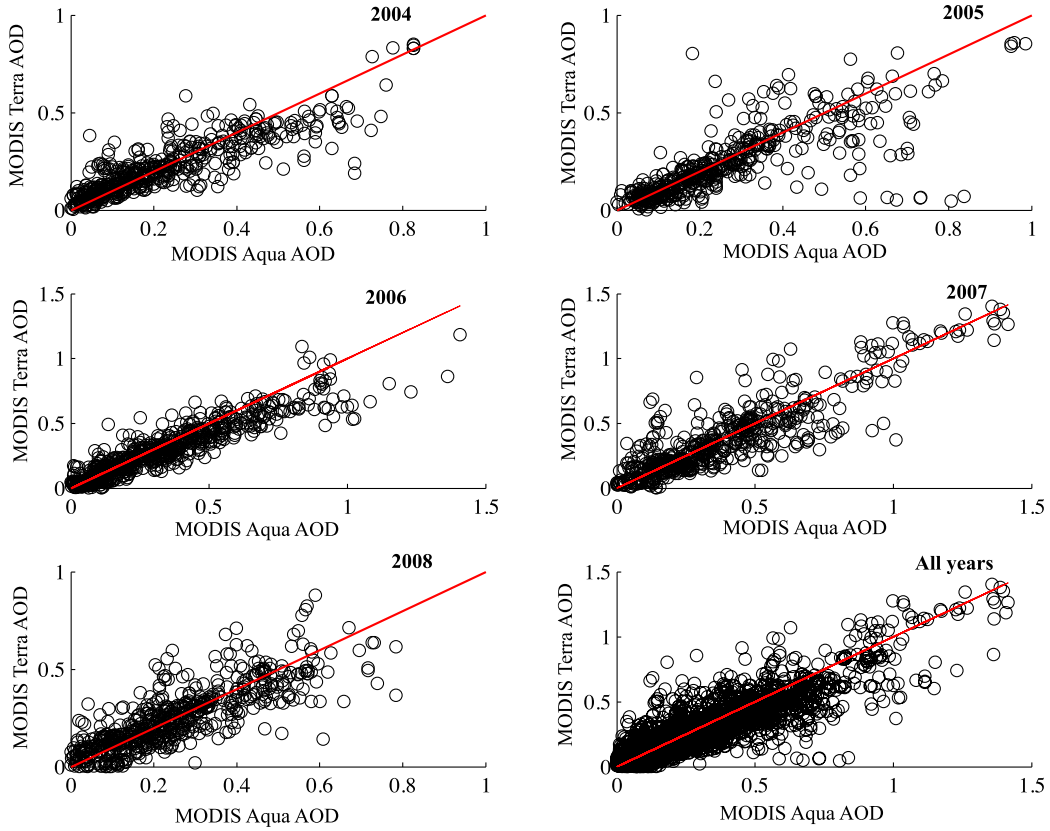

Figure 2.6: Scatterplots of MODIS Aqua AOD vs. MODIS Terra AOD. Red line represents 1:1 correspondence.

We consider the relationship between $PM_{2.5,24}$ and MODIS AOD aboard Terra and Aqua at each station through analyses of scatterplots. For instance, Figure 2.7 shows MODIS Aqua AOD vs. $PM_{2.5,24}$ at Gwinnett. This site is chosen to be illustrative of the other stations, as all the stations show the same general behavior as discussed below. We use the values of AOD > 0.7 and $PM_{2.5} > 35.5 \mu g/m^3$ to broadly define

quadrants to help to describe the different types of relations between AOD and $PM_{2.5,24}$. The scatterplots can be divided into quadrants, the NE quadrant is Q1, the NW quadrant is Q2, the SW quadrant is Q3, and the SE quadrant is Q4. These quadrants are representative of certain meteorological dynamic conditions. For instance, Q1 and Q3 are most likely associated with a well-mixed PBL such that aerosols are well distributed throughout the atmospheric column, thus satellite and ground-based measurements are in sync together. A vast majority of the data points lie within Q3. The points in Q3 have low AOD and $PM_{2.5}$ concentrations below 35.5 µg/m^3, which correspond to the green and yellow AQI ranges, see Table 2.1. However, Q1 describes data points with both high AOD and high $PM_{2.5}$ measurements (i.e., orange and higher AQI).

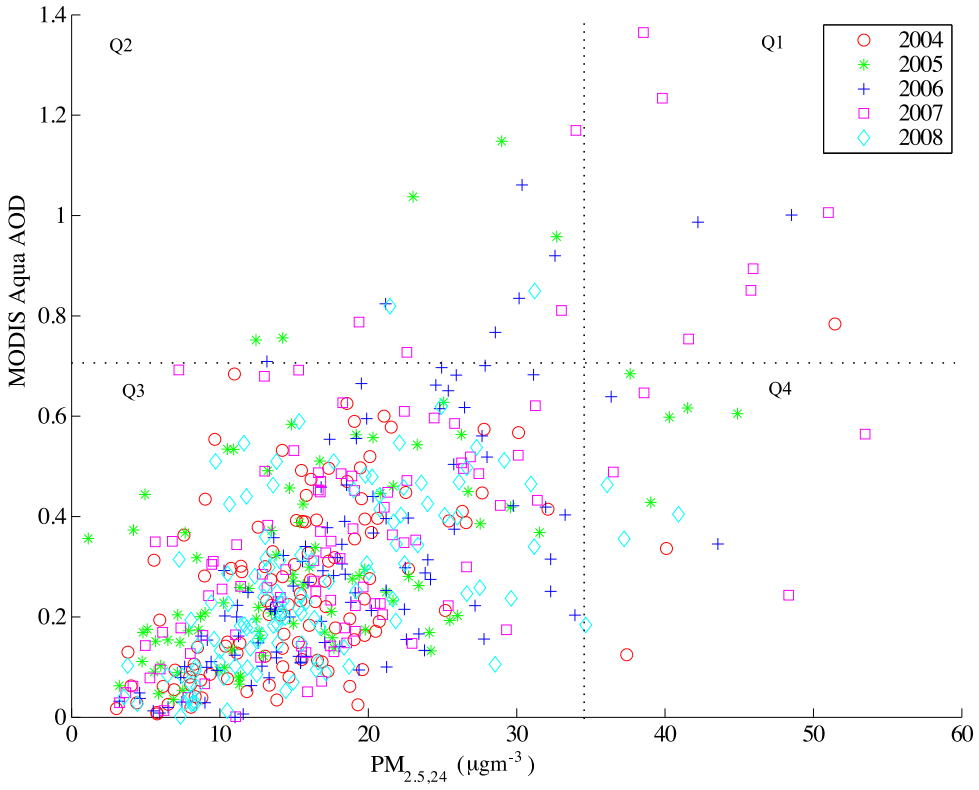

Figure 2.7: Scatterplot of MODIS Aqua AOD vs. $PM_{2.5,24}$ at Gwinnett. See text for explanation of notations.

In most cases, quadrants Q2 and Q4 can distinguish between different sources of air pollution. The points within Q2 have high AOD but low $PM_{2.5}$ concentrations. This situation could arise from long-range transport of aerosols into the area. The long-range transport of aerosols generally occurs above the boundary layer. Subsequently, these aerosols do not necessarily impact ground-based measurements (see discussion in previous section). However, it is possible that those aerosols can become entrained within the boundary layer due to changing dynamics and can impact ground-based measurements further downwind. Finally, Q4 has data points that coincide with high $PM_{2.5}$ concentrations and relatively low AOD. More than likely, these points represent increasing $PM_{2.5}$ concentrations of local source emissions. A possible scenario where this could occur is a strong inversion. In late spring and summer in Georgia strong inversions occur that trap all the local sources of pollution, e.g., cars and power plants, close to the surface by hindering vertical mixing. Additionally, the points in this quadrant could be indicative of smaller spatial scale (sub-pixel) events that are difficult to detect from satellites.

We have discussed what factors could possibly influence the $PM_{2.5}$-AOD relationship; the following analysis involves determining the robustness of the $PM_{2.5}$-AOD relationship through correlations. For a majority of the stations, both Aqua and Terra are correlated with $PM_{2.5}$. Correlation coefficients for Aqua vary between 0.37 – 0.76, and Terra has r-values of 0.25 – 0.68 (see Table 2.4 and Table 2.5). MODIS Terra and Aqua produce correlations that are similar to each other. Table 2.4 and Table 2.5 summarize the correlation coefficient (r), the slope, the y-intercept, and the number of

observations. In 2007, MODIS aboard Terra and Aqua have the highest correlations across all of the stations. The higher means of Terra AOD do not result in better agreement with $PM_{2.5}$, except in 2007 when Terra has higher r-values than Aqua. Terra also produces more variability in the correlation coefficients across the stations in comparison to Aqua. The seasonality of AOD and $PM_{2.5}$ is reflected in the values as well. Spring produces higher correlations than summer. The results presented here are somewhat different than the results from *Gupta and Christopher* [2009]. In their study, they presented correlations between observed $PM_{2.5}$ and estimated $PM_{2.5}$ from AOD for both a two-variable and multivariate linear regression. Our correlations and slopes show more variance than their reported values. Some of the differences between their work and ours could be due to the different time periods under consideration, as well as different approaches to ascertaining the $PM_{2.5}$-AOD relationship. We also compared our linear correlation coefficients and r-values to those of *Zhang et al.* [2009]. Our r-values were similar to theirs; however, our slopes and y-intercepts were slightly higher than theirs. Different spatial and time domains likely explain the differences found between their work and ours. This supports further the strong regional dependence of the AOD-$PM_{2.5}$ regression as was pointed by past studies [*Engel-Cox et al.*, 2004; *Weber et al.*, 2010] as well as highlights problems in determining a single regression line for accurately computing $PM_{2.5}$ from AOD data.

Table 2.4: Slope, Y-intercept, correlation coefficient (r), and number of observations of seasonal $PM_{2.5,24}$ vs. MODIS Terra AOD. Dash denotes missing data. Bold numbers are significant at $\alpha = 0.05$.

Location	Year	2004		2005		2006		2007		2008	
	Season	Spring	Summer	Spring	Summer	Spring	Summer	Spring	Summer	Spring	Summer
Confederate Ave.	Slope	-	-	0.03	0.01	0.01	0.01	0.02	0.02	0.00	0.01
	Y-intercept	-	-	-0.24	0.30	-0.05	0.14	-0.12	-0.03	0.11	0.11
	r	-	-	**0.87**	0.22	**0.62**	**0.37**	**0.81**	**0.62**	0.15	**0.44**
	#	-	-	6	35	59	66	57	53	54	61
Gwinnett	Slope	0.02	0.01	0.02	0.01	0.01	0.01	0.02	0.02	0.01	0.01
	Y-intercept	-0.05	0.13	-0.02	0.23	0.00	0.11	-0.01	0.08	0.10	0.16
	r	**0.68**	**0.51**	**0.66**	**0.50**	**0.62**	**0.44**	**0.76**	**0.67**	**0.29**	**0.41**
	#	53	48	46	38	67	53	61	53	54	63
McDonough	Slope	0.02	0.01	0.01	0.01	0.01	0.01	0.02	0.02	0.01	0.01
	Y-intercept	-0.03	0.09	0.04	0.25	0.02	0.18	-0.05	0.03	0.09	0.17
	r	**0.54**	**0.64**	**0.51**	**0.38**	**0.53**	**0.40**	**0.70**	**0.67**	0.25	**0.34**
	#	54	44	56	39	57	70	59	59	51	61
Newnan	Slope	0.01	0.01	0.01	0.00	0.01	0.01	0.02	0.02	0.00	0.01
	Y-intercept	0.00	0.16	0.02	0.28	-0.03	0.21	-0.05	0.09	0.11	0.08
	r	**0.44**	**0.46**	**0.57**	0.30	**0.73**	**0.37**	**0.78**	**0.61**	0.16	**0.56**
	#	55	32	40	35	57	63	57	57	49	62
S. Dekalb	Slope	0.01	0.01	0.01	0.00	0.01	0.01	0.02	0.02	0.01	0.01
	Y-intercept	-0.02	0.14	0.06	0.33	-0.01	0.15	-0.04	-0.03	0.10	0.19
	r	**0.54**	**0.49**	**0.56**	0.22	**0.59**	**0.40**	**0.78**	**0.69**	0.19	**0.33**
	#	54	44	56	35	55	63	59	55	54	66
Walton	Slope	-	-	0.01	0.00	0.01	0.02	0.02	0.02	0.01	0.01
	Y-intercept	-	-	-0.03	0.28	0.03	0.06	-0.03	0.05	0.05	0.19
	r	-	-	**0.65**	0.28	**0.51**	**0.51**	**0.76**	**0.68**	**0.35**	0.23
	#	-	-	32	36	55	64	53	56	49	59
Yorkville	Slope	0.02	0.01	0.02	0.01	0.02	0.01	0.02	0.02	0.01	0.01
	Y-intercept	-0.02	0.08	-0.04	0.24	-0.06	0.08	-0.05	0.00	0.03	0.11
	r	**0.45**	**0.60**	**0.74**	**0.38**	**0.62**	**0.51**	**0.74**	**0.76**	**0.50**	**0.51**

Table 2.5: Slope, Y-intercept, correlation coefficient (r), and number of observations of seasonal $PM_{2.5,24}$ vs. MODIS Aqua AOD. Dash denotes missing data. Bold numbers are significant at $\alpha = 0.05$.

Location	Year	2004		2005		2006		2007		2008	
	Season	Spring	Summer	Spring	Summer	Spring	Summer	Spring	Summer	Spring	Summer
Confederate Ave.	Slope	-	-	0.01	0.01	0.01	0.01	0.01	0.02	0.02	0.01
	Y-intercept	-	-	0.10	0.29	-0.09	0.11	0.03	0.02	-0.09	0.07
	r	-	-	0.18	**0.37**	**0.70**	**0.41**	**0.54**	**0.51**	**0.54**	**0.51**
	#	-	-	6	42	57	59	45	47	49	58
Gwinnett	Slope	0.01	0.01	0.01	0.01	0.02	0.01	0.01	0.02	0.01	0.01
	Y-intercept	0.00	0.19	0.10	0.21	-0.04	0.11	0.10	0.10	0.02	0.14
	r	**0.51**	**0.40**	**0.39**	**0.49**	**0.70**	**0.46**	**0.56**	**0.59**	**0.46**	**0.46**
	#	60	54	47	44	60	50	51	50	48	67
McDonough	Slope	0.02	0.01	0.01	0.01	0.02	0.01	0.02	0.02	0.01	0.01
	Y-intercept	-0.07	0.12	0.08	0.29	-0.02	0.14	-0.01	0.07	-0.02	0.07
	r	**0.56**	**0.54**	**0.47**	**0.38**	**0.67**	**0.46**	**0.62**	**0.65**	**0.58**	**0.53**
	#	58	46	49	43	54	58	43	55	52	61
Newnan	Slope	0.01	0.01	0.01	0.01	0.02	0.01	0.02	0.02	0.01	0.01
	Y-intercept	-0.01	0.23	0.12	0.21	-0.05	0.17	-0.02	0.09	0.05	0.15
	r	**0.40**	**0.43**	0.26	**0.56**	**0.70**	**0.45**	**0.71**	**0.61**	**0.37**	**0.50**
	#	56	38	39	44	57	56	42	52	49	58
S.Dekalb	Slope	0.01	0.01	0.01	0.01	0.02	0.02	0.01	0.02	0.01	0.01
	Y-intercept	0.02	0.13	0.10	0.30	-0.07	0.09	0.05	0.01	0.02	0.06
	r	**0.41**	**0.52**	**0.42**	**0.42**	**0.76**	**0.54**	**0.53**	**0.63**	**0.40**	**0.56**
	#	60	48	51	42	54	55	46	53	52	61
Walton	Slope	-	-	0.01	0.01	0.02	0.02	0.01	0.02	0.01	0.01
	Y-intercept	-	-	0.14	0.23	-0.04	0.06	0.07	0.08	0.02	0.04
	r	-	-	0.23	**0.41**	**0.61**	**0.51**	**0.50**	**0.63**	**0.42**	**0.51**
	#	-	-	36	39	52	61	44	50	45	57
Yorkville	Slope	0.02	0.02	0.01	0.01	0.02	0.02	0.01	0.02	0.02	0.01
	Y-intercept	-0.01	0.06	0.04	0.20	-0.02	0.06	0.08	0.05	-0.04	0.15
	r	**0.41**	**0.59**	**0.51**	**0.56**	**0.59**	**0.57**	**0.49**	**0.72**	**0.59**	**0.47**
	#	52	44	44	42	58	53	49	55	50	61

To avoid problems with the AOD-$PM_{2.5}$ regression, here we propose another approach for utilizing the multi-year AOD data in air quality applications. In this approach the AQI designations of $PM_{2.5}$ concentrations are used to categorize the AOD. For instance, all AOD data points that correspond to $PM_{2.5}$ concentrations between 0 – 15.4 $\mu g/m^3$ are considered to be Code Green AOD. This classification methodology is used for all six categories of AQI. This categorized AOD is then used to determine a threshold that can probabilistically separate days of air quality exceedances from days without exceedances.

Figure 2.8 and Figure 2.9 show AQI classified MODIS aboard Aqua/Terra AOD for 2006 at Gwinnett. Figure 2.8a and Figure 2.9a are results for Terra, and Figure 2.8b and 7b are for Aqua. In Figure 2.8 the upper panel is Code Green AOD, and the bottom panel is Code Yellow AOD. The panels on the left are frequency histograms and on the right are cumulative histograms of AOD. In Figure 2.8, Code Green and Yellow AOD have similar frequency and cumulative distributions. The cumulative distributions for both satellites are interpreted as 80% of Code Green AOD are below 0.35, and 80% of Code Yellow AOD are below 0.65. In Figure 2.9 the upper panel is Code Orange AOD and if present the bottom panel is Code Red AOD. Code Orange and Red AODs have different distributions. It is not surprising that Code Red AOD is skewed toward higher AOD. The closely related relationship between AOD and $PM_{2.5}$ suggests that high AOD will occur in cases of high $PM_{2.5}$. Code Orange AOD is associated with AOD of 0.75 for Aqua and 0.65 for Terra. The lack of Code Red AOD makes determination of thresholds difficult and would require analysis of longer AOD records.

The broad thresholds (80%) discussed above yielded overestimation in the Code Orange and Red categories. To more accurately match the $PM_{2.5}$-derived AQI, we used different thresholds for each satellite. For this we calculated AOD thresholds for Gwinnett for all years. The yearly threshold levels, e.g., 80%, 90%, and 95% were averaged to create AQI categorized AOD thresholds specifically tuned for Gwinnett. Figure 2.10 shows our AOD-derived AQI and $PM_{2.5}$-dervived AQI at Gwinnett. Specifically for Terra we used the 80% threshold for green AQI and 95% for yellow and orange AQI. The exact cut-offs for Terra AOD are: Code Green AOD is below 0.26, Code Yellow AOD is 0.26 – 0.72, Code Orange AOD 0.72 – 1.0, and Code Red AOD is everything greater than 1. For Aqua we used the 80% threshold for green AQI and 90% for yellow and orange AQI. AOD cut-offs for Aqua are slightly different than for Terra. Aqua AOD thresholds are: Code Green AOD is below 0.28, Code Yellow AOD is 0.28 – 0.69, Code Orange AOD is 0.69 – 1.15, and Code Red AOD is everything over 1.15.

While we only show pie charts based upon the new AQI designations, there are few differences between them and pie charts produced with AOD-derived AQI using old designations. The differences occur mostly within the yellow and orange AQI categories, as these are the AQI designations that were proposed to be changed in accordance with the revised $PM_{2.5}$ NAAQS 24-hr standard. Though these figures (AOD-derived pie charts) are not an exact match for the $PM_{2.5}$-based AQI, they provide information at an easily understandable and relatable manner. Having probabilistic means to describe the incidence of AOD over metro Atlanta allows for this threshold approach to be extrapolated for use in areas without $PM_{2.5}$ monitors. In particular, AQI categorized AOD has great applicability to suburban and rural areas in the state of Georgia and the other

rural areas across the country, because this approach is not bound strictly by achieving high correlations between $PM_{2.5}$ and AOD. Another advantage to this method is that it can be used in real-time to provide a quick assessment of the air quality for a specific region that does not require any additional computing or forecasting resources.

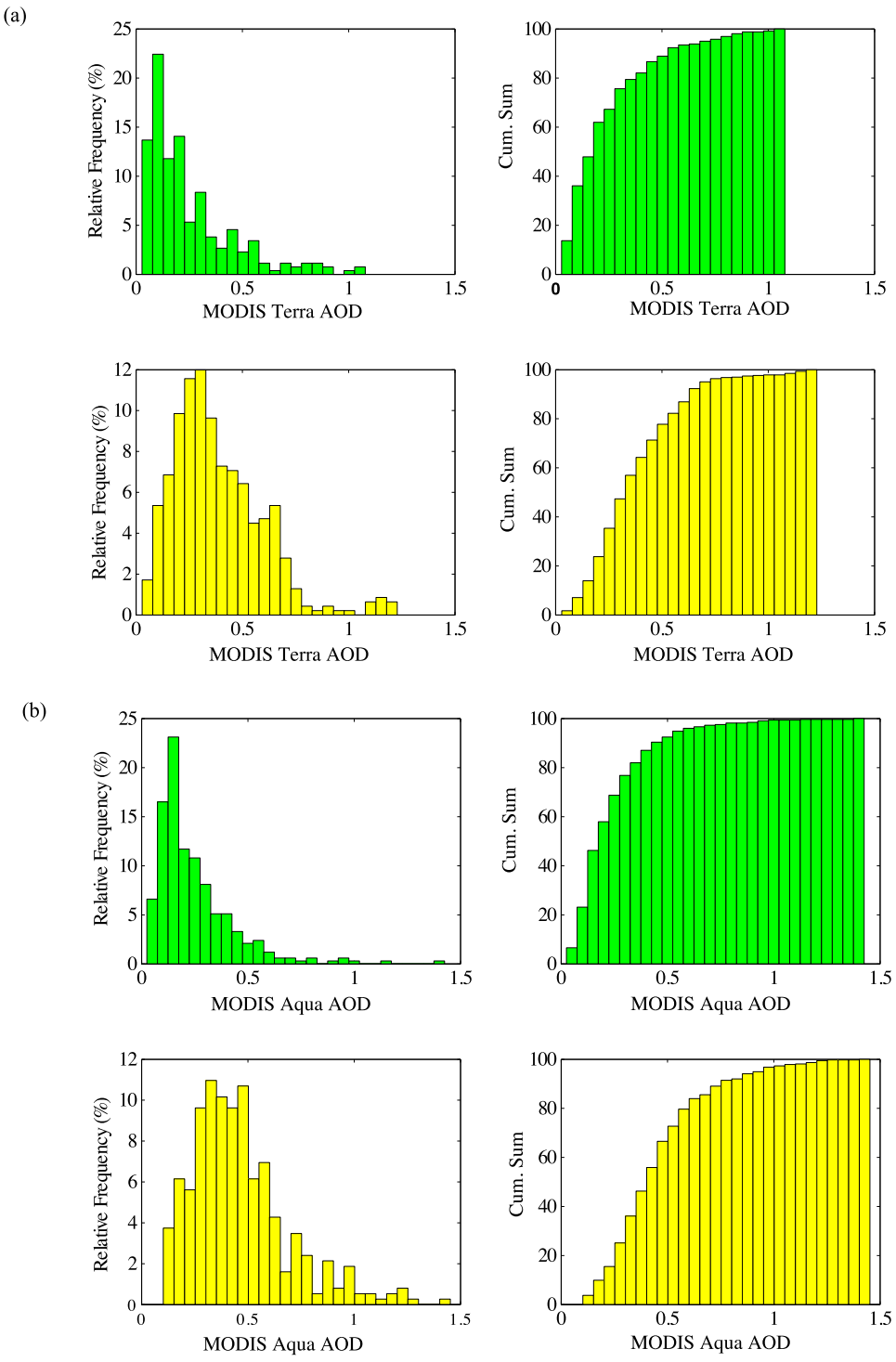

Figure 2.8: (a) Relative frequency histograms and cumulative frequency histograms of Code Green and Code Yellow MODIS Terra AOD at Gwinnett for 2006. (b) Same as (a), except for MODIS Aqua AOD.

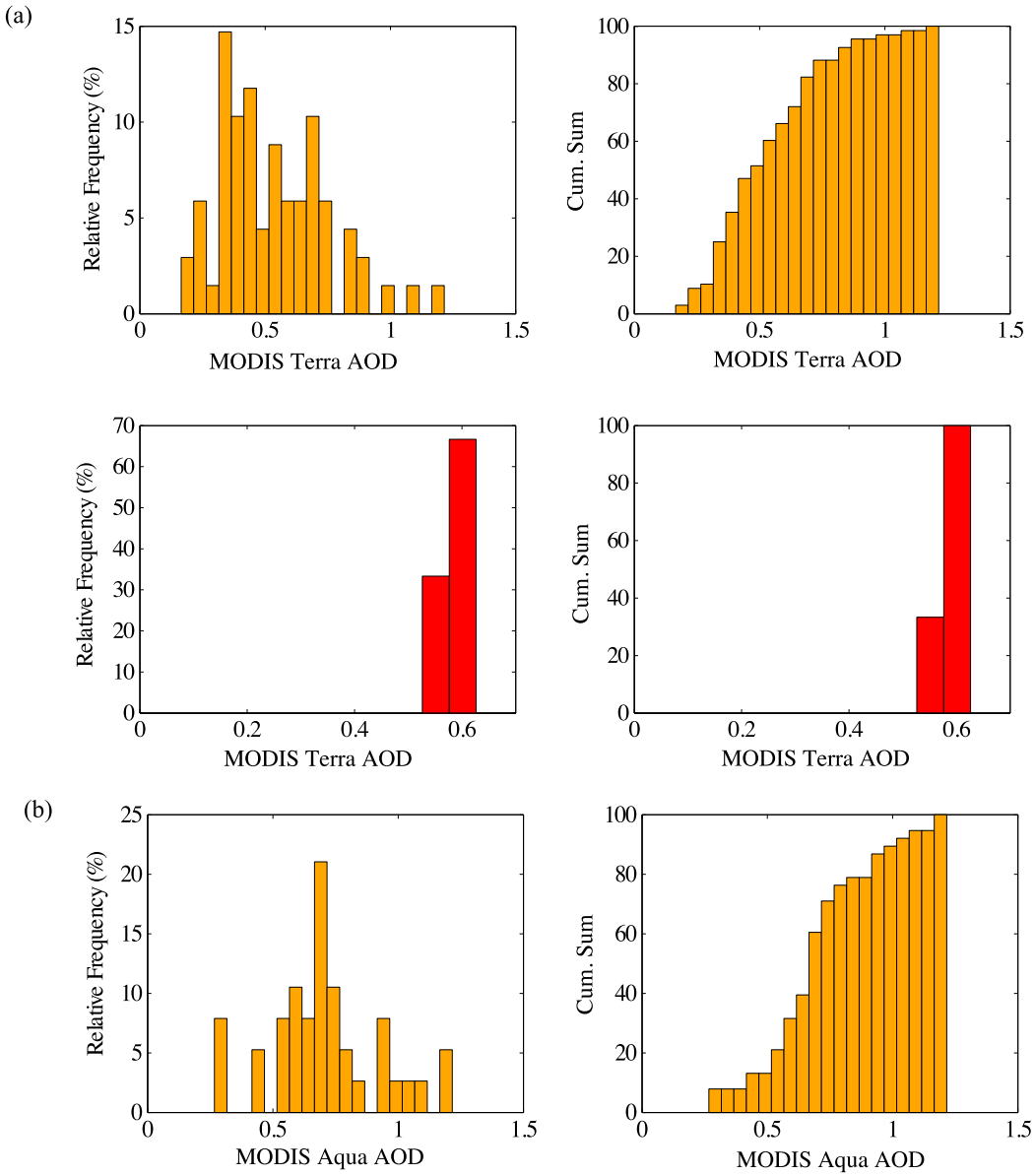

Figure 2.9: (a) Relative frequency histograms and cumulative frequency histograms of Code Orange and Code Red MODIS Terra AOD at Gwinnett for 2006. (b) Relative frequency histograms and cumulative frequency histograms of Code Orange MODIS Aqua AOD for 2006.

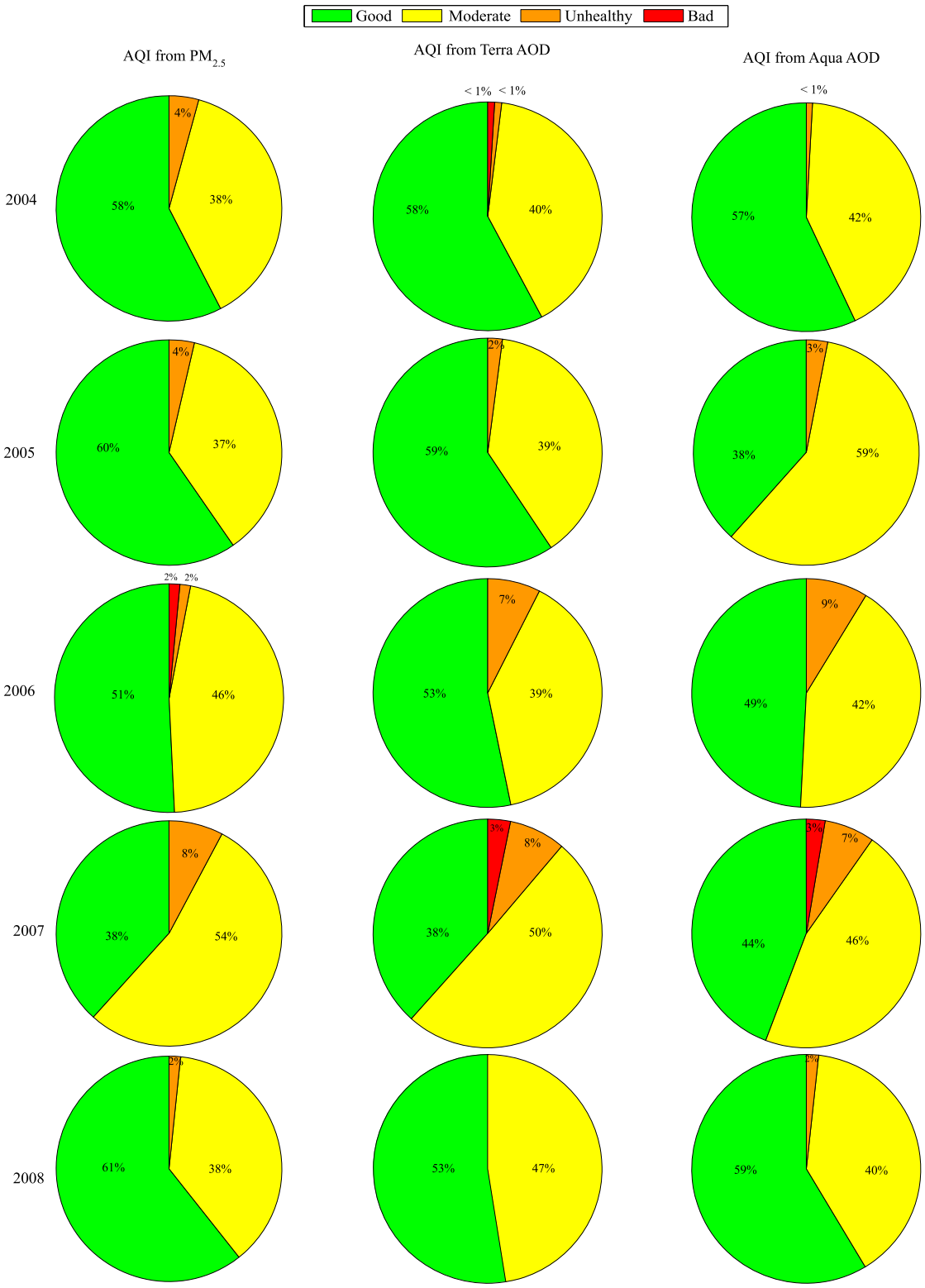

Figure 2.10: Piecharts of $PM_{2.5}$-derived AQI, MODIS Terra AOD-derived AQI, and MODIS Aqua AOD-derived AQI at Gwinnett.

2.4 Chapter Summary

Utilization of multi-year remotely sensed data allows for a broader perspective view of air quality. Local air quality is affected by a number of factors including regional emissions, temperature, atmospheric dynamics, and traffic patterns. Satellite data also allow for viewing the transport features/aerosols that could impact air quality with time. This research presented a multi-year analysis of spring and summer data from 2004 - 2008 in metropolitan Atlanta. Our research focused upon the synergy between ground-based measurements of $PM_{2.5}$ and NASA satellite observations in the terms of Aerosol Optical Depth (AOD) from MODIS and the Aerosol Index (AI) from OMI. MODIS AOD is a derived measurement from both MODIS instruments onboard the Terra and Aqua satellites. OMI onboard Aura is an instrument that measures the absorbing aerosols in the UV-spectrum. Our research goals were to understand the variability within the $PM_{2.5}$ and AOD data records, assess the strength of the $PM_{2.5}$-AOD relationship, and probabilistically determine AOD thresholds that relate directly to AQI categories, as an alternative to the $PM_{2.5}$-AOD linear regression approach.

Results for the $PM_{2.5}$ analysis show that $PM_{2.5}$ differences are likely due to station location, with the highest averages of $PM_{2.5}$ occurring at urban sites and the lowest averages occurring at rural sites. Across the all seven $PM_{2.5}$ stations the springtime means show less variability than summertime means. MODIS AOD has captured the same yearly behavior seen in $PM_{2.5}$, yet on a seasonal basis the summertime has AOD values double that of the spring. OMI AI does not have a discernable seasonal variability. Background levels of AI for the Atlanta metro area are around 0.3. Eighty percent of AI is below 0.5; therefore, AI values higher than this could be indicative of mid- and long-

range transport of wildfires smoke into the area. The results of linear regressions between $PM_{2.5}$ and AOD are r-values above 0.5 for a majority of sites with maximum r-values of 0.8 for Terra and 0.7 for Aqua. Interestingly, Terra produced higher correlation coefficients than Aqua in 2007, while in other years the satellites have similar r-values. Given various problems in establishing a robust $PM_{2.5}$-AOD regression, we proposed using statistical analysis of AOD data to relate AOD directly to AQI via probabilistic measures based upon the multi-year record of AOD values for a certain area. Applying this approach to the Atlanta metropolitan area, we determined that 80% of green AQI days occur with AOD of 0.35 or less, and 80% of yellow AQI days occur with AOD of 0.65. These probabilistic AOD cutoffs can be used to quickly access the AQI classifications without the dependence upon ground-based measurements. There is some agreement between $PM_{2.5}$ based AQI and satellite based AQI. Further work will need to be done to better tune the methodology for orange and red AQI, given the relatively low frequency of those AQI colors.

The great advantage of using the probabilistic approach to relating AOD to AQI is that it can be tuned for different regions of interest. Once AOD thresholds are established they can be used in real-time general assessments of the state of air quality on a daily basis. This method could also be applied to geostationary satellites (e.g., the National Oceanic and Atmospheric Administration's (NOAA) GOES [*Prados et al.*, 2007]) where half-hourly data from the satellites can provide quick, real-time information about air quality throughout the day. Finally, the use of long-term timeseries of AOD can be used to quantitatively determine if air quality policies are effective in bettering air quality. Longer term studies on air quality policies' impacts can be obtained by extending the

AOD timeseries into the future with launch of the VIIRS (Visible Infrared Imager Radiometer Suite) instrument planned as part of the NPOESS (National Polar-Orbiting Operational Environmental Satellite System) program [*Lee et al.*, 2006].

CHAPTER 3

COMBINED CAPABILITY ASSESSMENT OF SATELLITE AND GROUND BASED DATA TO ASSESS IMPACTS OF BIOMASS BURNING ON AIR QUALITY WITHIN THE SOUTHEASTERN U.S.

3.1 Introduction

In this study, we examine the impact of a large wildfire episode that occurred in the spring of 2007 on air quality in the Atlanta metropolitan area by exploring the utility of multi-satellite data, especially new data provided by the A-Train satellite constellation (http://nasascience.nasa.gov/earth-science/a-train-satellite-constellation).

Many past studies have explored the use of satellite data in air quality applications (see a recent review by *Hoff and Christopher* [2009]). The majority of them have focused upon establishing a linear regression between surface level particulate matter ($PM_{2.5}$ or PM_{10}) and satellite-derived aerosol optical depth (AOD), mainly from MODIS. Using the single or multiple regression approaches, the $PM_{2.5}$/AOD relationships have been developed at the regional scales in the U.S. [*Engel-Cox et al.*, 2005] and for selected cities in the U.S. southeast [*Gupta and Christopher*, 2008b]. This body of work has demonstrated various differences in $PM_{2.5}$-AOD regressions revealing the role of specific region-dependent factors. However, only a few studies have used satellite data in addressing the impact of wildfires on air quality in large cities [*Liu et al.*, 2009a]. Furthermore, some studies (e.g., Gupta et al. 2006) have reported low $PM_{2.5}$ /AOD correlations in the case of fires that are expected to be affected by the region-dependent type of burning vegetation, fire regimes, meteorological conditions controlling the smoke

transport, among some other regional factors. The sole use of AODs, which reflects the columnar aerosol loading, limits the delineation of involved factors such as sources, composition, and vertical distribution of particulate matter. New data from the A-Train constellation, especially observations of the vertical profiles of aerosols and their types performed by the CALIPSO space lidar, offer a better opportunity to examine the impact of fires on air quality, as well as the value of $PM_{2.5}$/AOD relationships.

In spring of 2007 Atlanta was affected by the largest wildfire in southeastern U.S. history that burned along the Georgia (GA) – Florida (FL) state border in the Okefenokee Swamp National Wildlife Refuge. Atlanta is located approximately 240 miles north of the fire center. The fire burned over 300,000 acres in total, and transport of smoke affected the larger part of the U.S. southeast. The main goal of this paper is to examine multiple-satellite data as a tool for characterizing wildfire impacts on a large urban area, addressing the specifics of swamp fires and their impact on the Atlanta metropolitan area. Our specific goals are to (1) examine the dynamics of $PM_{2.5}$ and AOD retrieved from MODIS aboard Terra and Aqua satellites and the $PM_{2.5}$-AOD relationship in the case of high smoke loadings (exceedance days), (2) examine the capability of CALIPSO lidar to detect and identify smoke and quantify the vertical structure of AODs, (3) identify the wildfire signatures through the analysis of OMI data, and (4) perform an in-depth analysis of smoke events that caused the largest impact on air quality across the Atlanta metro area in May of 2007 through a combination of multi-satellite data. Section 2 briefly introduces the data and methodology used in this study followed by the results presented in Section 3. In out discussion section, we use the methodology developed in earlier sections and apply it to the wildfire of 2011. This wildfire occurred in the same location

as the fire in 2007, and a comparison on these fires could provide insights into the dynamics that control wildfire impacts to air quality. Finally, we conclude with a summary in Section 5.

3.2 Data and Methodology

3.2.1 Ground-based $PM_{2.5}$ Data

For this chapter, we use the same notation of $PM_{2.5}$ subsets ($PM_{2.5,T}$ and $PM_{2.5,A}$) with the exclusion of the 24-hr averaged $PM_{2.5}$. Figure1.1 shows the location of seven stations in the metropolitan Atlanta area that were used in our study. We will be using the same $PM_{2.5}$ stations as in Chapter 2. For details on this dataset, please see Section 2.2.1. The stations are abbreviated as the following: Confederate Ave – Con; Gwinnet – Gwi; McDonough – McD; Newnan – New; S. Dekalb – Sde; Walton – Wal; Yorkville – Yor. For this study we use $PM_{2.5}$ measurements for May 2007.

3.2.2 Satellite data products

3.2.2.1 MODIS Data

We analyzed the most recent MODIS Level 2, Collection 5 data that are provided by NASA LAADS (http://ladsweb.nascom.nasa.gov/index.html) for May 2007. A search radius of 0.5° and 0.25° was used to select all MODIS pixels around a station's latitude and longitude following the approach of *Engel-Cox et al.* [2004] and *Gupta and Christopher* [2008a]. Those pixels were averaged to create a co-located, coincident dataset of AODs from MODIS on Terra and Aqua for each respective $PM_{2.5}$ station. Two

search radii (0.5° and 0.25°) were considered to address the role of spatial heterogeneity of smoke and implications for correlations between coincident $PM_{2.5}$ and MODIS AODs.

In Section3.4, we use MODIS AOD to analyze the wildfire of 2011. Here we use AOD from May1 – July 31, 2007, 2009, 2011 to compare fire and non-fire years.

3.2.2.2 OMI Data

The Ozone Monitoring Instrument (OMI) on board the Aura satellite takes measurements in the near-ultraviolet (UV) for retrievals of gases and aerosols. In this chapter, we use OMI AI broadly centered of the same lat/lon box as in Chapter 2 (Section2.2.2) since we are more focused on broader regional effects of the wildfires. We use OMI AI for May 2007 and for a number of days during the summer 2011 due to retrieval errors of the OMI sensor (see Section 3.4).

3.2.2.3 CALIPSO Data

CALIPSO (Cloud-Aerosol Lidar and Infrared Pathfinder Satellite Observations) includes a space-borne lidar, which measures vertical profiles of backscattering 24 hours a day with near global coverage in 16 days. The CALIPSO lidar (CALIOP) takes measurements in three channels 532 nm parallel, 532 nm perpendicular, and 1064 nm [*Winker et al.*, 2009]. The CALIOP has a nominal vertical resolution of 30 m and horizontal resolution of 333; however, aerosol products are retrieved at coarser resolutions. The CALIPSO Level 2 algorithms identify features and classify these as clouds or aerosols. The feature finding algorithms use changes in the profiles of attenuated backscatter to identify features [*Vaughan et al.*, 2009] and the cloud aerosol discrimination algorithm uses attenuated backscatter intensity, color ratio and volume

depolarization ratio to separate clouds from aerosols [*Liu et al.*, 2009b]. The aerosol sub-typing algorithm uses integrated attenuated backscatter and depolarization ratio to identify clean marine, clean continental, dust, polluted continental, polluted dust, and smoke aerosols [*Omar et al.*, 2009]. The Version 3 data products used in this study consist of the attenuated backscatter profile, the vertical feature mask, and the CALIOP-derived AOD [*Omar et al.*, 2009]. Data were obtained from the NASA Langley Atmospheric Science Data Center (http://eosweb.larc.nasa.gov/). The CALIOP-derived AOD is reported at 5 km horizontal resolution while the number of vertical layers (and hence the vertical resolution of AODs) varies from scene-to-scene. We focus on examining the CALIPSO capability in identifying the smoke plumes, resolving their vertical layered structure, and determining AODs of resolved layers.

3.3 Results

3.3.1 Analysis of Ground-based Data

According to the Georgia Department of Natural Resources, during May of 2007 there were six days (May 4, 16, 22, 26, 27, and 31) that the daily NAAQS for $PM_{2.5}$ was exceeded (http://www.georgiaair.org/tmp/exceedances/index.php?yr=2007). All these exceedance cases were associated with wildfire smoke transported to the Atlanta metropolitan area.

Figure 3.1 shows the diurnal cycle of hourly $PM_{2.5}$ at the seven sites for the six exceedance days. An interesting finding is that most of the exceedance cases are from stations outside the I-285 perimeter (McDonough, Newnan, Walton, and Yorkville. These sites reached the exceedance level before the more centrally located stations of Confederate Ave., Gwinnett, and South Dekalb. In fact, the two furthest removed stations

from the metro area, Newnan and Yorkville, consistently recorded some of the highest concentrations, 280 μg/m^3, and 180 μg/m^3 respectively. The centrally located stations had maximum concentrations around 180 μg/m^3 for Confederate Ave., 175 μg/m^3 for Gwinnett, and 247 μg/m^3 for South Dekalb in comparison to non-exceedance days where typical maximum concentrations are around the mid 20s μg/m^3. Maximum concentrations at all stations were greater than the level commonly considered as very unhealthy air quality, further stressing the significance of the adverse impacts of wildfires on urban air quality.

The spatiotemporal distribution of smoke differs from the common pattern of urban pollution in Atlanta. In this instance, the common pattern of pollution refers to urban areas having higher concentrations than rural areas as well as how the diurnal cycle varies from different representative stations [*Butler et al.*, 2003; *Edgerton et al.*, 2006]. Understanding the normal (non-fire) $PM_{2.5}$ concentration gradient is important to understanding how the wildfire causes changes to that pattern. The wildfire created an exaggerated diurnal cycle; where the overnight/morning concentrations were sometimes three to four times higher than normal, see Figure 3.2. Although examination of Figure 3.2 reveals some similarities in the $PM_{2.5}$ dynamics between the stations, various differences are apparent. Figure 3.2 also shows that, in most cases, the $PM_{2.5}$ concentrations were higher during the MODIS Terra overpasses compared to $PM_{2.5}$ coincident with MODIS Aqua that might have implications to the $PM_{2.5}$ –AOD relationships.

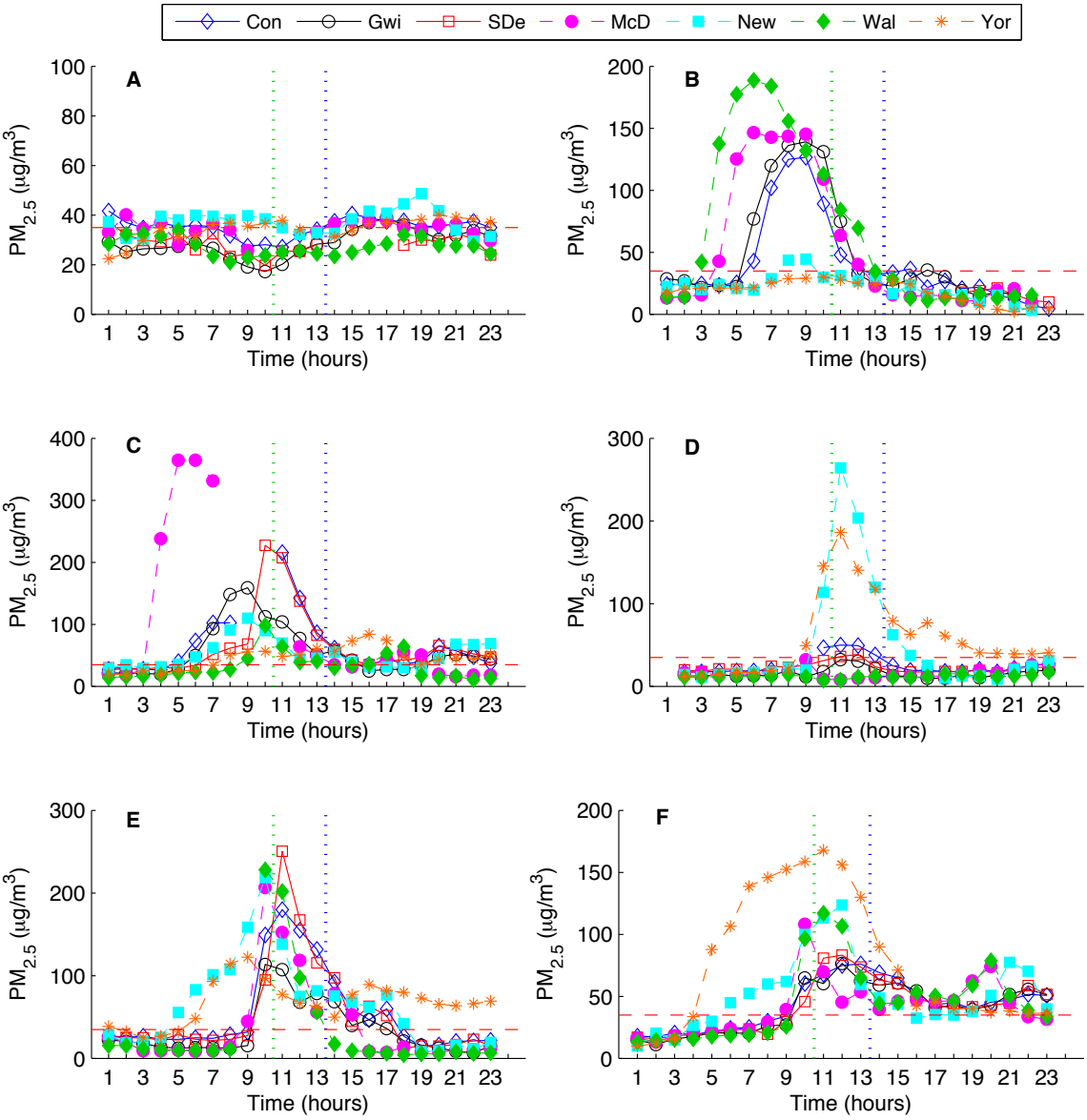

Figure 3.1: $PM_{2.5}$ diurnal cycle. (A) Exceedance day May 4, (B) Exceedance day May 16, (C) Exceedance day May 22, (D) Exceedance day May 26 , (E) Exceedance day May 27, (F) Exceedance day May 31. Red dashed line is NAAQS daily standard of 35.5 $\mu g.m^3$; green and blue dotted lines represent Terra and Aqua equatorial overpass times respectively. Station abbreviations, see Section 3.2.1.

To further examine the differences in the behavior of $PM_{2.5}$ across the stations during satellites' overpasses, we subtracted $PM_{2.5,T}$ and $PM_{2.5,A}$ values observed at the Confederate Ave. station from those observed at the other six stations. We chose to use Confederate Ave. as the baseline because it is centrally located, and it generally has the

highest concentrations during May. These timeseries for the entire month of May are shown in Figure 3.3. Positive differences indicate that the station reported a higher concentration than Confederate Ave. On non-exceedance days, the absolute differences among the stations are within 10 $\mu g/m^3$, while much larger differences are clearly seen in the case of exceedances. These differences also vary from one case to another. For instance, on May 25 Newnan and Yorkville stations have absolute difference values greater than 80 $\mu g/m^3$, followed by differences of over 60 $\mu g/m^3$ on May 26, and finally on May 27 have differences between 30–60 $\mu g/m^3$. Overall, the analysis of ground-based data demonstrated that the wildfire increased $PM_{2.5}$ concentrations across the metro area in a non-uniform way, as might be expected. Our analysis suggests that the counties furthest from the city, specifically to the west and south, were impacted more than other stations as shown by the differences between them in Figure 3.2 and Figure 3.3. Wildfires have been shown to create a heterogeneous spatial distribution of pollution concentrations in other areas as well [*Wu et al.*, 2006]. Focusing on two exceedance cases (May 22 and 31) in Section 3.3.3.3 we explore how the multi-sensor satellite data can aid in air quality assessments by providing the larger scale perspective. We chose to closely examine these two days because both days have high $PM_{2.5}$ concentrations and have the broadest range of satellite data available for analysis. But first we examine the linkage between MODIS AOD data and ground $PM_{2.5}$ data.

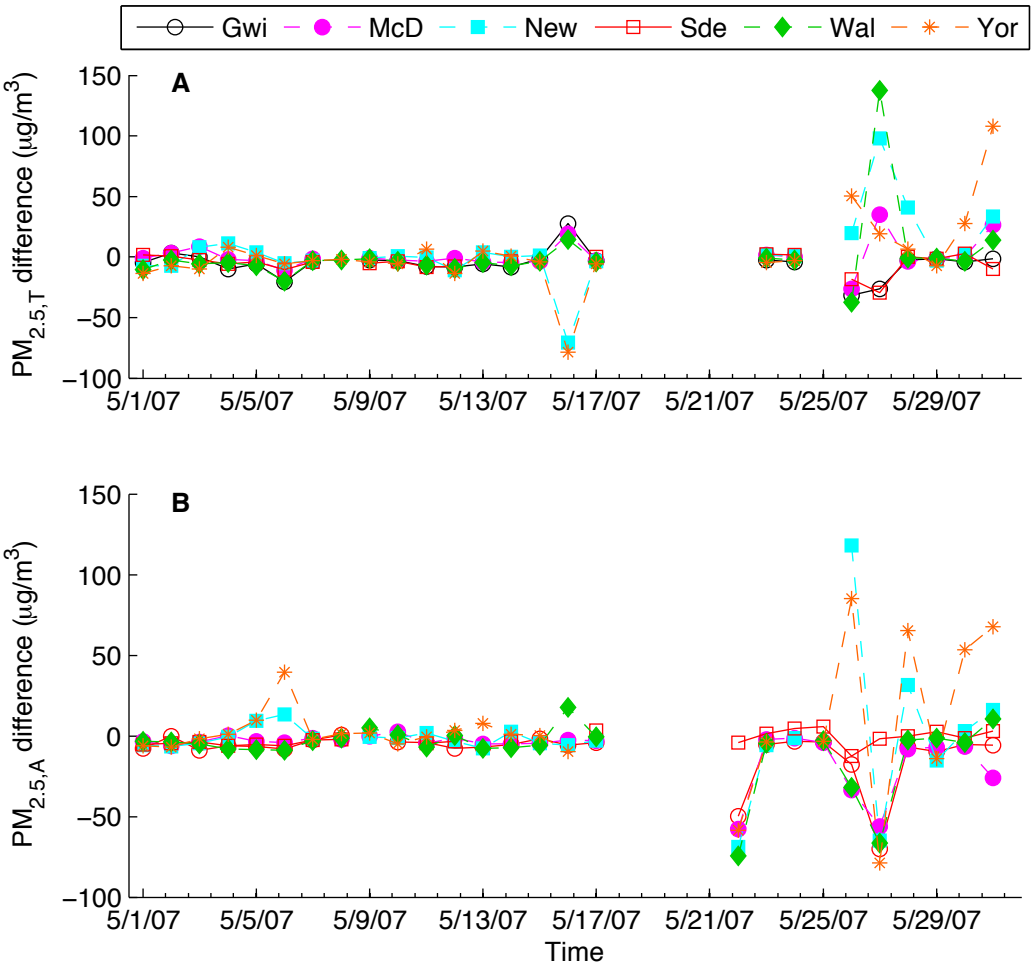

Figure 3.2: Timeseries of the difference curves of PM2.5 concentrations, where difference = each station's concentrations – Confederate Ave.'s concentrations (A) $PM_{2.5,T}$ (B) $PM_{2.5,A}$. Open symbols are urban stations; filled symbols are rural stations. Station abbreviations, see Section 3.2.1.

3.3.2 Examination of $PM_{2.5}$ and MODIS AOD Relationships

Our analysis of MODIS data confirms that for the month of May retrieved AOD show elevated values with varying spatial distributions. We found that the MODIS can capture the heterogeneity associated with the different concentration gradients of $PM_{2.5}$ on a day-by-day basis. Visible imagery from MODIS Terra and Aqua showed thick cloud

cover over Atlanta on both days. The presence of clouds also resulted in missing AODs on other days, especially for Aqua overpasses.

The days of high AOD values from both satellites generally occur on the same days of $PM_{2.5}$ exceedances. On May 22, 27, and 31 Terra AOD values were greater than 0.8 while Aqua AOD values were as high as 0.7 – 0.9. There was a period of elevated AOD values around May 12 that did not corresponded to surface $PM_{2.5}$ concentrations in Atlanta; however, there was a $PM_{2.5}$ exceedance in Macon, Georgia, which is located south of Atlanta. The most likely explanation for the discrepancy of ground-based $PM_{2.5}$ and AOD is that the wildfire aerosols that were causing the exceedance in Macon were located aloft over Atlanta on that day. Unfortunately, there were no co-located CALIPSO passes to corroborate this.

We show in Figure 3.1 that $PM_{2.5}$ values were higher at the times of MODIS Terra overpasses than MODIS Aqua. Figure 3.3 presents the timeseries of AOD collocated with the McDonough and Yorkville stations, showing that Terra does record higher AODs compared to Aqua. McDonough and Yorkville stations were chosen to be representative of suburban and rural conditions, respectively. Figure 3.3 also presents the difference between using a search radius of 0.5° (Figure 3.3(A and C) and a search radius of 0.25° (Figure 3.3(B and D). Using the smaller radius results in fewer points, but lessens the effects of overlapping AOD measurements at the stations. Given the low number of data points, it is difficult to determine the general behavior of AOD.

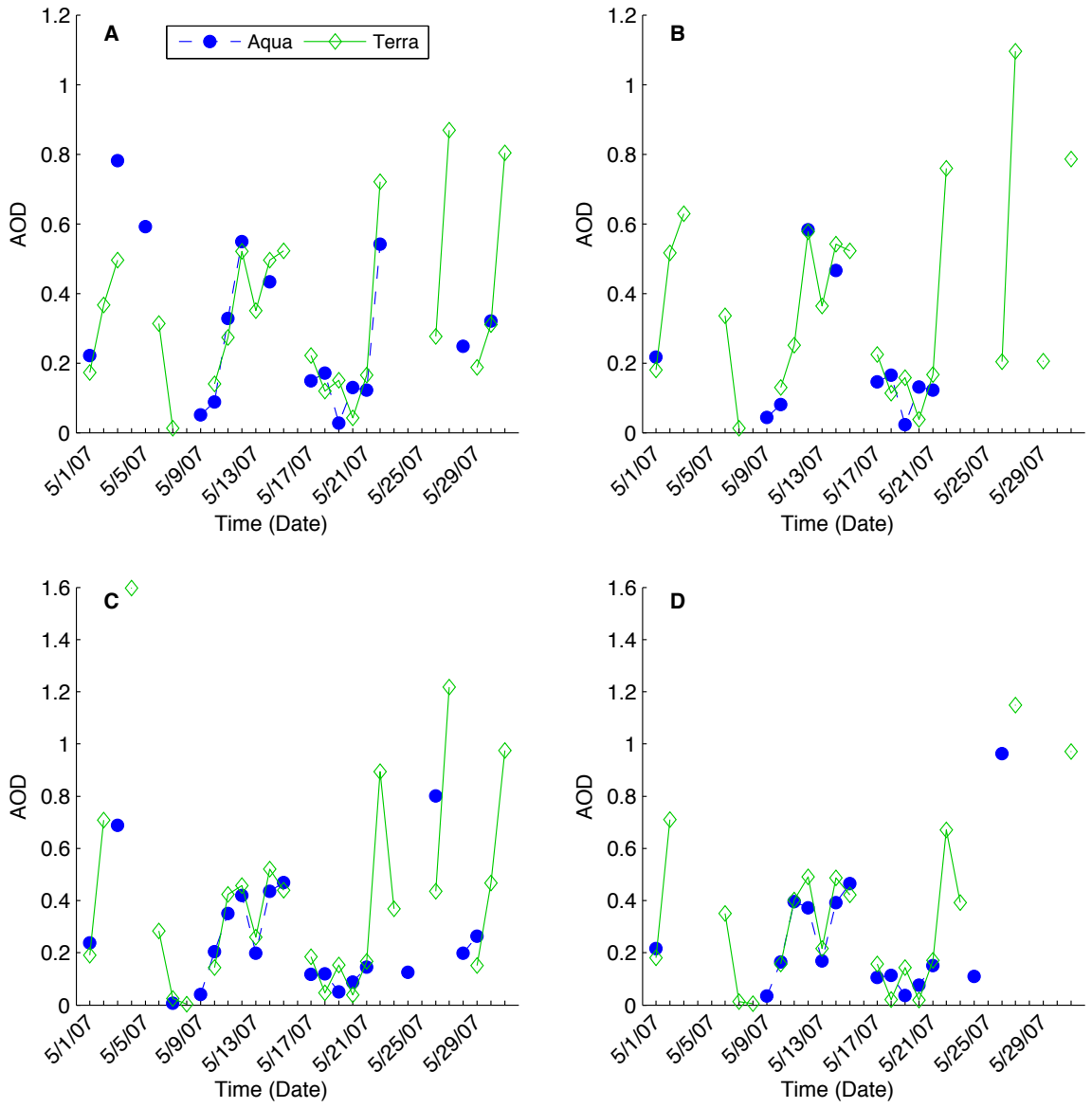

Figure 3.3: Timeseries of MODIS AOD for May 2007 (A) MODIS AOD over McDonough for 0.5° radius, (B) MODIS AOD over McDonough for 0.25° radius, (C) MODIS AOD over Yorkville for 0.5° radius, (D) MODIS AOD over Yorkville for 0.25° radius. Blue squares represent MODIS Aqua and green triangles represent MODIS Terra. Missing data is shown by gaps.

Yet, the high peaks in Figure 3.3 correspond to the peaks (up or down) shown in Figure 3.2, which indicate agreement on the six exceedance days. Figure 3.1 shows how the wildfire causes a heterogeneous response across the stations, and this could potentially explain the differences in correlation values shown in Table 3.1. $PM_{2.5,A}$ and

$PM_{2.5,T}$ are positively correlated with the respective MODIS AODs with statistical significance above 95% for a majority of stations. The correlation coefficients with Terra vary between 0.59 – 0.89, while Aqua has correlations between 0.56 – 0.72. Newnan, which had relatively higher $PM_{2.5}$ concentrations, has the highest correlations for both satellites. In comparison, r-values from the correlation between AODs with smaller (0.25°) search radius and $PM_{2.5}$ are well correlated for both satellites. Regression coefficients are 0.63 - 0.89 (Aqua) and 0.52 – 0.9 (Terra). Our statistical analysis results show a broad range of values, which is not seen in Figure 6 of *Christopher et al.* [2009]. Their correlation analysis only considers four $PM_{2.5}$ stations in Georgia, with possibly three stations from metro Atlanta, and their analysis considered $PM_{2.5}$-24 hour averages. Nevertheless, our study and *Christopher et al.* [2009] both found higher linear correlations with Terra, despite the fact that the PBL dynamics favors the correlation between MODIS Aqua AODs and $PM_{2.5}$ because of the Aqua's afternoon time orbit. In summary, MODIS can provide visual imagery that allows for tracking the smoke plumes and AOD data related to total aerosol loading. However, MODIS provides only two measurements per day, so being able to track the evolution of biomass burning is hindered. Additionally, cloud cover reduces the number of satellite observations. MODIS satellite data could be used most effectively in multi-day events to compensate for the possibility of reduced observations, especially during the spring and summer months when biomass burning and cloudiness are more frequent.

Table 3.1: Correlation values (r-values) and number of coincident observations (#) between $PM_{2.5}$ and MODIS AOD using 0.25° and 0.5° as search radii for MODIS pixels. Numbers in bold are statistically significant at $\alpha = 0.05$.

		Radius = 0.5°				Radius = 0.25°			
Station	Location	r-values		#		r-values		#	
	(Lat, Lon)	Terra	Aqua	Terra	Aqua	Terra	Aqua	Terra	Aqua
Con	(33.81°. -84.38°)	**0.90**	**0.89**	17	9	**0.82**	**0.57**	16	20
Gwi	(33.96°, -84.07°)	**0.81**	**0.63**	17	11	**0.77**	**0.64**	17	20
McD	(33.43°, -84.16°)	**0.85**	**0.82**	17	8	**0.81**	0.52	12	17
New	(33.40°, -84.74°)	**0.89**	**0.70**	16	10	**0.89**	**0.72**	13	18
SDe	(33.68°, -84.29°)	**0.77**	**0.72**	15	6	**0.72**	0.35	11	17
Wal	(33.70°, -83.60°)	**0.52**	**0.82**	17	10	**0.57**	0.26	14	18
Yor	(33.93°, -85.04°)	**0.83**	**0.84**	17	11	**0.59**	**0.56**	13	20

3.3.3 Characterization of Spatial (Horizontal and Vertical) Distribution of Smoke Plumes

3.3.3.1 Biomass Burning Signatures from OMI

In the case of May 2007, smoke aerosols were originating primarily from swamp wildfires. This type of wildfire differs from the seasonally driven biomass burning in other regions such as Africa, Australia, and S. America that were previously studied using OMI or TOMS [*Ahn et al.*, 2008; *Dirksen et al.*, 2009; *Livingston et al.*, 2009]. Nevertheless, our analysis reveals that OMI AI detects swamp smoke reasonably well, allowing us to examine the spatial evolution of the smoke plumes and implications to air quality.

Figure 3.4 shows the dynamics of the wildfire plume viewed through OMI AI for 25-30 May. We show the positive and negative AI values (shown in gray) to represent absorbing and non-absorbing aerosols, respectively. One consistent feature from all the days is an area of high AI located near the central border of GA-FL. The shape of the elevated AI remains oblong and stretches horizontally following the state border. The elevated values of AI ($1.5 < AI < 3.0$) are a persistent feature of the plume transport that remains throughout May 25-30, and near the epicenter AI values > 3.6 are reported. Our results using OMI data to identify the spatial extent of the wildfire aerosols are complementary to the modeling work done by *Christopher et al*. (2009) in terms of the predicted location of the wildfire plume. They use a model driven by estimated fire emissions from the GOES satellite. While Terra AOD didn't capture the plume due to heavy cloud cover, the model predicted the plume extent along the GA-FL border, and our OMI results provide independent verification of the model on May 25. Our results suggest that OMI AI identified plume transport and distinguished between absorbing and non-absorbing aerosols through the use of positive and negative AI.

While we have shown that OMI AI is able to detect aerosols from a swamp wildfire, AI has not proven to be effective at identifying urban pollution in the Atlanta metro area. It is possible that larger industrialized areas with a stronger carbonaceous signal (e.g., Ohio River Valley) might have a stronger signal detectable by OMI. The U.S. southeast is dominated by mostly non- UV absorbing aerosols, which allows for easy detection of transport of wildfire aerosols.

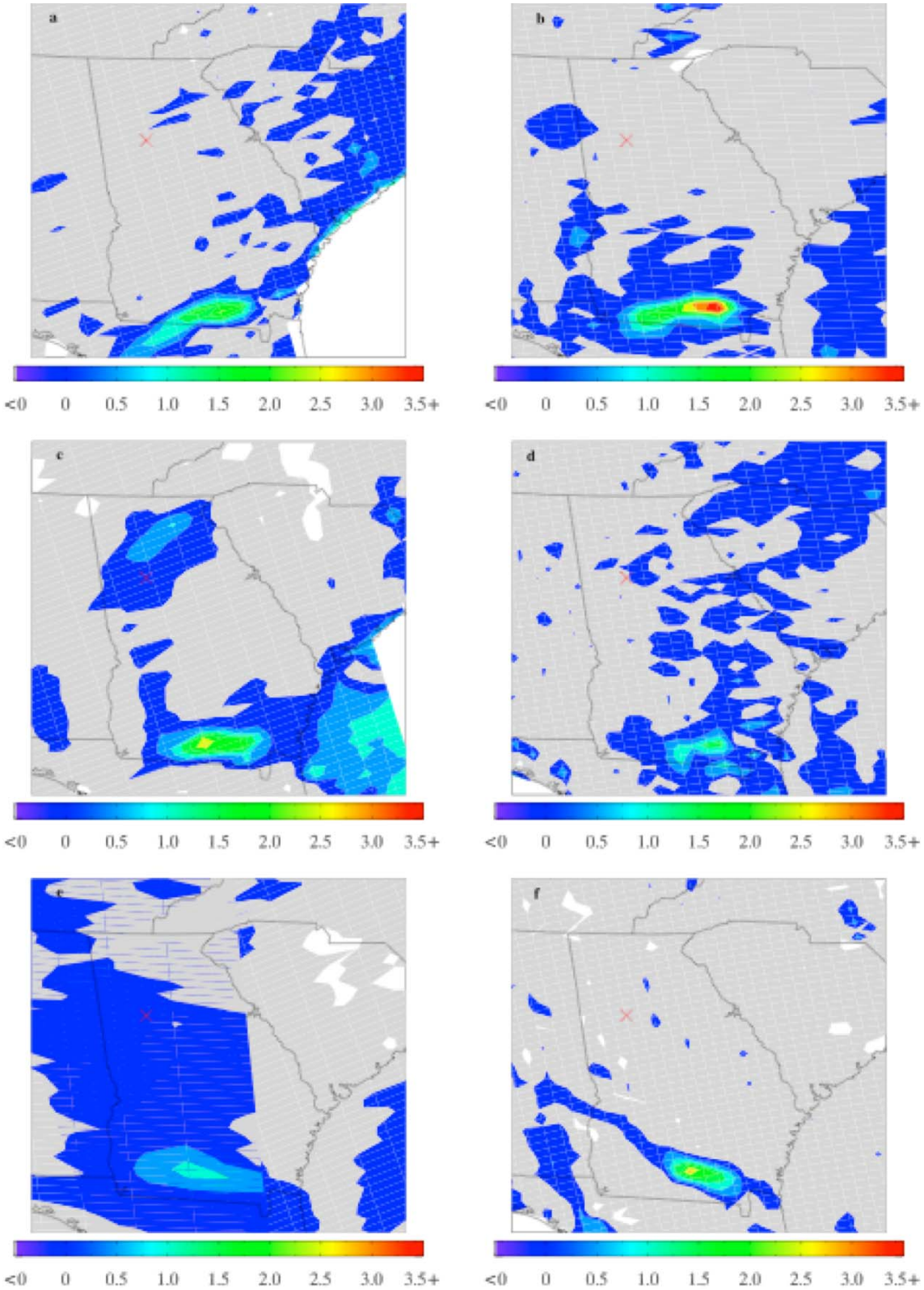

Figure 3.4: OMI AI on consecutive days: (A) May 25, 2007 through (F) May 30, 2007. Negative AI shown in gray. Red X represents Atlanta, GA.

3.3.3.2 Analysis of Aerosol Vertical Profiles Using CALIPSO

CALIPSO had 15 passes over the state of Georgia during May 2007. Eight overpasses were during the day, and seven were during the night. Of the seven night time passes, the two closest to Atlanta were on May 14 and 30, and the two closest to the wildfire were on May 7 and 23. There were overpasses on the exceedance days May 16 and 26, but the passes are not located near metro Atlanta. *Bhoi et al.* [2009] discussed the vertical profiles of the attenuated backscattering coefficient from overpasses near the fire over land (April 30 and May 3) and ocean (May 18). *Christopher et al.* [2009] presented the vertical profiles of the attenuated backscattering coefficient from only one CALIPSO pass near Birmingham, Alabama, on May 24. Neither of the above studies has addressed the vertical feature mask, classification of the aerosol type, and AOD derived from CALIPSO. Examination of these CALIPSO products is important to better understand how CALIPSO data can be used in air quality applications. To that end, here we present a detailed analysis of CALIPSO passes that were closest to Atlanta (May 14) and the wildfire area (May 7). Additionally, we summarize findings from the daytime overpasses on May 5, 10, 12, and 19 to better understand the wildfire's impacts on air quality.

A night time pass has much less noise in the lidar retrievals, making it easier to identify features. In Figure 3.5(A) the red box highlights an area of high backscattering indicative of increased aerosol concentrations observed on May 7 near the wildfire epicenter.

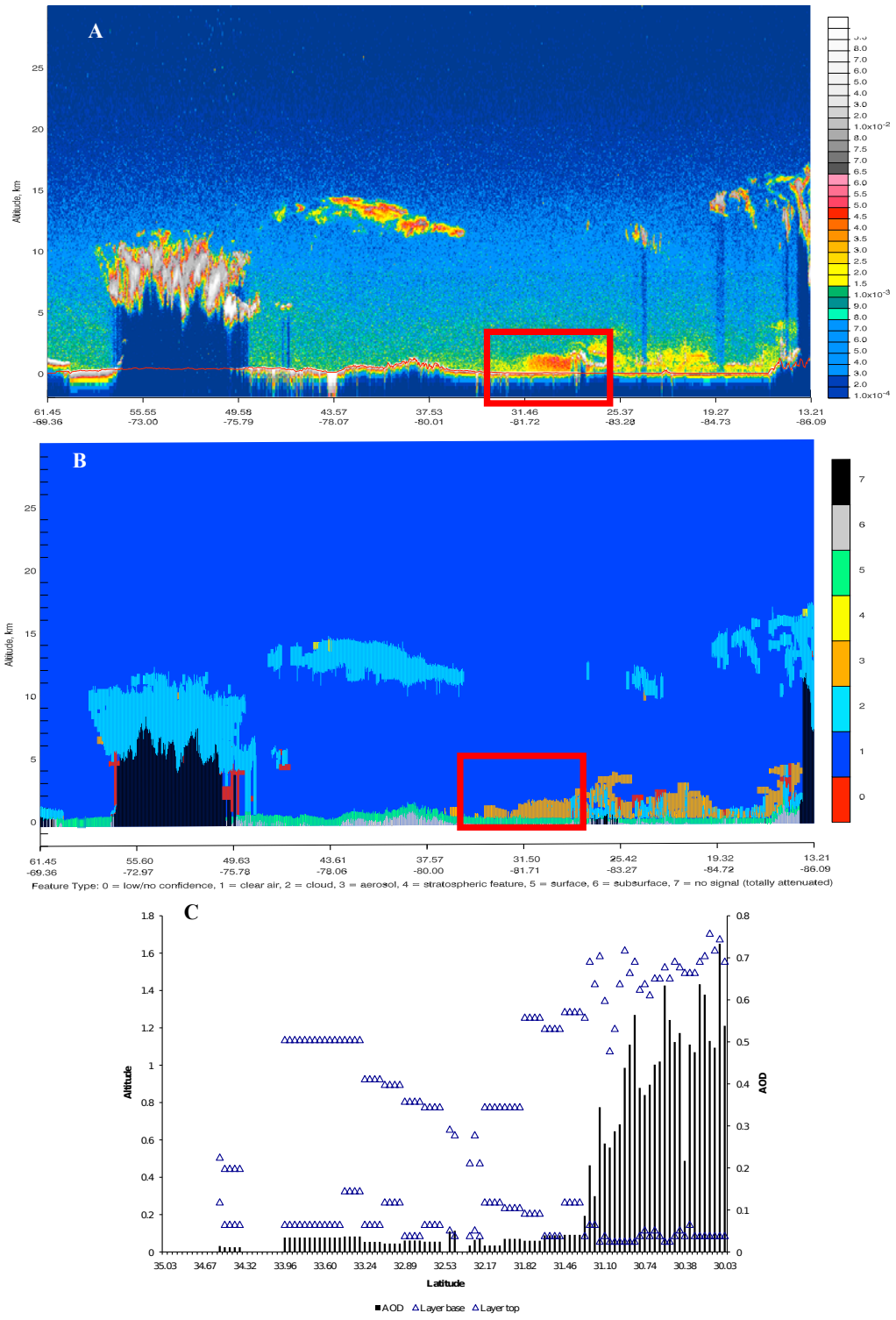

Figure 3.5: CALIPSO nighttime images of May 7, 2007 overpass near fire. (A) Total Backscattering at 532nm, (B) Vertical feature mask, (C) Layer height in blue triangles and AOD in black columns for the CALIPSO pass shown by a red box.

In the vertical feature mask the area highlighted by the red box in Figure 3.5(B) is categorized as aerosol. The aerosols are further analyzed by the CALIOP algorithm to determine their subtype (e.g., biomass burning, polluted continental, dust, etc.). The area highlighted by the boxes in Figure 3.5 is sub-typed as polluted dust and desert dust that is clearly an algorithm error. This misclassification is due to the fact that the depolarization ratio of this aerosol layer is non-zero, and the CALIOP algorithm defaults to the layer being classified as dust because of the well-known fact that non-spherical dust particles cause significant depolarization. This classification error was reported to the CALIPSO science team.

On May 7 the lidar shows the layer being close to the ground and extending to about 1.5 km, which is consistent with a low nocturnal PBL. The optical depth of this layer varies along the ground track from optically thin around 0.01 to optically thick at values above 0.5 (see Figure 3.5(C)). To determine the effect of the aerosol misclassification on AOD, we re-calculated AOD values using the correct lidar ratio for biomass burning aerosol. Resulting AODs increased by almost 50%.

We also examine a night time pass on May14, which tracks through central Georgia near Atlanta. In Figure 3.6(A) the red box shows an area of high backscattering indicative of aerosols that is corroborated by Figure 3.6(C) showing the highlighted areas as aerosols. In this case CALIPSO detects multiple layers. The CALIOP algorithm again misclassifies the lower layer as dust with a second layer being correctly detected as smoke. We believe that all the layers are smoke associated with biomass burning. The AODs along the ground track reach a maximum of 0.6 for the first layer and 1.2 within

the second layer (see Figure 3.6(D)). By correcting the lower level AODs to match with the correct aerosol type, AODs nearly doubled in comparison to the original values.

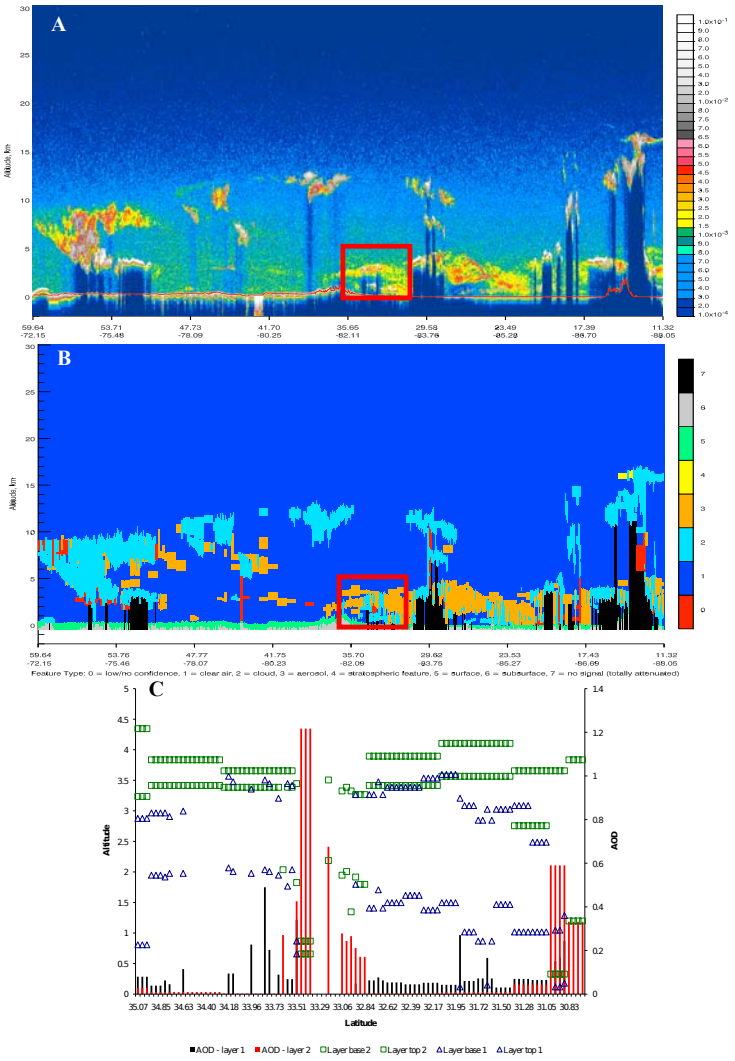

Figure 3.6: Same as Figure 3.5, except for nighttime May 14, 2007 overpass near Atlanta, (C) Two layers are shown with first layer in triangles and second layer in squares; AOD for first layer in red columns and second layer in black columns (for the CALIPSO pass shown by a red box).

The high values of AOD imply that the smoke layer is dense, thick and well developed vertically. The high AODs from CALIPSO are similar to MODIS AOD on exceedance days (e.g., May 26 - 27). Though a recent study by Kittaka that compared column-averaged AOD from CALIPSO with MODIS Aqua found that for the Southeastern U.S.

CALIPSO AOD are biased low in comparison [*Kittaka et al.*, 2011]. We agree with the authors in that CALIPSO's uncertainty in selecting the appropriate lidar ratio, which affects the aerosol subtyping and AOD, could be a potential source of the bias. The smoke layer extends from just above the surface to 4.5 km. The height of the smoke layer indicates that the plume has been lifted aloft and within the region of the atmosphere where aerosol transport takes place. *Bhoi et al.* [2009] report vertical height of the plume to vary between 2.5 km over land and 4 km over ocean. Christopher et al. (2009) identify wildfire aerosols located 2 – 3 km above the surface. The combination of these results points to the wildfire plume being quite variable throughout May 2007.

We analyzed daytime CALIPSO overpasses to understand the implications to air quality. We present the dates of May 5, 10, 12, 19 2007 as examples, see Figure 3.7. The other daytime overpasses (May 21, 26 and 28) repeat the ground-tracks for the dates previously mentioned e.g. May 5, 10, 12. Atmospheric boundary layer dynamics is a major controlling factor in surface concentrations. On all four dates, CALIPSO identified a well developed smoke layer, with the layer thickness of about 1 km, Figure 3.7(A-D). In some instances, there are two aerosol layers identified. Another consistent feature is that for the month of May, the daytime aerosol layer over Georgia is around 0.5 – 2 km in height. Afternoon boundary layer heights during this same time period vary between 2.5 – 3 km. This implies that the nighttime inversion likely traps the smoke aerosols close to the surface.

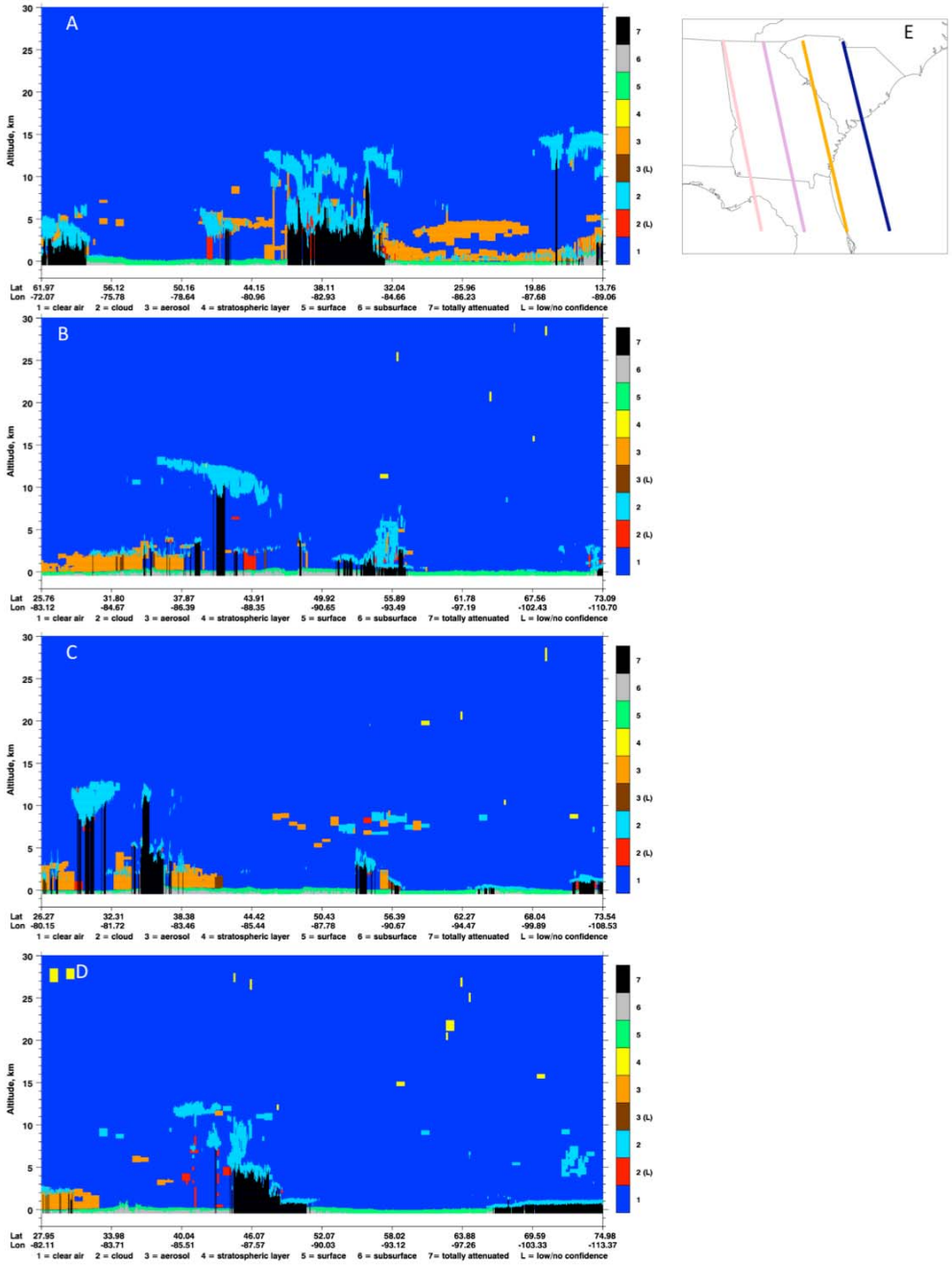

Figure 3.7: CALIPSO Vertical feature masks of daytime overpasses (A) May 5, 2007, (B) May 10, 2007, (C) May 12, 2007, (D) May 19, 2007, (E) CALIPSO satellite overpass tracks (pink) May 10, 2007, (purple) May 19, 2007, (orange) May 12, 2007, (navy) May 5, 2007 (E) Geographic representation of daytime overpasses shown in A-D.

This could explain why most exceedances occur in the early morning hours. Analyses of the nighttime overpasses yield different results. A majority of nighttime overpasses show

two layers where one layer is closer to the ground (similar to Figure 3.7), and the other (higher) layer is located around 3 – 4 km. In summary, CALIPSO adds valuable information about the vertical profile of aerosols. In relation to air quality studies, we have shown that CALIPSO is capable of detecting boundary layer aerosols, but that the capability is tempered by the longer overpass repeat cycle of 16 days and distance between overpasses.

3.3.3.3 Integrated Event Analysis

In the following analysis we explore the complementary nature of multiple sensor data focusing on May 22 and 31. These two cases were chosen because these days reached very high $PM_{2.5}$ concentrations and had the most amounts of data available from satellite and ground-based monitors. We use ground-based, satellite data and back trajectory analyses [*Draxler*, 2006] from HYSPLIT to provide understanding of the evolution of air quality in metro Atlanta from a local, state, and regional perspective. Unfortunately, CALIPSO due to its repeat cycle was unable to provide data near Atlanta during any of the six exceedance events.

Event – May 22, 2007

The majority of the southeastern U.S. was dominated by a large high pressure system that was centered over Georgia throughout May 20-21. This system moved off the GA-SC coast bringing southeasterly flow to the metro Atlanta area. By 8 AM, a majority of sites, except the eastern most of Walton, had reached exceedance levels (see Figure 3.1(C)). The high pressure system provided cloud-free conditions across Georgia. When MODIS Terra flew over the southeast U.S. at 16:10 GMT (11:10 AM EST), all sites

reported $PM_{2.5}$ concentrations above 50 μg/m^3. The two biomass burning aerosol plumes are clearly seen in the MODIS Terra true color images (Figure 3.8(A)), with one located over the Georgia-Alabama border and another one in central Georgia. Accordingly, retrieved AODs across the stations were above 0.8, with the exception of Walton. In the plume over central Georgia, AOD values > 1 were over the urban stations Confederate Ave., Gwinnett and South Dekalb (Figure 3.8(C)). Some monitors stopped reporting data causing gaps in the timeseries shown in Figure 3.1(C). The remaining three rural sites recorded maximum concentrations between 50 -100 μg/m^3, whereas the urban and suburban sites reported maximum concentrations of 100 – 225 μg/m^3. By early afternoon, convective processes along with southeasterly winds lowered the ground level $PM_{2.5}$ concentrations. A visible image from MODIS Aqua shows more cloud cover, yet the plume over central Georgia is still visible (Figure 3.8(B)). Aqua AOD of 0.3 over all Atlanta is lower than the reported Terra AOD (Figure 3.8(D)). Figure 3.8(E) shows an area of absorbing aerosols where AI > 3 located just west of the wildfire epicenter. Also, back trajectory analysis from HYSPLIT (Figure 3.8(F)) depicts descending parcels of air arriving in the Atlanta metro area having originated in the southeastern part of the state in the vicinity of the wildfires. The HYSPLIT analysis supports that the plumes shown in both MODIS Aqua and Terra RGB images are associated with transported biomass burning aerosol.

The elevated levels of aerosols that caused poor air quality in Atlanta moved further west (downwind) impacting Alabama and Mississippi on May 23–25. *Christopher et al.* (2009) attribute the poor air quality event to a decrease of PBL height that allowed the sinking of smoke aerosols mixing that degraded air quality near the surface. Our

analysis of surface weather maps, show that during May 23- 25, another high pressure system is located of the mid-Atlantic coast. As time progresses to late on 24 May, the system has shifted further south in the Atlantic pushing the area of increasing wind speeds towards the west and southwest. Thus, the entire period of May 22 – 25 could be seen as one event with impacts in multiple urban areas downwind of the wildfire.

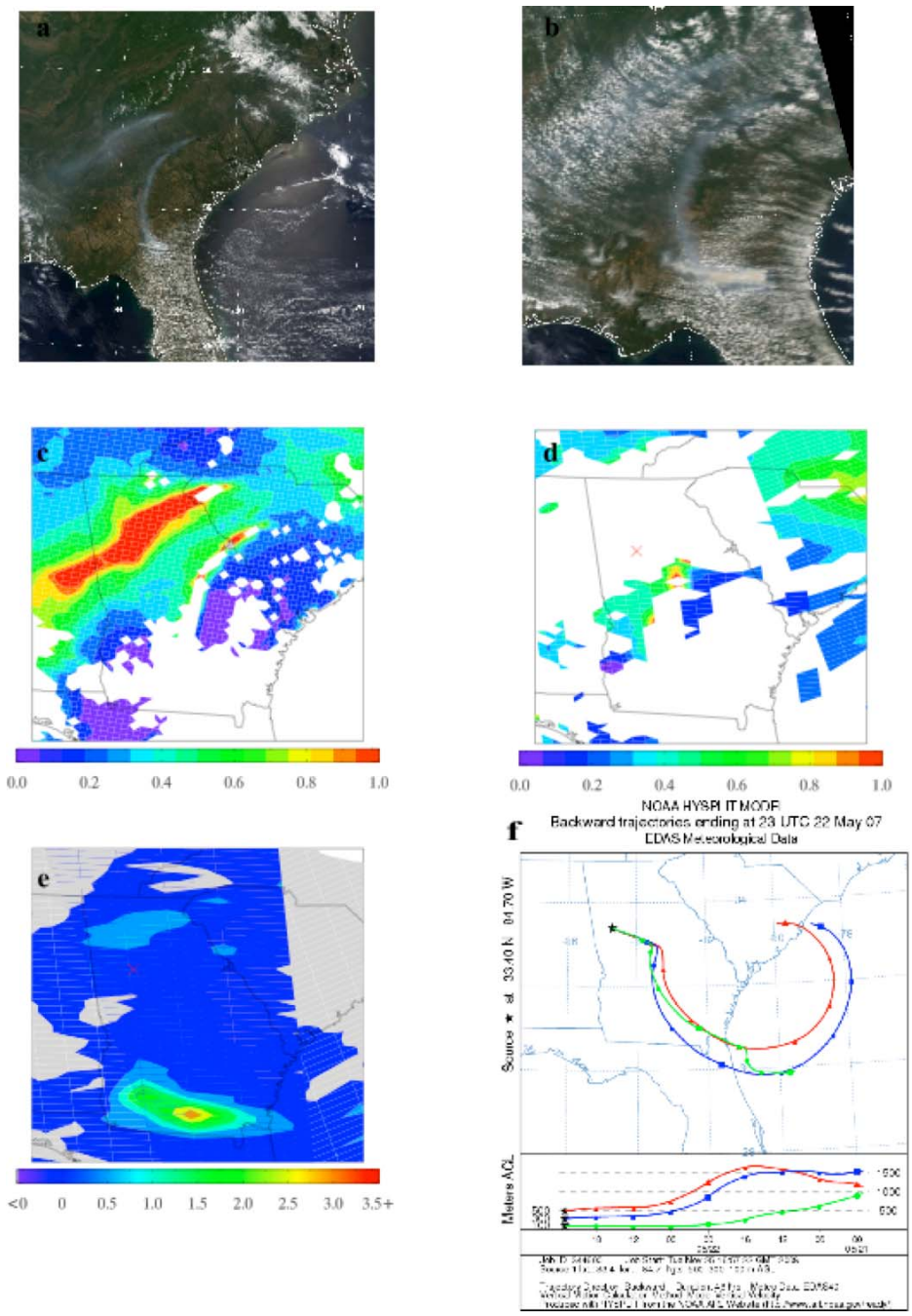

Figure 3.8: Multiple satellite perspectives on May 22, 2007: (A) MODIS Terra RGB image, (B) MODIS Aqua RGB, (C) MODIS Terra AOD, (D) MODIS Aqua AOD, (E) OMI AI, (F) HYSPLIT backtrajectory. Red X represents Atlanta, GA.

Event –May 31, 2007

The synoptic dynamics on this day was similar to that of 22 May. The region was again controlled by a high pressure system. The $PM_{2.5}$ concentrations appear to rise

across the area in an eastward progression. Beginning around 4 AM, the western-most stations of Newnan and Yorkville record elevated $PM_{2.5}$ concentrations, breeching exceedance levels within the next hour (Figure 3.1(F). All stations surpass exceedance levels by 10 AM. Back trajectories (not shown) confirm that air in the metro area transects the area on the wildfire, thus bringing increased levels of PM to Atlanta. The trajectories on May 31 appear very similar to the trajectories on May 22 shown in Figure 3.9. A difference from May 22 is that the highest exceedances are at rural stations. By 11 AM, Newnan, Walton, and Yorkville have concentrations very close to double that of the urban stations (see Figure 3.1(F)). Furthermore, all the rural stations record maxima for the day above 100 $\mu g/m^3$, whereas the urban stations have maxima between 74 – 83 $\mu g/m^3$. Visible images from MODIS Terra (Figure 3.9(A)) and Aqua (Figure 3.9(B)) show what appears to be haze associated with the wildfire below higher-level clouds. The amount of cloud cover does not inhibit MODIS Terra from retrieving AOD over the Atlanta area, but retrievals for the remainder of the state are sparse. AODs for the area are greater than 0.78 (Figure 3.9(C)). Unfortunately, MODIS Aqua is unable to make any AOD retrievals for southern Georgia due to the large amount of clouds (Figure 3.9(D)). Despite the cloud cover, OMI AI is able to detect elevated amounts of absorbing aerosols slightly west - northwest of the wildfire epicenter (Figure 3.9(E)). In comparison to May 22, the area of highest AI values is located entirely within central Georgia. This could explain why the southernmost stations experienced elevated $PM_{2.5}$ concentrations before the rest of the metro Atlanta area. The map of $PM_{2.5}$ across the U.S. shows elevated concentrations in the states east of the Mississippi River with the highest concentrations in the metro Atlanta area (Figure 3.9(F)). Afternoon vertical mixing lowers

concentrations throughout the area; however, the concentrations remain above exceedance level until the early hours of June 1.

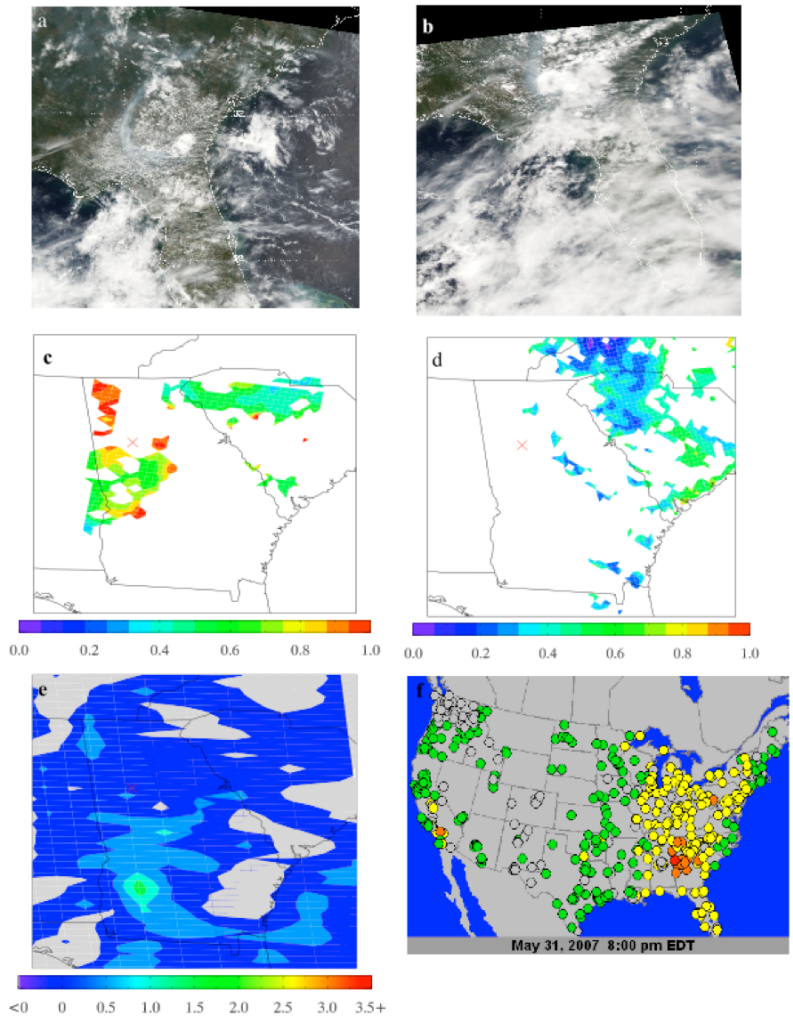

Figure 3.9: Multiple satellite perspectives on May 31, 2007: (A) MODIS Terra RGB image, (B) MODIS Aqua RBG image, (C) MODIS Terra AOD, (D) MODIS Aqua AOD, (E) OMI AI, (F) $PM_{2.5}$ map of SE U. S. from www.airnow.gov. Red X represents Atlanta, GA.

3.4 Discussion

The techniques showcased earlier in this manuscript, reflect a methodology that can be used in other wildfires. In late April 2011, a lighting strike occurred within the Okefenokee Swamp National Wildlife Refuge, which started a wildfire named the Honey Prairie Complex Fire. In July 2011, another fire started just north of the wildfire refuge, and its name is the Sweat Farm Again Fire. This fire is occurring in nearly the same location as the fire studied earlier in this manuscript, and this new fire allows for direct comparison with the fire of 2007. As of September 19, 2011 the fire complex (Honey Prairie and Sweat Farm Again) has consumed over 320,000 acres. During peak burn periods, the extent of the drought in 2011 is more severe (exceptional drought) across more of the state than in 2007 (http://droughtmonitor.unl.edu/monitor.html).

The two fires' impacts on aerosol concentration as measured by MODIS AOD are show in Figure 3.10. Unlike the 2007, the 2011 fire has a much longer burn period, which has extended further into the summer months. To better highlight the direct aerosol contribution of the wildfire these timeseries are area averaged in a 4° x 4° box centered over the wildfire refuge, and for comparison a non-fire year (2009) was added. Both wildfire years show increased aerosol concentrations with the 2011 fire having 15 days where MODIS Terra AOD > 0.5. Though it should be noted that the 2007 wildfire had more days of high MODIS Terra AOD (AOD >0.7) compared to the 2011 wildfire (2 days). This is not a surprising finding, in that the 2007 wildfire was shorter in duration, but consumed more acreage.

In comparing the 2011 wildfire to a non-fire year (2009) there are some appreciable differences. Monthly averages of MODIS Terra AOD covering May – July

are higher in 2011 than in 2009. The monthly averages for May 2009 = 0.2071, May 2011 = 0.2496; June 2009 = 0.3067, June 2011 = 0.3955; July 2009 = 0.2552, July 2011 = 0.3237. Not surprisingly the standard deviation of MODIS Terra AOD are higher in 2011 (May = 0.1207, June = 0.1913, July = 0.1938) than in 2009 (May = 0.0736, June = 0.1285, July = 0.0817).

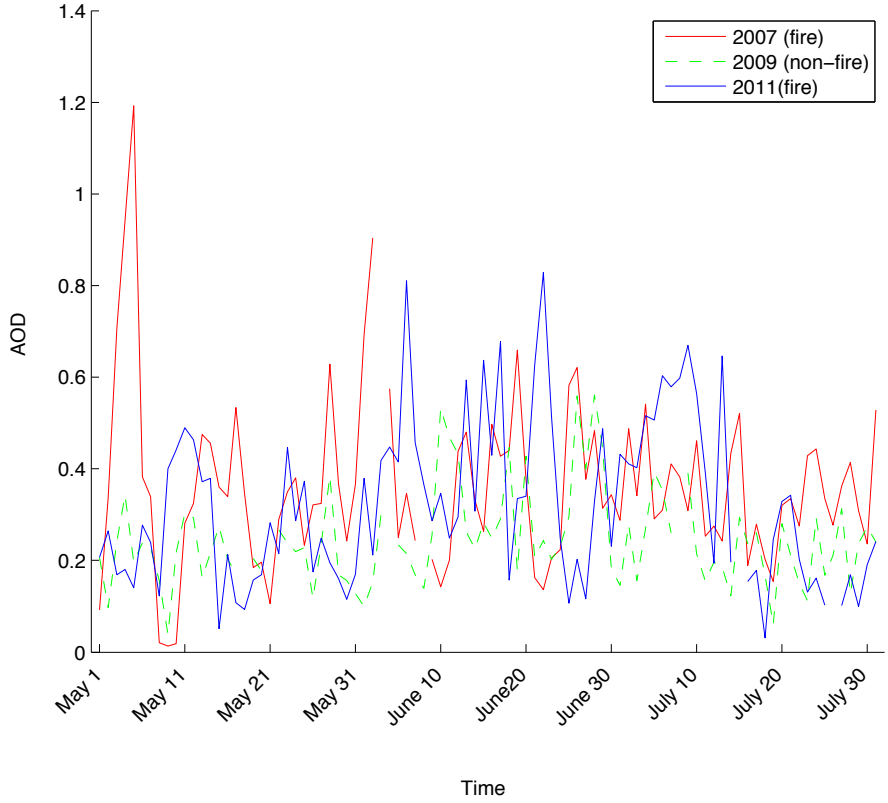

Figure 3.10: Timeseries of MODIS Terra AOD for May – July 2007, 2009 and 2011.

An analysis using OMI AI would be fitting for this discussion; however, the OMI sensor was experiencing row anomalies that affect the Level 1B and Level 2 data products, which lead to either no retrievals being made or erroneous retrievals at the edges of those row anomalies within the scan. Thus a timeseries comparison is not appropriate, yet there are a number of days where AI > 0.5 which suggests the presences

of absorbing aerosols. On June 6th, AI = 0.99 which coincides with an elevated MODIS AOD value of about 0.79. Savannah, GA, which is less than 180 miles away from the refuge, experienced an air quality exceedance on this day. Also, between June 21-22nd there were elevated AOD values (0.623 and 0.828 respectively) which coincided with an high OMI AI value of 1.36 taken on June 21st, see Figure 3.10. During this time span most of the smoke was blown offshore as shown in the visible image from MODIS Terra, see Figure 3.11. MODIS Aqua also measured increased AOD, but it should be noted that the elevated AOD retrievals occur mostly over water. No cities in GA had air quality exceedances during this time range, but Jacksonville, FL, which is less than 75 miles away from the refuge experienced air quality exceedances.

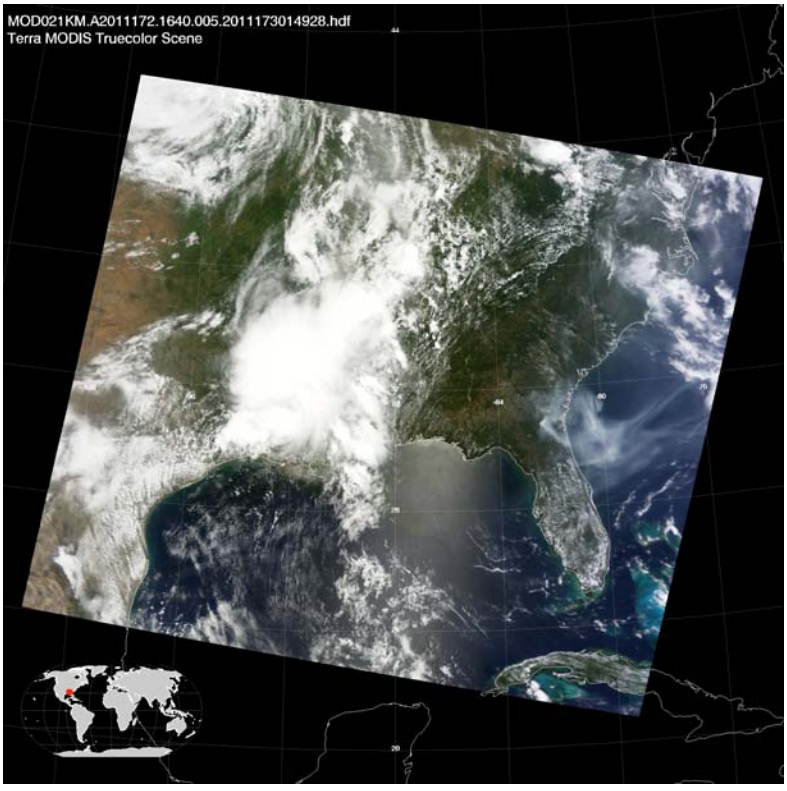

Figure 3.11: Visible image from MODIS Terra on June, 21 2011.

Unfortunately, there is little to be gained by CALIPSO. Though the fire was longer in duration, the space-borne lidar did not detect any wildfire signatures over this region. On the days where AOD was highest, there were not any overpasses nearby, thus a missed opportunity for a multi-sensor analysis. It would have been beneficial to determine if the CALIPSO science team had indeed corrected the problems mentioned earlier in the results section e.g. incorrect lidar ratio.

From 2003 until 2007 the metro Atlanta area never had a TEOM-measured air quality exceedance. One could hypothesize that in a warming climate; the number of wildfires in the U. S. southeast could increase thus resulting in more poor air quality events. Potentially a warmer climate could lead to more severe droughts that are larger in size, severity and duration. Though wildfires are an integral part of the swamp/bog ecosystem, the impacts from fires like this are increased as more people move towards the coasts in U.S. This research has shown a robust methodology that provides insights into peat-based wildfires and their remotely sensed signatures. Yet, if anything, our research has shown that studying wildfire impacts from satellites require a person to understand the capabilities and limitations of satellite data. In cases where the satellite data has missing retrievals due to cloud contamination or the inability to separate aerosol and cloud effects, maybe interpolation schemes can be used to fill-in the missing data. Ultimately a person must decide based on the available data provided what is a wildfire effect.

3.5 Chapter Summary

The goal of this study was to examine multiple-satellite data as a tool for understanding biomass burning impacts on an urban area, focusing on the specifics of

swamp wildfires and their impact on the Atlanta metropolitan area. In May 2007, the wildfire caused six exceedance days where smoke aerosols pushed ambient concentrations of $PM_{2.5}$ to extremely high levels (> 100 $\mu g/m^{-3}$), producing a visible haze layer on some days and causing degradation in air quality. We have shown that MODIS AODs were able to characterize the dynamics of surface $PM_{2.5}$ over the Atlanta metro area. The urban $PM_{2.5}$ stations correlated well with MODIS Terra, while MODIS Aqua AODs have somewhat lower r-values for all of the $PM_{2.5}$ stations. By using a smaller radius (0.25°), r-values for both satellites increased for most stations. Correlation values for Terra using the smaller radius varied between 0.52 – 0.9, and Aqua had r-values of 0.63 – 0.89. The range of correlation coefficients underscores the variability seen across all the stations and highlights potential biases in selecting which stations to correlate with AOD. To compensate for this, the use of as many stations as possible could be beneficial.

OMI measured AI values greater than three near the vicinity of the wildfire epicenter. OMI AI also provided satellite verification of model-predicted AODs reported by *Christopher et al*. [2009] when MODIS AODs were not available. Our CALIPSO analysis found that the wildfire plume was dynamic. A thick layer of smoke near the surface was persistent throughout the study period; however, our analysis presented evidence of a smoke layer aloft where it could be advected to other areas. When studied sequentially, we found that the plume height varied from around 1.5 km near the fire to 3 – 4.5 km further downwind from the fire.

Our analysis has shown that CALIPSO is adept at identification and classification of aerosol layers; however, the current (Version 2) algorithm does not always correctly identify the type of aerosol. In our case, there was a persistent misclassification of smoke

as polluted dust that resulted in lower AOD values. A strength of CALIPSO data is the ability to discriminate between elevated aerosol loads within the PBL (e.g., in the case of May 7) and those aloft (May 14). Aerosols within the PBL most affect air quality locally, while those aloft may affect air quality downwind later in time. This vertical distribution, especially in the case of wildfires, provides valuable information for constraining air quality models. However, the narrow lidar footprint results in infrequent coincident observations with ground sites so the relationship between ground $PM_{2.5}$ and CALIPSO-derived AOD seems to be of limited use.

Large urban areas have poor air quality due to local sources and/or the transport of aerosols into the local air shed. While we have quantified the effects of biomass burning in metro Atlanta, additional research is needed to understand the extent to which fires can impact air quality in other large metropolitan areas. Multi-satellite data can be used to aid in understanding biomass burning impacts on a large urban area's air quality, especially in causal determination of poor air quality episodes which can be important to local and state environmental managers.

CHAPTER 4

ANALYSES OF SEASONAL AND INTERANNUAL VARIABILITY OF ATMOSPHERIC AEROSOLS IN THE U. S. SOUTHEAST FROM GROUND AND SPACE BASED MEASUREMENTS OVER THE PAST DECADE

The work presented in this chapter has been published in Atmospheric Measurement Techniques Discussions [Alston et al., 2011b].

4.1 Introduction

As mentioned in the Introduction, solar dimming relates to increases in aerosol concentration that prevent incoming solar radiation from reaching the surface, while solar brightening refers to decreases in aerosol concentration that results in increased surface solar radiation. *Dutton et al.* [2006] analyzed twenty seven years of NOAA/GMD surface solar irradiance data from five remote sites and concluded that while the sites span a large geographic area, the behavior of surface solar irradiance was similar (decreasing then increasing with time) across the sites. *Wild et al.* [2009] provide updates of surface radiation measurements through 2005 and present evidence that brightening across large areas is ongoing and that anthropogenic contributions are an important factor in this phenomena. *Streets et al.* [2009] use model-predicted aerosol optical depth (AOD) to determine the regional nature of solar dimming/brightening. Their results indicate that the U.S., Europe and Russia have decreasing AOD values over a twenty-five year (1980 – 2005) period, and these regions also have a strong linear relationship between AOD and surface radiation.

Ground based measurements of aerosols can provide high temporal concentration data over an extended period of time, yet these measurements are generally limited in their geographic coverage. A majority of ground based measurement sites are mostly in areas with high population densities. Additionally, ground based measurements are at best representative of aerosols in the lower atmosphere, mainly in the planetary boundary layer (PBL); as such, these measurements miss aerosols aloft, especially transport events.

Satellites provide atmospheric column measurements that are ideally representative in a well-mixed PBL and have regional viewing perspectives; however, satellite retrievals of aerosols are associated with a number of problems, especially over land such as deserts or urban environments. *Liu and Mishchenko* [2008] found that MODIS and MISR retrievals can disagree on a regional basis; yet, *Kahn et al*. [2009; 2011] attempt to disprove those findings in concluding that MISR (Multi-angle Imaging Spectroradiometer) and MODIS retrievals are in agreement and provide details on the causes of the discrepancies between the two. Given the regional nature of aerosols and inherent difficulties and limitations in both satellite and ground based observations, it is important to utilize multiple sensors in aerosol analysis in order to develop as accurate understanding of aerosol behavior as possible.

The goal of this study is to characterize aerosols in the U.S. Southeast through analysis of ground and space based measurements from 2000 – 2009, with the emphasis on seasonal and interannual aerosol variations. The specific objectives are to examine the temporal changes of ground based $PM_{2.5}$ and AODs from MODIS and MISR over the past ten years, determine common features and differences between these data records, determine if there is a discernible trend, and if a trend is present, what are the

implications of such for the region in the context of the dimming/brightening phenomena. We analyzed ten years of AOD from MODIS and MISR onboard Terra and eight years for MODIS onboard Aqua over a 5° x 5° box that encompasses the state of Georgia. This analysis also uses ten years of filter-based $PM_{2.5}$ data provided by the EPA, and all available data from Georgia-run continuous $PM_{2.5}$ monitors. This paper is organized as follows. Section 4.2 Introduces the data and methods used in this study. Section 4.3 presents the results, and Section 4.4 concludes with a summary and discussion.

4.2 Data and Methodology

4.2.1 Ground Based $PM_{2.5}$ data

As mentioned in Section 2.2.1, we use two different surface $PM_{2.5}$ measurements: continuous from TEOMs and filter-based from the EPA. We have already discussed the $PM_{2.5,TEOM}$ dataset in Section 2.2.1. The filter-based data set is provided by the EPA Air Quality Monitoring System (http://www.epa.gov/airexplorer/index.htm). The data from this network are used for air quality regulatory purposes, e.g. attainment/non-attainment designations. Each monitor uses EPA-defined reference methods described in 40 CFR Part 53 (http://ecfr.gpoaccess.gov/cgi/t/text/textidx?c=ecfr&tpl=/ecfrbrowse /Title40/40cfr53_main_02.tpl), and they must meet high quality control measures. Due to high level of quality control, there is usually a time lag from the measurement, the analysis, and finally making the data publically available. Each station serves a different purpose; as such there are different repeat cycles. Population exposure monitors have daily concentrations; while the majority of sites have a 3-day repeat cycle. Monitors that capture background conditions have a 6-day repeat cycle. Similar to our methodology for

the $PM_{2.5,TEOM}$ dataset, we only use EPA sites completely within Georgia state lines, subsequently we use data from 29 sites in total for both types of monitors. This dataset will be annotated as $PM_{2.5,FRM}$. Over half of the $PM_{2.5,FRM}$ stations have data that encompass 2000–2009, and the $PM_{2.5,FRM}$ station locations are shown in Figure 2.1. To separate out Atlanta's influence from the remainder of the state, we split each $PM_{2.5}$ dataset into subsets depending on the geographical location of the considered sites. Ultimately, we have three subsets for each $PM_{2.5}$ dataset. We calculate a statewide mean for the *All GA* subset. The *Atlanta* subset is the mean exclusively using Atlanta sites. The last subset *Outside Atlanta* uses sites outside Atlanta for the calculated mean. For the $PM_{2.5,TEOM}$ datasets, hourly means are averaged to create daily means. Those daily means are then used in subsequent analyses. Given the repeat cycle associated with the $PM_{2.5,FRM}$ dataset, fill values were used to fill-in the gaps in the data record where measurements were not taken. Those complete timeseries were used in subsequent analyses.

4.2.2 Satellite Data

4.2.2.1 MODIS Data

The analysis is performed with MODIS Collection 5 Level 2 data, which have a nominal resolution of 10x10 km^2 at nadir. The variable of most importance to this study is "Optical_Depth_Land_and_Ocean" at the 550 nm wavelength which incorporates only the highest quality retrievals. We use daily AOD data from 2000 - 2009.

4.2.2.2 MISR Data

The Multi-angle Imaging SpectroRadiometer (MISR) flies onboard of the Terra satellite together with MODIS. MISR is a multi-angle imaging instrument consisting of nine cameras with view angles of ±70.5°, ±60.0°, ±45.6°, ±26.1°, and 0° (nadir), operating in four spectral bands centered at 446 nm (blue), 558 nm (green), 672 nm (red), and 867 nm (near infrared). In global observing mode, the spatial resolution of the red band is 275 m in all nine cameras, the other bands are re-sampled to 1.1 km resolution in all the cameras, except the nadir, which preserves the full 275 m resolution in all four bands. The common swath width is ~400 km and global coverage is obtained every nine days at the equator and more frequently at higher latitudes [*Diner et al.*, 2002]. MISR operational aerosol retrievals are performed at 17.6 km horizontal resolution, and particle size, shape, and single-scattering albedo are retrieved in addition to aerosol optical depth (AOD) [*Martonchik et al.*, 2002; *Martonchik et al.*, 2009]. A global comparison of coincident MISR and AERONET sunphotometer data showed that overall about 70% to 75% of MISR AOD retrievals fall within 0.05 or 20% of AOD, and about 50% to 55% are within 0.03 or 10% of AOD, except at sites where dust or mixed dust and smoke are commonly found [*Kahn et al.*, 2010]. MISR data were obtained from NASA Langley ASDC (Atmospheric Science Data Center). The analysis is performed with MISR version 22 Level 2 aerosol data. The used AOD values are "best estimate AOD" at MISR green (558 nm) band that combines the land and ocean AOD products.

For each satellite, we create a subset based on the latitude/longitude box 30°N – 35°N and 80°W - 85°W. All the satellite pixels contained within that latitude/longitude box are averaged together to create a regional mean AOD value on a daily basis for each satellite sensor. The daily mean AOD values are used in the subsequent analyses. For spatial

analysis the nominal Level 2 products are used to create maps of AOD from both Terra instruments. The daily granules are averaged on a global grid (0.25° x 0.25° for MODIS and 0.2° x 0.2° for MISR). These grids are then averaged to create seasonal means of AOD fields for the ten year time period covering the aforementioned latitude/longitude box.

4.3 Results

4.3.1 Seasonal Cycle

Where available, we analyzed 10 years of $PM_{2.5,TEOM}$, $PM_{2.5,FRM}$, and AOD data from MODIS Terra and Aqua, and MISR Terra to investigate the seasonal aerosol signatures over the U.S. Southeast. Considering only spring and summer seasons in our previous study [*Alston et al.*, 2011a] we found that $PM_{2.5}$ and AOD have different seasonal traits with AOD values almost doubling during the summer compared to values in the spring. Here we calculated 10-yr (if available) averages of each month for both the satellite and $PM_{2.5}$ datasets. The results are shown in Figure 4.1. In analyzing a full calendar year instead of just spring and summer, here we determine that summer (June – August) AOD (0.32 – 0.35) is almost tripled from wintertime (December – February) AOD (0.08 – 0.1). MODIS Terra has the highest average AOD. Generally speaking, both Terra sensors (MODIS and MISR) have higher AOD than MODIS Aqua. During the summer months the difference between the MODIS AOD sensors and MISR AOD is about 0.1. While the difference between the MODIS AOD sensors at its highest is about 0.025. The noted 3x increase cannot be fully attributable to $PM_{2.5}$ increases over the same period. The different $PM_{2.5}$ datasets behave differently, with $PM_{2.5,TEOM}$ doubling concentrations

during the summer whereas $PM_{2.5,FRM}$ shows only a modest increase over the same period (~10.0 μg/m^3 during the winter to ~18.0 μg/m^3 during the summer). It is possible that some of the differences seen between the datasets are that the $PM_{2.5,TEOM}$ dataset only has 7 years of data compared with 10 years of the EPA dataset. Another possibility could be due to the differences in measurement techniques used. The standard error (standard deviation/number of observations) of the means of both datasets show more variability during the warmer months, see Figure 4.2.

Timeseries of monthly mean data for each year are shown in Figure 4.2. The winter months have the lowest values of AOD and $PM_{2.5}$, while the summer months have the highest. Specifically, July and August have the highest AOD values with maximums over the years varying between 0.5 – 1.5, with January and December having the lowest values between 0.2 – 0.55. MODIS Aqua has a much tighter AOD envelope with wintertime AOD values between 0.05-0.08 and summertime AOD values between 2.5 – 0.5. The year 2007 has anomalously high values in all the datasets. For a majority of the year, the satellite datasets have small amounts of interannual seasonal variability, with the highest amounts of interannual variability occurring in the summer.

The $PM_{2.5}$ datasets have more interannual variability than the satellite datasets. By breaking the $PM_{2.5}$ datasets into different geographic regions allows us to evaluate the effect of the large urban area of Atlanta on the region as a whole. Atlanta concentrations from both $PM_{2.5,TEOM}$ and $PM_{2.5,FRM}$ have more variability throughout the year when compared to stations outside the Atlanta metropolitan area, see Figure 4.3 and Figure 4.4. Our results suggest that during the summer there is a complex dynamic relationship between regional background $PM_{2.5}$ concentrations and anthropogenic emissions that lead

to Atlanta having a 50% or more increase in surface concentrations that are not observed elsewhere in the state.

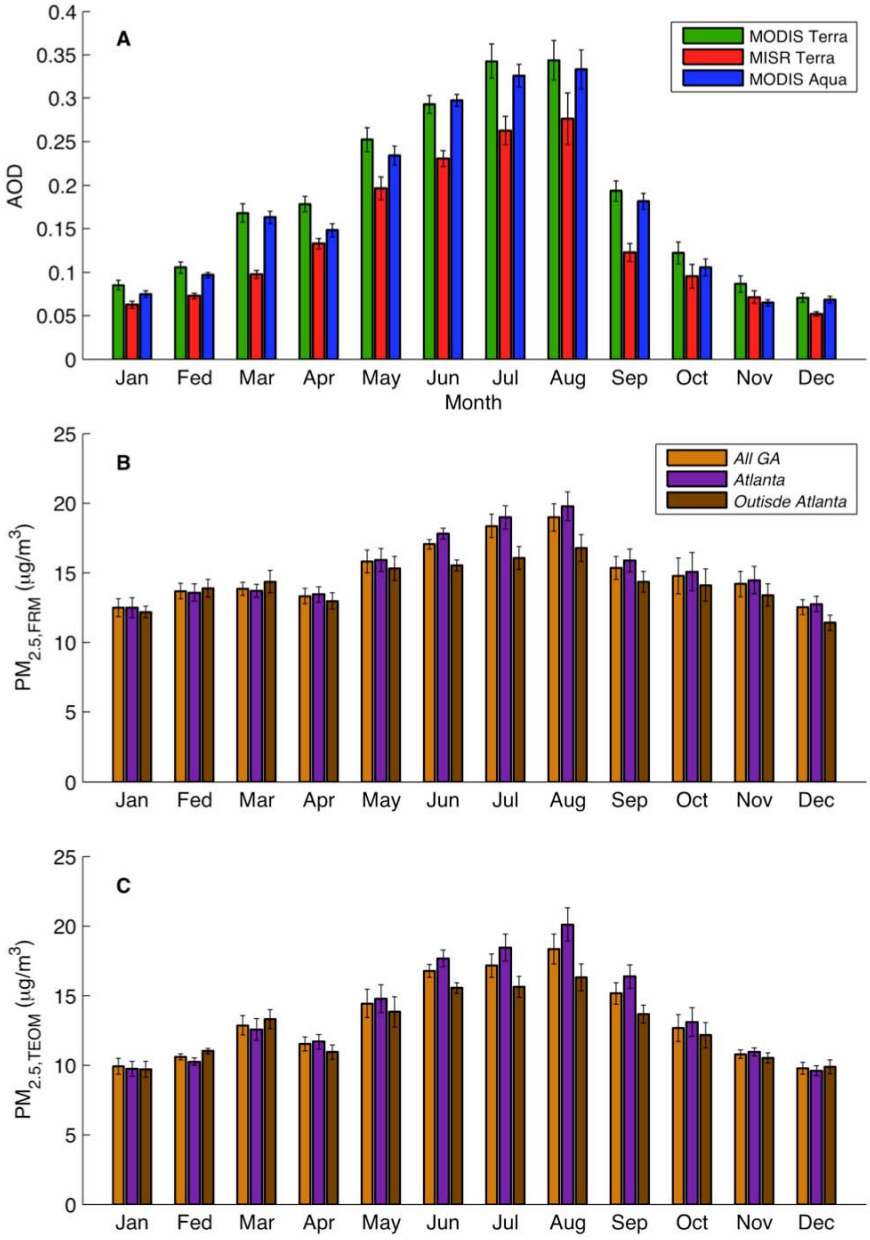

Figure 4.1: (A) Bar plots of ten-year means by month for MODIS Terra AOD, MISR Terra AOD and MODIS Aqua AOD. (B) Same as (A) except for $PM_{2.5,FRM}$ *All GA* ($\mu g/m^3$), $PM_{2.5,FRM}$ *Atlanta* ($\mu g/m^3$) and $PM_{2.5,FRM}$ *Outside Atlanta* ($\mu g/m^3$). (C) Same as (A) except for $PM_{2.5,TEOM}$ *All GA* ($\mu g/m^3$), $PM_{2.5,TEOM}$ *Atlanta* ($\mu g/m^3$) and $PM_{2.5,TEOM}$ *Outside Atlanta* ($\mu g/m^3$). Whiskers represent +/- standard error of the mean for each respective dataset.

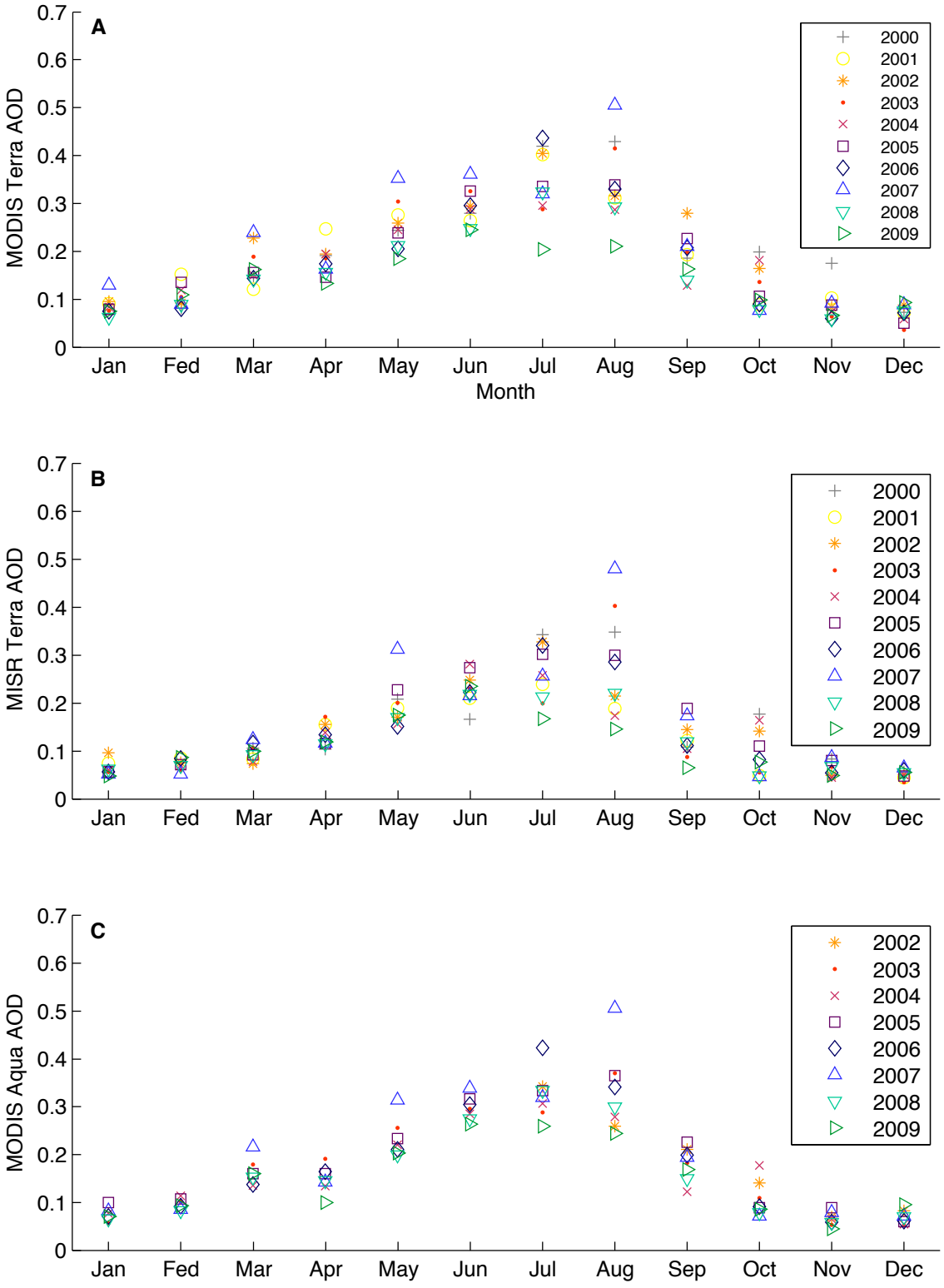

Figure 4.2: (A to C) Multi-year plots of monthly means for MODIS Terra AOD, MISR Terra AOD and MODIS Aqua AOD.

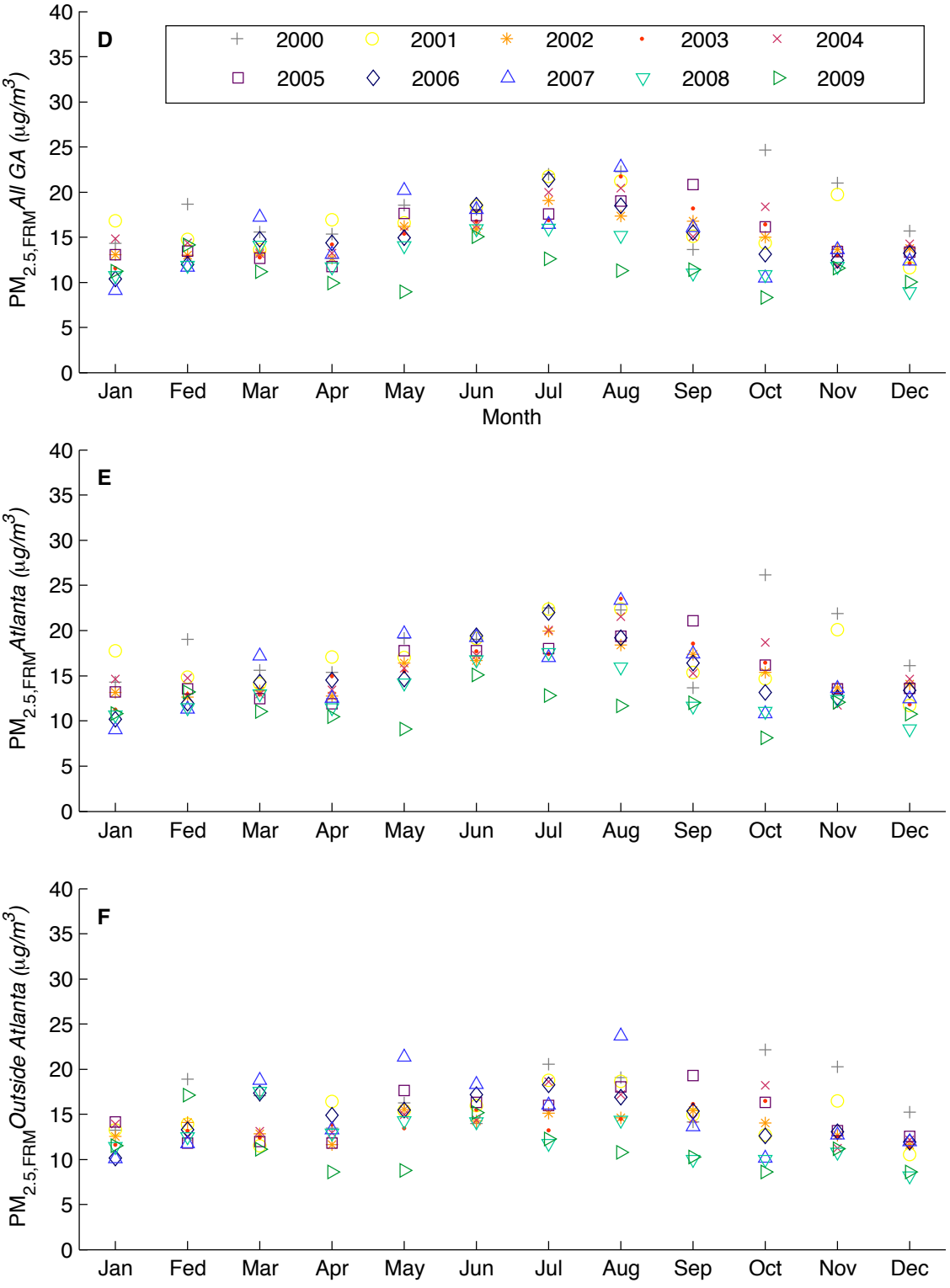

Figure 4.3: (D to F) Multi-year plots of monthly means for $PM_{2.5,FRM}$ *All GA* (µg/m^3), $PM_{2.5,FRM}$ *Atlanta* (µg/m^3) and $PM_{2.5,FRM}$ *Outside Atlanta* (µg/m^3).

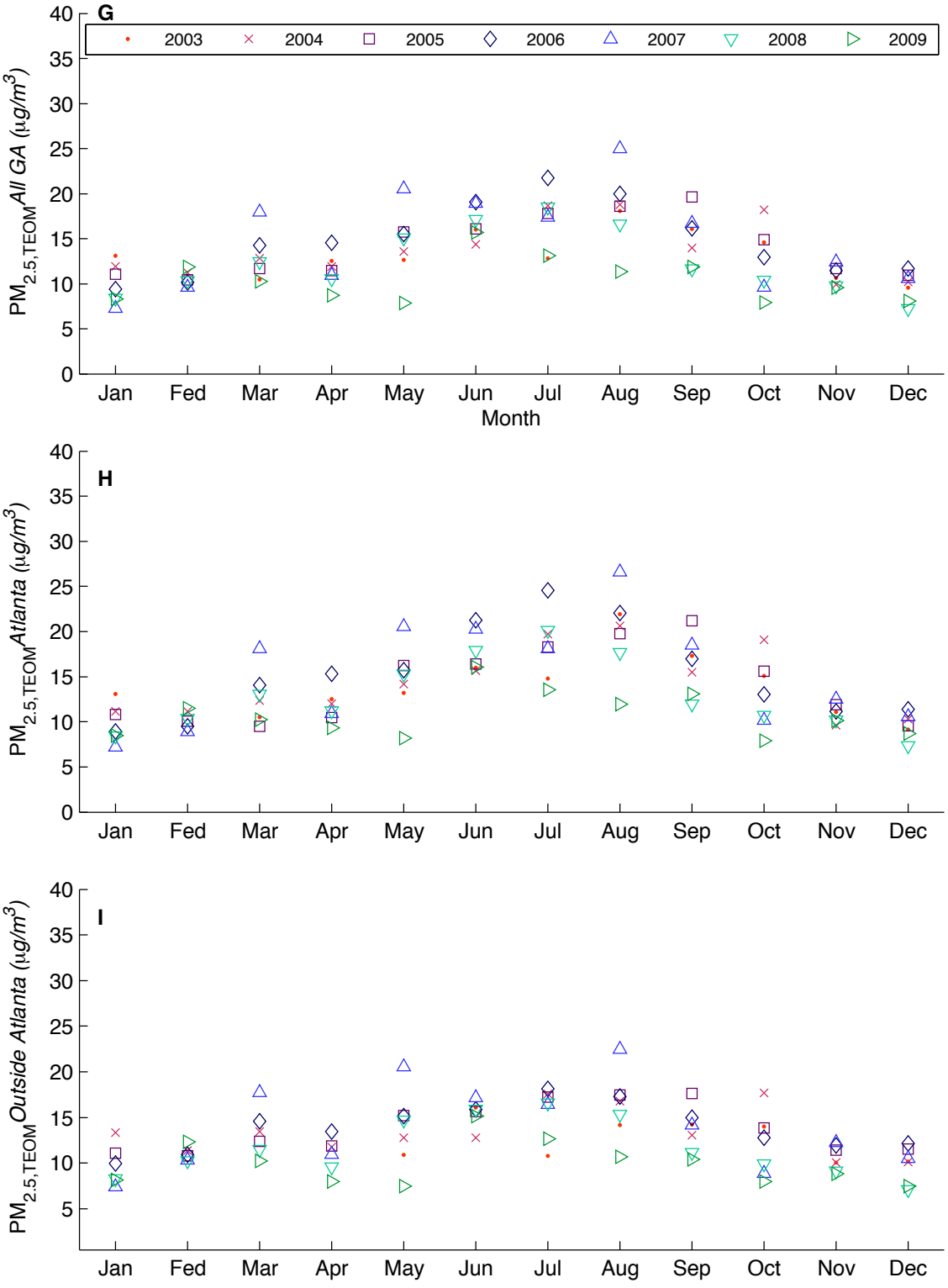

Figure 4.4: (G to I) Multi-year plots of monthly means for $PM_{2.5,TEOM}$ *All GA* (µg/m^3), $PM_{2.5,TEOM}$ *Atlanta* (µg/m^3) and $PM_{2.5,TEOM}$ *Outside Atlanta* (µg/m^3).

Our analysis to this point has shown relatively good agreement between the satellite sensors. To further investigate the agreement between sensors, specifically MODIS Terra and MISR Terra, we analyze seasonal coincident AOD monthly means. We define each season in standard fashion: winter (December, January and February), spring (March, April and May), summer (June, July and August), and fall (September, October and November). Figure 4.5 presents the comparison of AODs. In most seasons, MODIS reports higher AOD values than MISR. Although our results from Figure 3 show that on a monthly basis the differences between the two sensors are smallest during the fall and winter, our seasonal analysis (Figure 4.5) shows more variance between the sensors. Not surprisingly, the linear regression slopes (0.33 for winter and 0.54 for fall) are not close to 1, and the subsequent correlation coefficients are 0.33 and 0.57, respectively. The outliers in scatterplots are possibly due to retrieval biases, differences within the retrieval algorithms, and cloud effects. *Remer et al.* [2008] found that on a global scale, aerosols near clouds only occur less than 1% of the time over land; however, they note that AOD values near clouds can double the reported AOD due to subpixel cloud contamination [*Zhang et al.*, 2005], 3-D effects [*Wen et al.*, 2007], and increase of AOD due to increased humidity near clouds [*Koren et al.*, 2007]. Kahn et al. [2009] found that MODIS AOD values are lower than MISR AOD values for AOD below 0.2, which could be related to Collection 5 algorithm changes that allow for negative AOD retrievals. The spring and summer seasons produce the greatest agreement between the two sensors with correlation coefficients of 0.64 and 0.71, respectively. Hygroscopic growth of aerosols due to higher relative humidity in the summer also possibly influences the agreement between the sensors.

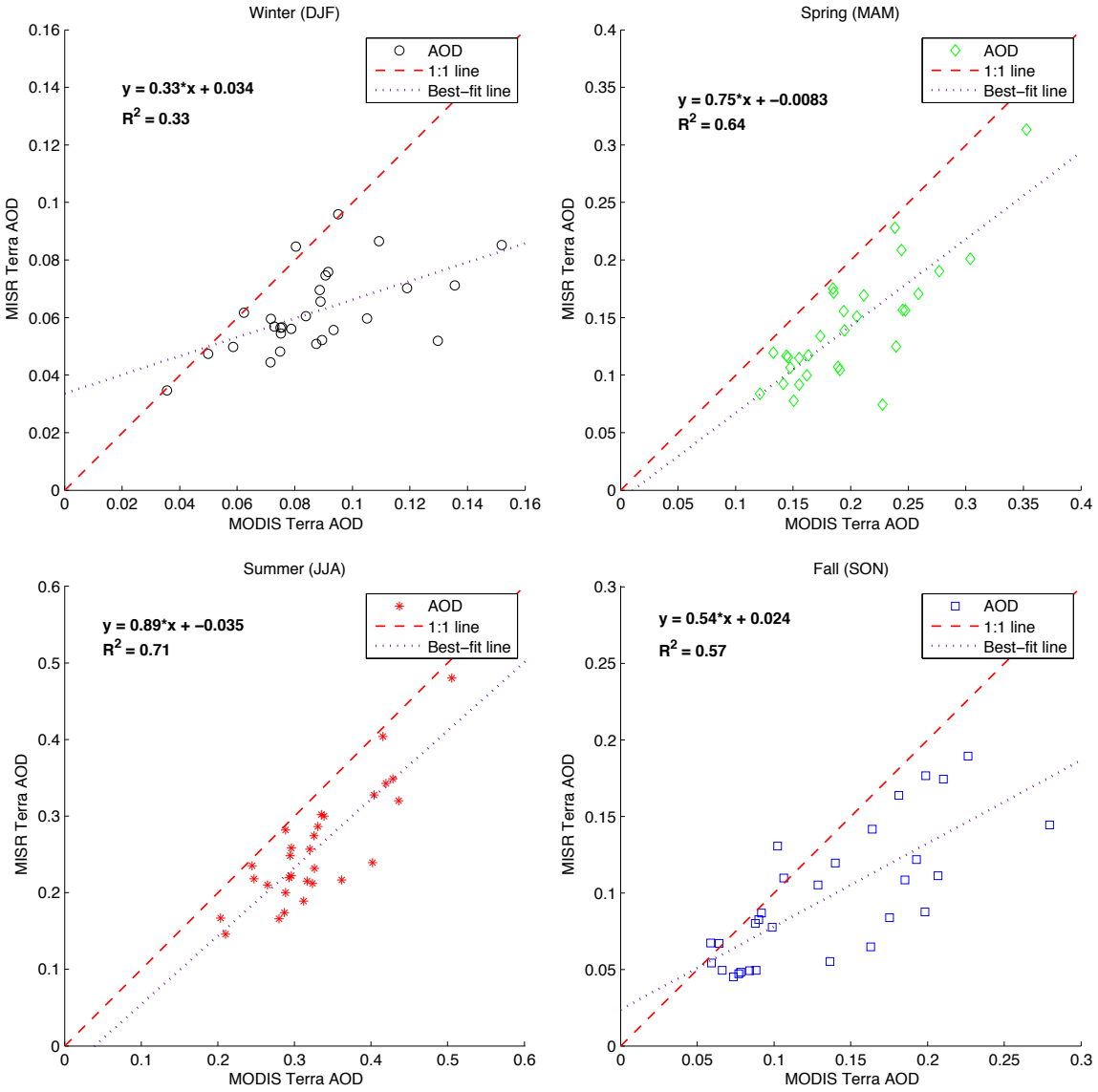

Figure 4.5: Seasonal scatterplots of MODIS Terra AOD vs. MISR Terra AOD. Red dashed line denotes 1:1. Purple dotted line denotes linear regression line.

An additional influence could be the weather pattern dynamics with the spring and summer seasons experiencing large-scale high pressure systems that can persist, which likely results in increased AOD values for both sensors despite their differences in viewing geometry. Interestingly, the signs of the y-intercepts are negative for spring and summer seasons. Possible explanations for this include that we do not force our linear

regressions through zero, and due to systematic underestimation of AOD by MISR [Kahn et al., 2009], the regression line is pulled downward. Nevertheless, our results suggest good agreement between the two sensors over the past ten years. Yet *Liu and Mishchenko* [2008] reported larger disparities between the two. We should note that *Liu and Mishchenko* [2008] only consider two months (January and July) from 2006, and they consider a region (Eastern U.S.) that is spatially larger than our area and contains multiple sources of aerosols (e.g., large metropolitan areas), while our area only contains one large metropolitan area, i.e., Atlanta.

Figure 4.6 shows how the seasonal means for each dataset change over time. As expected, spring and summer seasons show the most variance over the years. For instance, in the year 2000 MODIS Terra and MISR Terra had summer AOD means of 0.38 and 0.29, respectively, and by 2009 the means were 0.21 and 0.24. Also, even though our considered spatial domain is relatively small (5° by 5°), our seasonal means are similar in behavior to those of East North America as shown in *Remer et al.* [2008] where Level 3 1° x 1° globally gridded AOD are used for regional seasonal analysis, yet our seasonal means are higher. In the $PM_{2.5}$ datasets there appear to be different behaviors. The $PM_{2.5,FRM}$ values all appear to be decreasing with time. In 2000, $PM_{2.5,FRM}$ concentrations were around 22 $\mu g/m^3$, but by the end of the decade they had decreased to around 14 $\mu g/m^3$. The spring, fall, and winter seasons have similar behaviors, with summer being the exception. The three seasons also show similar behavior across all of Georgia, yet during the summer our results suggest that Atlanta is dominating concentrations across the state. The difference between the *All GA* and *Atlanta* means at

most varied around 2 µg/m^3, and there is a larger difference (4 µg/m^3) between the *All GA* means and the *Outside Atlanta* means.

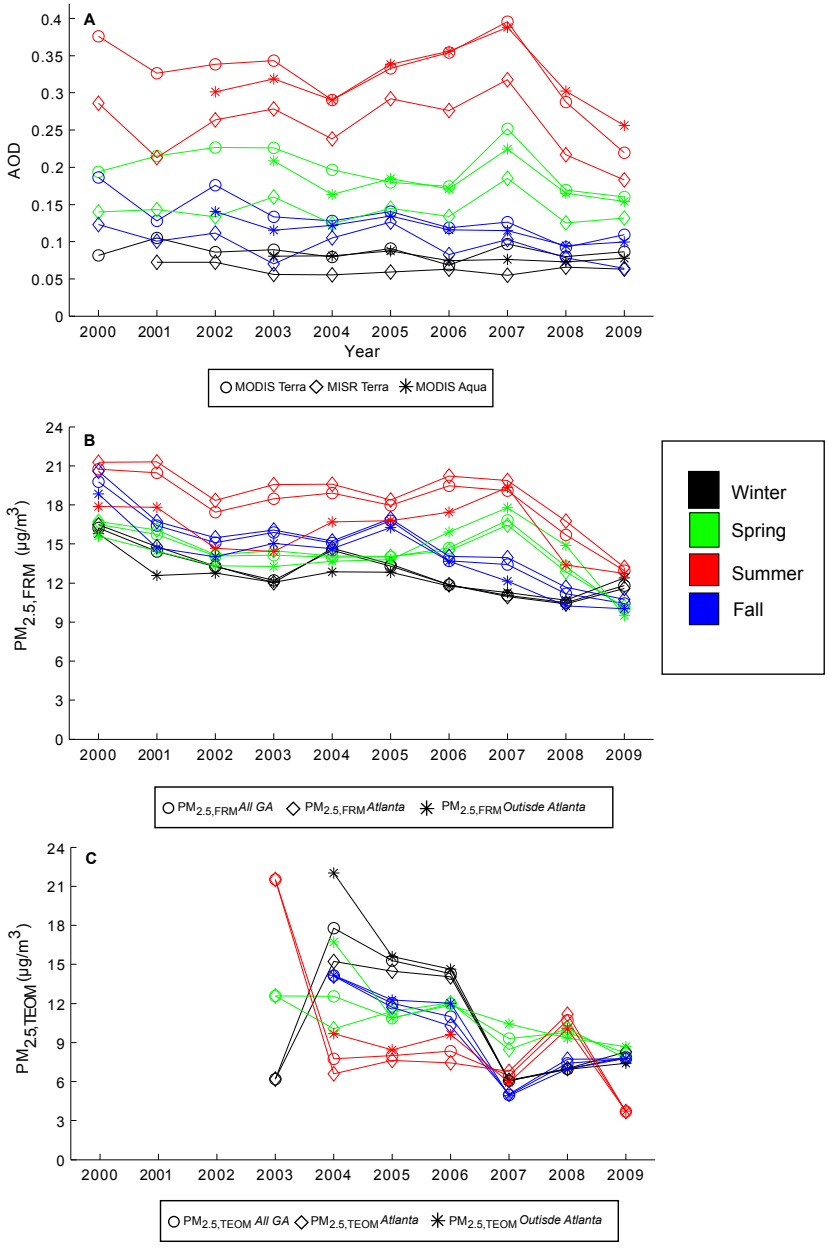

Figure 4.6: (A) Timeseries of seasonal means for MODIS Terra AOD, MISR Terra AOD and MODIS Aqua AOD. (B) Same as (A) except for $PM_{2.5,FRM}$ *All GA* (µg/m^3), $PM_{2.5,FRM}$ *Atlanta* (µg/m^3) and $PM_{2.5,FRM}$ *Outside Atlanta* (µg/m^3). (C) Same as (A) except for $PM_{2.5,TEOM}$ *All GA* (µg/m^3), $PM_{2.5,TEOM}$ *Atlanta* (µg/m^3) and $PM_{2.5,TEOM}$ *Outside Atlanta* (µg/m^3).

Alston et al. [2011a] highlighted how the spring of 2007 was anomalous in both AOD and $PM_{2.5}$ concentrations compared with other springs due to the large wildfire that burned for almost two months. It is likely that if the wildfire had not occurred, the spring means would decrease with time. Despite increased means for 2006 and 2007, the $PM_{2.5,TEOM}$ dataset appears to generally decrease with time.

The aerosol seasonality was also examined through an analysis of satellite AOD fields over the past 10 years. In particular, we were interested in understanding if there are any discernable AOD differences from the large metropolitan area of Atlanta and the remainder of the state. Seasonal maps of AOD from MODIS Terra and MISR Terra are shown in Figure 4.7: winter mean AOD (A and D), summer mean AOD (B and E), and the difference between the two seasons in (C and F). These maps, specifically the seasonal difference maps provide comparison to similar figures in *Goldstein et al.* [2009], see their Figure 1. Our spatial analysis does not strongly resemble the features seen in Goldstein et al., namely the large area of AOD (AOD > 0.25) over the broader southeastern U.S. It should be noted that a major difference between this study and theirs is that we use a finer resolution product (Level 2), which is gridded to finer resolution grid than is provided by the Level 3 (1° x 1°) monthly mean product used by *Goldstein et al*. The Level 3 products produces smoother appearing maps that can likely mask large point sources (e.g., industrialization, large metropolitan areas). This study also uses data from 2000 – 2009, whereas their study encompassed 2000 – 2007.

The MODIS maps suggest that the Atlanta area has slightly higher AOD from the remainder of the region, see Figure 4.7 (A-C). The MISR maps do not appear to capture the AOD signal in Atlanta as well as MODIS, see Figure 4.7 (D-F); however, both

sensors show very low AOD during the winter season with AOD values < 0.1, though there are some areas near the coastlines and over the ocean where AOD > 0.1 [*Chu et al.*, 2002; *Levy et al.*, 2005; *Kahn et al.*, 2007]. The summer season presents a more varied spatial representation. As noted early, there is almost a 3x increase from winter AOD values.

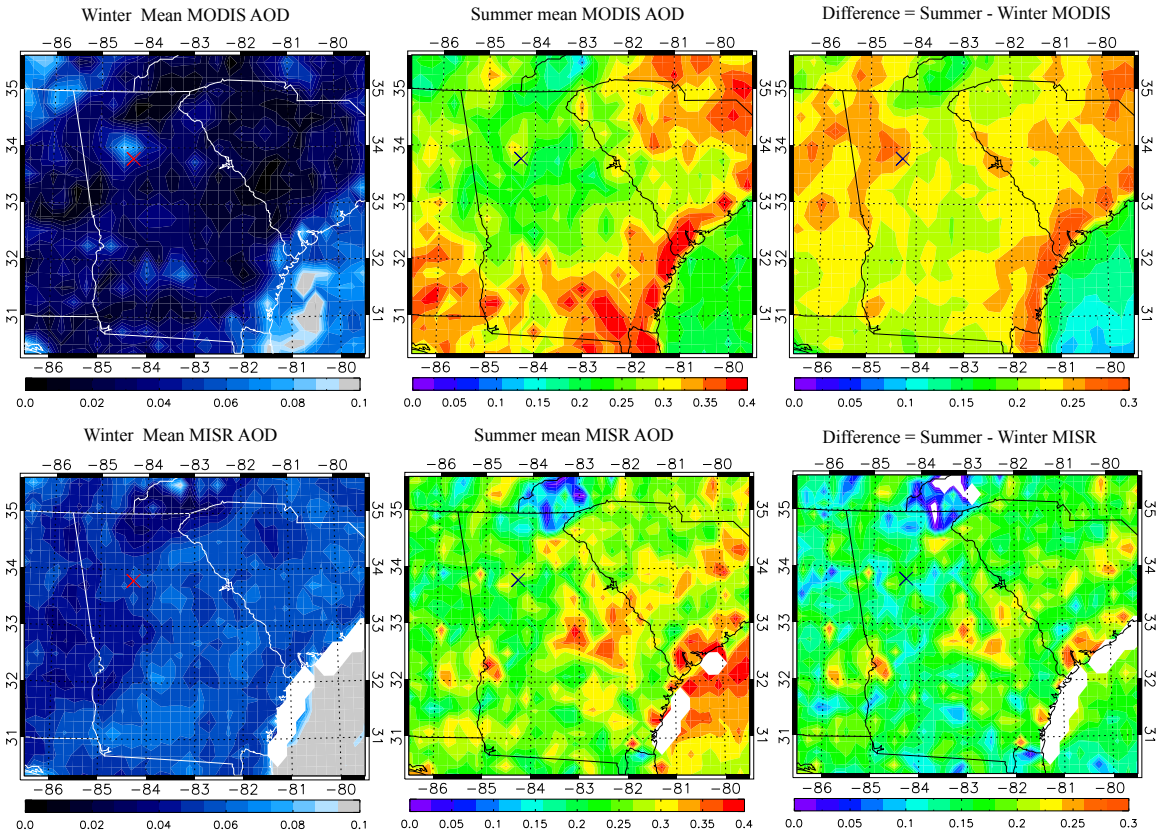

Figure 4.7: Maps of satellite AOD. (A) Winter mean AOD for MODIS Terra. (B) Summer mean AOD for MODIS Terra. (C) Difference between summer mean AOD minus winter mean AOD for MODIS Terra. (D) Same as (A) except for MISR Terra. (E) Same as (B) except for MISR Terra. (F) Same as (C) except for MISR Terra. In (A and D) the red 'X' denotes Atlanta, GA. In (B-C and E-F) the navy 'X' denotes Atlanta, GA.

One common feature between the sensors is that the background region (the region minus Atlanta) appears fairly uniform in AOD. The difference plots (Figure 4.7 (C and F) suggest variation across the region that is not seen in Figure 1 of *Goldstein et*

al. [2009]. In summary, the spatial analysis presented here shows slight differences between Atlanta and the remainder of the region at least from the MODIS Terra perspective, and this analysis shows more marked seasonality in spatial extent and magnitude than previously shown by *Goldstein et al*. [2009]. Finer scale spatial resolution of satellites will likely aid the differentiation of urban centers from background conditions. Until newer satellite sensors are available with finer resolution, regional scale analysis are likely to remain the current standard, which has implications for air quality forecasts that want to incorporate satellite data into these forecasts on a state or smaller scale.

4.3.2 Interannual Variability and Trends

To examine interannual variability of aerosol in the Southeast U.S., we analyzed monthly means of satellites AODs and ground based $PM_{2.5}$ data, including analyses of anomalies and trends. Figure 4.8 presents the timeseries of monthly mean AODs for MODIS Terra, MISR Terra, and MODIS Aqua, along with timeseries of monthly mean $PM_{2.5}$ concentrations for the two ground datasets. When viewed over the past ten years, the satellites have generally good agreement with each other. Though there are differences in AOD magnitudes between MODIS Terra and MISR Terra, their behavior over time is quite similar. The difference between minima (~ 0.1) and maxima (~ 0.4) for the MODIS sensors is about 0.3. Another way to put that is according to the MODIS sensor, AOD almost quadruples from the lowest values in winter to the highest values in summer. MISR appears to have quite dramatic fluctuations as well, with its minima ~ 0.3 and its maxima ~ 0.8. The interannual variability makes it difficult to determine if there is a trend over time.

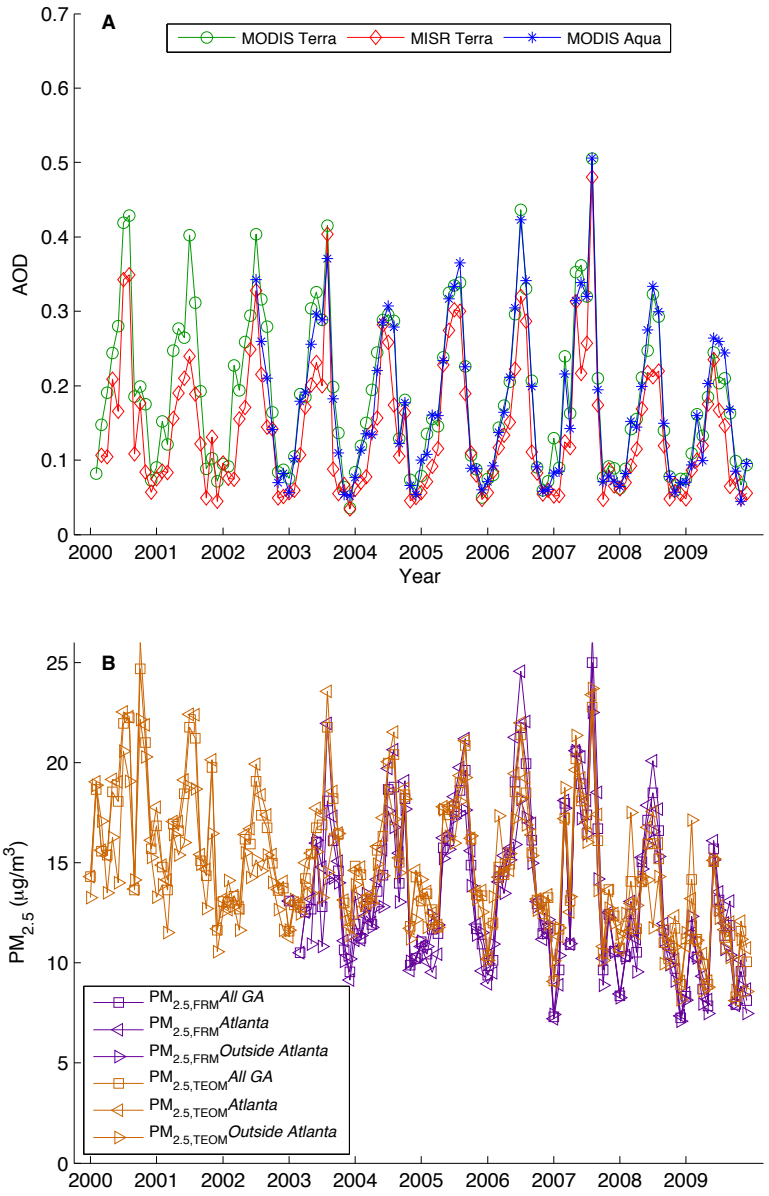

Figure 4.8: Timeseries of monthly means for satellite AOD and $PM_{2.5}$ ($\mu g/m^3$) datasets

In contrast, the $PM_{2.5}$ datasets show a distinctly decreasing trend over time. Both the maxima and minima for these datasets have decreased by 5- 8 µg/m3. The seasonality is present in the $PM_{2.5}$ datasets, but not as pronounced as the AOD datasets. When viewed together (both AOD and $PM_{2.5}$ datasets), the peaks and valleys in the timeseries

correspond well together. For instance, the correlation coefficient of MODIS Terra vs. $PM_{2.5,FRM}$ *All GA* and MISR Terra vs. $PM_{2.5,FRM}$ *All GA* is 0.72 and 0.73, respectively; however, the correlation coefficient of MODIS Aqua vs. $PM_{2.5,FRM}$ *All GA* is 0.8. Correlation analysis between the satellites and $PM_{2.5,TEOM}$ *All GA* yields 0.84, 0.81 and 0.84, respectively. Finally, Figure 4.9 presents AOD and $PM_{2.5}$ concentrations over the past 10 years in terms of yearly means calculated from monthly means. It is readily apparent that there is a decreasing trend across all datasets. One point of incongruity occurs in 2007. In the AOD datasets, 2007 is high compared with years 2006 and 2008, yet 2007 does not have this peak in the $PM_{2.5}$ dataset. *Alston et al.* [2011a] suggested that aerosols aloft associated with aerosol transport of local and long range haze and biomass burning events could be a likely explanation.

As shown in Figure 4.8 there is strong seasonality, which makes the determination of any increasing/decreasing trend difficult. The first step in the determination of a trend is to fit the timeseries with a linear regression. The second step is to access if the slope is statistically different from zero by using t-test for $\alpha = 0.05$. Though there was no trend easily detected in Figure 4.8, we fit each satellite AOD with a linear regression and determined that all the datasets did not have a statistically significant slope. As mentioned earlier, the $PM_{2.5}$ datasets appear to be decreasing with time. The linear regression for $PM_{2.5,FRM}$ all have slopes that are significant for $\alpha = 0.05$. In other words, the detected decrease in the timeseries is valid with some certainty. The $PM_{2.5,TEOM}$ datasets have more varied results.

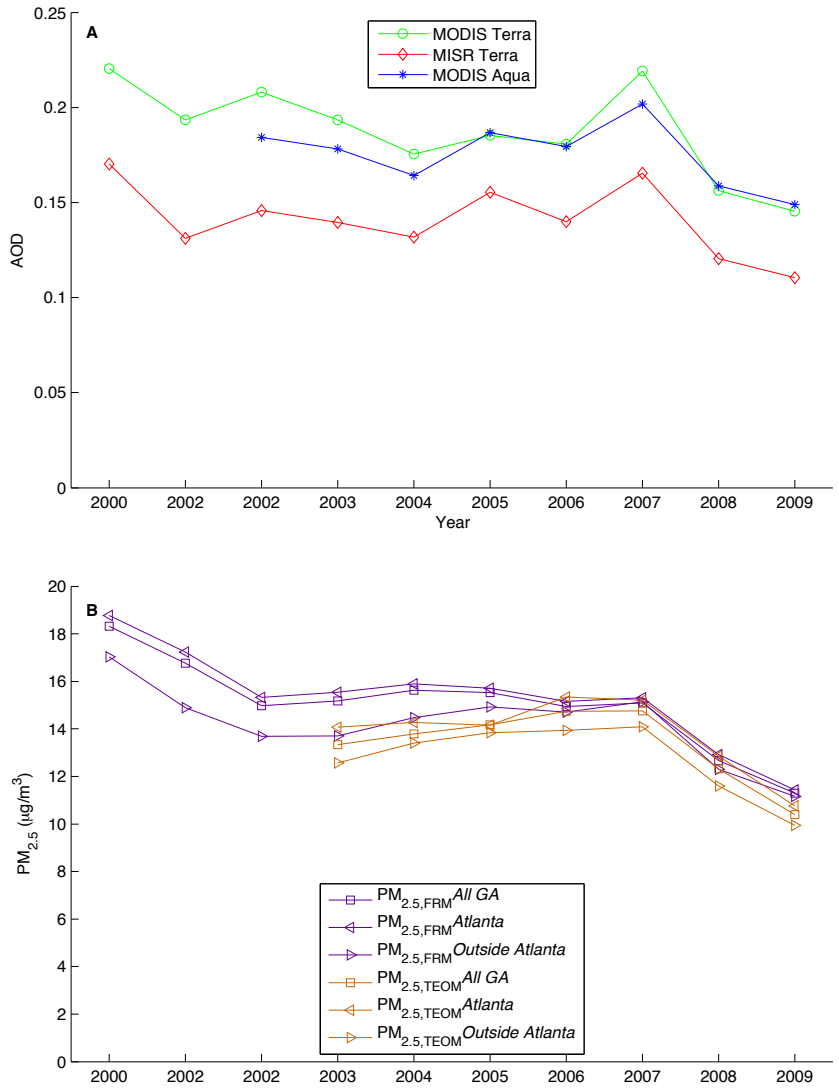

Figure 4.9: Timeseries of multi-year means for satellite AOD and $PM_{2.5}$ ($\mu g/m^3$) datasets

The slopes for $PM_{2.5,TEOM}$ *All GA* and *Atlanta* are not statistically significant, yet $PM_{2.5,TEOM}$ *Outside Atlanta* is significant. Our previous results suggest that metro Atlanta concentrations likely skew the statewide average towards higher values due to the majority of the TEOM monitors (7 or 60%) being in the metro Atlanta area. Our results also hint that the rest of the state is indeed experiencing decreasing $PM_{2.5}$ concentrations, but the anthropogenic emissions especially in the summer in the metro Atlanta are likely

masking this decreasing trend. Another possible explanation for why one $PM_{2.5}$ dataset shows a decreasing trend and the other does not is the difference in length of the data records. We believe that given the air quality control policies in place, the $PM_{2.5,TEOM}$ dataset will likely show a statistically decreasing trend given more time.

Ultimately, it is necessary to remove the seasonal signal in order to access the presence of any true trends. We calculate a ten-year mean of every month, and subtract each month from the 10-yr mean of that month. For example, if the ten-year January average is 0.18, then 0.18 is subtracted from each January in the dataset, thus we are using anomalies from the 10-yr monthly mean to detect trends over the past 10 years. The resulting timeseries of anomalies for both satellite and $PM_{2.5}$ datasets are shown in Figure 4.10. The anomaly timeseries are fit with linear regressions to determine the trend and are shown by the dashed line in Figure 4.10. MODIS Terra was the only satellite dataset to have a statistically significant slope. We believe the smaller range of MISR AOD is why that dataset does not have a significant slope, while the MODIS Aqua dataset is only 8 years long. It is possible that as time progresses the MODIS Aqua dataset will show a decreasing trend with certainty. By removing the seasonal component within the $PM_{2.5}$ datasets revealed statistically significant decreasing trends, see Figure 4.11 and Figure 4.12. The linear regression variables (slope and y-intercept) are summarized for each dataset in Table 4.1. The regression variables are calculated on a per decade basis. We hypothesize that removing the strong seasonality from those datasets the summertime peaks in concentrations were minimized thus allowing a true and statistically significant trend to emerge.

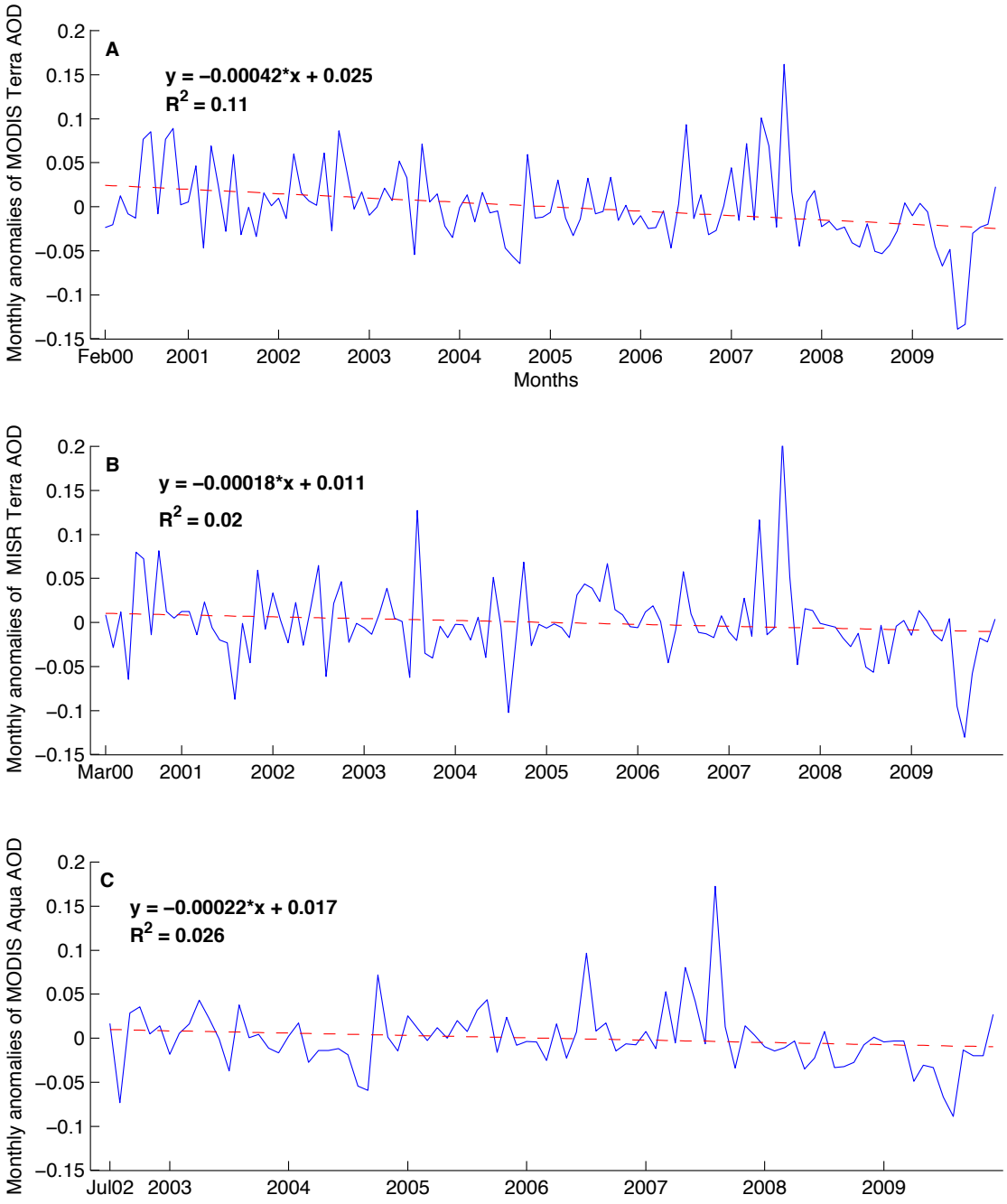

Figure 4.10: (A to C) Timeseries of monthly anomalies for MODIS Terra AOD, MISR Terra AOD and MODIS Aqua AOD. Dashed red lines denote linear regression trend line.

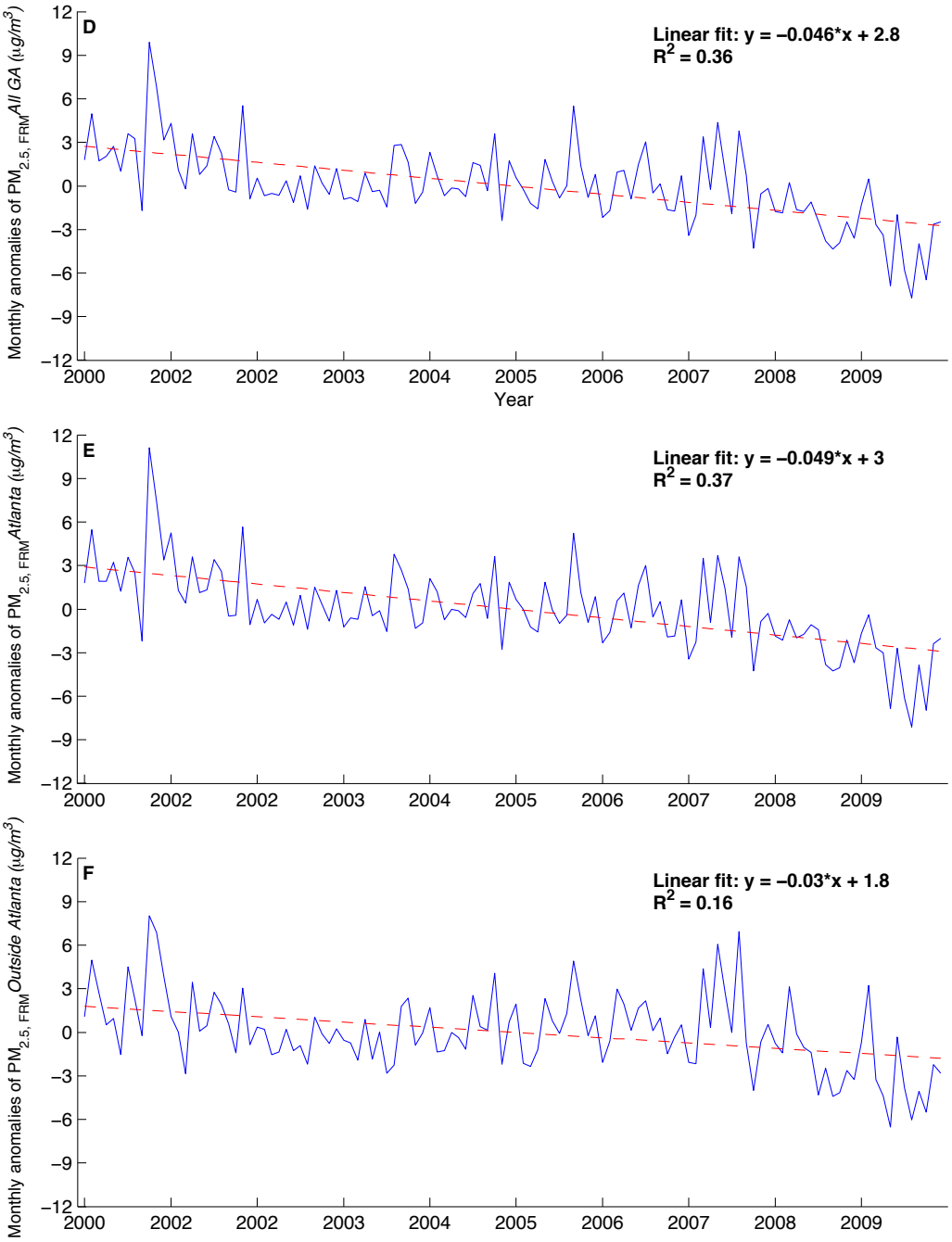

Figure 4.11: (D to F) Timeseries of monthly anomalies for $PM_{2.5,FRM}$ *All GA* (µg/m^3), $PM_{2.5,FRM}$ *Atlanta* (µg/m^3) and $PM_{2.5,FRM}$ *Outside Atlanta* (µg/m^3). Dashed red lines denote linear regression trend line.

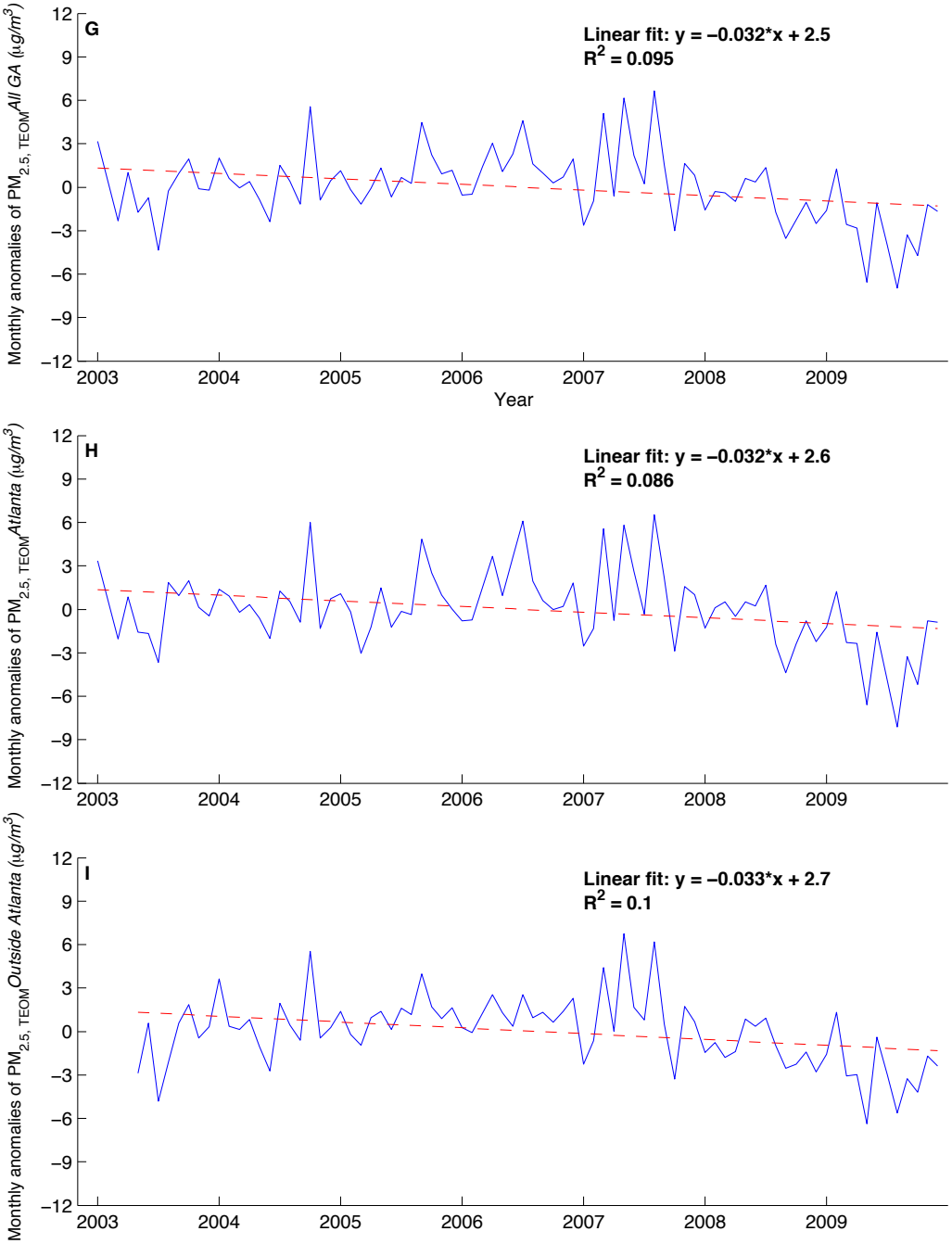

Figure 4.12: (G to I) Timeseries of monthly anomalies for $PM_{2.5,TEOM}$ *All GA* (µg/m^3), $PM_{2.5,TEOM}$ *Atlanta* (µg/m^3) and $PM_{2.5,TEOM}$ *Outside Atlanta* (µg/m^3). Dashed red lines denote linear regression trend line.

Table 4.1: Linear regression coefficients for satellite and $PM_{2.5}$ datasets. Significance is denoted in bold.

Dataset	Slope (AOD/month) or ($\mu g/m^3$ $month^{-1}$)		Y-intercept (AOD) or ($\mu g/m^3$)	
	Seasonal component	No seasonal component	Seasonal component	No seasonal component
MODIS Terra	-0.000415	-0.00434	0.214	0.025
MISR Terra	-0.000177	-0.000112	0.15	0.011
MODIS Aqua	-0.000219	-0.000275	0.196	0.017
$PM_{2.5,FRM}$ *All GA*	**-0.046**	**-0.0448**	17.75	2.781
$PM_{2.5,FRM}$ *Atlanta*	**-0.0488**	**-0.0472**	18.187	2.951
$PM_{2.5,FRM}$ *Outside Atlanta*	**-0.0301**	**-0.0302**	16.029	1.821
$PM2_{.5,TEOM}$ *All GA*	-0.0317	**-0.0319**	15.876	2.501
$PM_{2.5,TEOM}$ *Atlanta*	-0.0324	**-0.0319**	16.325	2.561
$PM_{2.5,TEOM}$ *Outside Atlanta*	**-0.0335**	**-0.0385**	15.876	2.696

4.4 Chapter Summary

We analyzed aerosol data from both ground based ($PM_{2.5}$) and space based (satellite AOD) platforms to examine the seasonality and interannual variations of the regional aerosol signal, and to detect if there was any discernable trends over the past ten years. We found that strong seasonality exists in both the AOD and $PM_{2.5}$ datasets where mean summertime AOD is nearly three times higher than mean wintertime AOD, and mean summertime $PM_{2.5}$ concentrations are almost twice as high as mean wintertime concentrations. Another factor that possibly influences the seasonality is the effect of hygroscopic aerosol growth during the summer months, given much higher relative humidity in the summer. Though satellite retrieval algorithms do not directly incorporate relative humidity, the retrievals are affected [*Wang and Martin*, 2007]. Additionally over

the past ten years, the $PM_{2.5}$ dataset used for regulatory purposes ($PM_{2.5,FRM}$) agree quite well with the satellite AOD measurements of aerosols. The correlation coefficients between $PM_{2.5,FRM}$ and AODs from MODIS Terra are 0.72, for MISR Terra are 0.73, and for MODIS Aqua are 0.8.

We found that MODIS onboard Terra and MISR onboard Terra agree well with each other during the warmer months with correlation coefficients of 0.67 for spring and 0.71 for summer. It is possible that cloud cover and inherent differences in sensor sensitivity explain the reduced agreement during the cooler months. Trend analysis was performed to establish baselines of different aerosol measures. We use t-tests of the slopes for $\alpha = 0.05$ to determine whether the calculated slopes are statistically different from zero. Trend analysis of monthly means AOD revealed that none of the satellite datasets shows a statistically significant negative trend. Yet the $PM_{2.5,\ FRM}$ monthly mean timeseries does have statistically significant negative trends. Given the strong seasonality, we removed the seasonal component to create monthly mean anomalies. Trend analysis of the monthly mean anomalies yielded that MODIS onboard Terra has a statistically significant negative trend, and all the $PM_{2.5}$ datasets have statistically significant negative trends. It should be noted that for MODIS onboard Terra, this detected trend could be impacted by degradation of the blue channel used in MODIS retrievals over land, yet even with this drift taken into account the retrieved values are within the acceptable error envelope [*Levy et al.*, 2010; *Kahn et al.*, 2011].

Our results question the *Goldstein et al.* (2009) hypothesis on a dominant contribution of SOA from biogenic emission to AODs in the region. AOD is a column-averaged measurement that cannot readily differentiate between sources without a priori

information. If the conversion rate between BVOC and SOA is primarily temperature driven, then if the temperature record was found to neither increase or decrease [*Menne et al.*, 2009] then biogenic SOA is unlikely to be the driver behind the negative trends in AOD. Following this reasoning the primary driver behind the negative trend appears to be anthropogenic sources which are monitored and controlled through air quality policies. Another facet of the *Goldstein et al*. [2009] hypothesis is that these BVOC associated SOA are formed in an aerosol layer aloft and thus ground based sensors would not likely capture the additional aerosol load of those aerosols. One would not expect trends in the $PM_{2.5}$ records, yet our results show decreasing seasonal and yearly trends. These results suggest that ground based monitors are measuring some portion of these SOA aerosols. Of course, this result requires additional measurement of aerosol profiles in this region for confirmation purposes. However, given the current state of measurement techniques it is not a simple exercise to differentiate between SOA of anthropogenic and biogenic sources (Weber et al., [2007]). Finally, the spatial analysis presented here somewhat agrees with that shown in *Goldstein et al*. [2009]. Of significance is that our results are different in spatial features (not smooth continuous fields of AOD) and magnitude (the difference between summer and winter is higher).

Our analysis suggests that air quality policies and controls placed upon $PM_{2.5}$ precursors have resulted in appreciable decreases in aerosols in the U.S. Southeast. Our results also suggest that this region is experiencing solar brightening associated with decreasing concentrations of aerosols. Ground based measurements of solar irradiance in the region would be necessary to confirm our conclusions. Currently, there is no such monitoring being done. Our analysis also provides a useful baseline for naturally derived

aerosols representative of background conditions in this region of the U.S. Establishing the background helps to delineate the $PM_{2.5}$ contributions of the metropolitan area of Atlanta. Thus, it is likely that future air quality control strategies will need to focus upon the anthropogenic component, while also incorporating naturally occurring aerosols. Additionally, the air quality control policies that have likely resulted in solar brightening might have potential climatic trade-offs. As such these longer-term analyses are critical for evaluation of the air pollution regulatory policies, and these analyses can serves as baselines of measures that can be used to access impacts of future policies and climate change. The methodology applied here is readily applicable to regions that have sufficient ground based aerosol measurements so long as the chosen area is large enough for sufficient satellite coverage. The need for finer scale resolution satellite sensors will aid a host of applications seeking to do more detailed regional and local scale analyses. Users of satellite data need to be aware of possible bias within the data at land-water boundaries, which is an important consideration given that so many highly populated areas are near coasts. It is possible that with newer sensors better treatment of these issues will be addressed. Our future work will focus upon the climatic impacts of the decreasing aerosol trend on this region.

CHAPTER 5

CLIMATIC RADIATIVE FORCING OF AEROSOLS IN THE SOUTHEASTERN U.S.: ASSESSMENT BASED ON DECADAL SATELLITE DATA AND RADIATIVE TRANSFER MODELING ANALYSIS

5.1 Introduction

In the U. S. aerosols have distinct compositions based upon region, see the U.S. EPA's report of Our Nation's Air (http://www.epa.gov/airtrends/2010/index.html). Aerosols in the Southeastern U.S. are dominated by sulfates and organic carbon, with remaining contributions from nitrates, elemental carbon (or black carbon, BC) and crustal material. Several previous studies assessed TOA radiative forcing in the Southeastern U. S. *Carrico et al*. [2003] estimated TOA forcing to understand the radiative effects of urban aerosols on climate. Recently, *Goldstein et al*. [2009] estimated the radiative forcing (ΔF = -3.9 Wm^{-2}) associated with secondary organic aerosols (SOA) formed from biogenic emission during the summertime in the U. S. Southeast. Their calculated forcing is less than the estimate from *Carrico et al.* [2003] (ΔF = -11 ± 6 Wm^{-2}) taken during the summer of 1999. The Goldstein study used a mean value of summer aerosols from seven years of aerosol optical depth (AOD) measured by the MISR (Multi-angle Imaging SpectroRadiometer) and MODIS instruments on the NASA Terra satellite. Both studies used a first order approximation (see Eq.5.1) to assess the TOA forcing. While this research provides an interesting starting point in understanding the radiative impacts of aerosols in the Southeastern U.S., it only provides a snapshot of summertime conditions

as shown by the one calculated value of TOA forcing. To date, there have been over ten years of satellite data from Terra that can now be used to assess how TOA forcing responds over the longer time period.

The first order approximation of TOA forcing can be defined as (Haywood and Shine, [1995]):

$$\Delta F = -DS_0 T_{atm}^2 (1 - A_c)\omega_0 \beta AOD\left((1 - R_s)^2 - \frac{2R_s}{\beta}\left(\frac{1}{\omega_0} - 1\right)\right) \qquad (5.1)$$

where D the is fractional day length, solar constant (S_0) = 1370 Wm^{-2}, T_{atm} is the atmospheric transmission, A_c is the fractional cloud amount, ω_0 the is single scattering albedo, β is the up-scatter fraction, and R_s the is surface reflectance. *Goldstein et al.* [2009] only considered changes in AOD by keeping the other variables constant. A single scattering albedo of 0.972 was used as a representative value of the optical properties of aerosols in the Southeastern U.S. Also, they chose to use a fixed surface albedo value of 0.15 and fractional cloud cover amount of 0.6 to be representative of the region. Many of these variables can now be measured by satellite that provide a unique opportunity to assess the TOA radiative forcing of aerosols taking into account the decadal variations in aerosol AOD, cloud faction and surface albedo. The *National Research Council Report* [2005] advocates for the better understanding of regional variations in the radiative forcing as well as for long-term monitoring of radiative forcing variables.

Goldstein et al. [2009] suggested that the negative TOA forcing produces a cooling at the surface. Earlier analysis of surface temperature using the GISS global climate model suggested that over the past hundred years the U. S. Southeast had cooled [*Hansen et al.,* 1999]. However, recent reanalysis of surface temperature records point towards a different conclusion, namely that the Southeast has neither warmed nor cooled

[*Menne et al.*, 2009]. If the latter is accurate, that has implications on whether the haze that persists in the Southeast is indeed responsible for cooling as Goldstein et al. hypothesized.

In Chapter 4, our analysis of ten years of data has revealed distinct seasonality with respect to aerosol concentration and AOD, but that is only part of the story. The chemical composition of aerosols in this region changes with season as well [*Butler et al.*, 2003; *Edgerton et al.*, 2006; *Edgerton et al.*, 2009]. Chapter 4 results also supported differences between the urban area of Atlanta and the remainder of the state (see Section 4.3.1). *Tombach and Brewer* [2005] found that the region is fairly homogeneous in sulfate, which happens to be the largest contributor to aerosols by mass, while organics were homogeneous as well. Organics are the second largest contributor to aerosols by mass. Nitrates were found to be homogeneous as well, but in considerably lower concentrations. Interestingly, *Blanchard et al*. [2011] found that in the Atlanta area, organic carbon and black carbon (BC) have noted higher concentrations from the surrounding region. The differences between the urban center and the remainder of the region are likely anthropogenic influenced. As mentioned earlier, a way to ascertain the impact of anthropogenic aerosols is through TOA estimates of forcing. However, the approximation given by Eq. 5.1 cannot capture the complexity of aerosol composition To have a more accurate estimate of forcing, a full-scale radiative transfer model can be used that includes optical properties of aerosols computed from measurements of the chemical speciation of aerosols. The radiative transfer model can also be used to address the differences between summer and winter aerosols. The model can also explore the

radiative impacts of certain conditions that have been raised earlier in this dissertation, namely biomass burning [*Panicker et al.*, 2010] and aerosol layers located aloft.

This study seeks to (1) assess the regional TOA aerosol direct radiative forcing and its dynamics over the past decade in the U. S. Southeast by taking into account changes in cloud cover, surface albedo, and aerosol concentration through AOD; and (2) quantify the radiative impacts of representative aerosols occurred during the summer and winter seasons both at the TOA and surface. In the first part of this chapter, we used AOD, cloud fraction and surface albedo data from MODIS and MISR from March 2000 – December 2010. Our first order approximation of TOA radiative forcing assessment focuses on determining the seasonal and interannual variations of these variables across the region of interest and associated dynamics of the TOA radiative forcing, especially the presence of trends. The second portion of this chapter focuses upon full-scale optical and 1-D radiative modeling of Southeastern U. S. aerosols to determine the differences between the urban and background areas during the summer and winter seasons. We assemble different mixtures of aerosol species representative of winter and summer aerosols through the use chemical speciation measurements of $PM_{2.5}$ and optical properties of those species. The mixtures are then used as input into an optical model whose results then serve as input into a 1-D radiative transfer model. We also quantify the radiative impacts of biomass burning as seen during the years 2007 and 2011, and test the Goldstein hypothesis of an organic layer aloft. The chapter is organized as follows. Section 5.2 describes the types of data and methodologies used in the first order approximation of TOA radiative forcing and presents the results. Section 5.3 presents the results of the radiative transfer modeling. Finally, section 5.4 concludes this chapter with

a combined summary from both the estimated radiative forcing assessment and the radiative transfer modeling analysis.

5.2 First-Order Radiative Forcing Assessment Based on Decadal Satellite Data

5.2.1 Data and Methodology

This research utilizes aerosol products from MODIS and MISR along with cloud fraction and surface land albedo from MODIS. This study uses Collection 5 Level 2 over land aerosol product MOD04 from MODIS (see Chapter 2 for further information on MODIS). Level 2 data are separated into five-minute granules. One variable of interest to this study is "Optical_Depth_Land_and_Ocean" which is measured at 550 nm. This product combines the corrected optical depth over land and ocean with the best data quality (QA Confidence flag = 3).

MISR AOD used in this analysis is version 22 Level 2 aerosol data, which have a 17.6 km resolution at nadir (see Chapter 4 for further details). The AOD values used are "best estimate AOD" at MISR green (558 nm) band. MISR also has in their standard product a variable that estimates single scattering albedo (ω_0 or SSA), which is used in this analysis.

This study uses a 5° x 5° latitude/longitude box centered over the Southeastern U.S. The box's coordinates are 30-35 °N and 80-85°W. The AOD values associated with the pixels contained within the box are averaged together for each day from March 1, 2000 - December 31, 2010. The daily AOD means are then averaged to create monthly means. These data files were obtained from NASA Goddard Space Flight Center's LAADS (Level 1 and Atmosphere Archive and Distribution System).

This study also uses the same MODIS product to obtain cloud cover information. Specifically the "Cloud_Fraction_Land" subset is used. Cloud fraction is simply the ratio of the number of cloudy/probably cloudy pixels to the total number of pixels within a granule during the cloud-top algorithm processing [*Platnick et al.*, 2003]. The same lat/lon box is used for obtaining cloud fraction over the Southeastern U.S for the same time period.

The final dataset used in this analysis is a Level 3 CMG (Climate Modeling Grid) Albedo product (MCD43C3) at 0.5° x 0.5° resolution provided by Dr. Schaaf (*personal communication*). Albedo is a measure of a surface reflectivity that depends on the surface type. MCD43C3 is a combined product that uses both MODIS sensors as inputs. This product is available in 16-day aggregates every 8 days, which results in a maximum of 46 Albedo measurements over a year.

The MODIS Albedo products are generated using the Ross-Thick/Li-Sparse-Reciprocal BRDF model [*Ju et al.*, 2010]. The model parameters are estimated independently for each gridded pixel location by inversion of against the MODIS observations (surface reflectance and solar and viewing geometry values) sensed in the 16-day retrieval period [*Schaaf et al.*, 2002]. For more detailed explanation of the Albedo/BRDF algorithm please see [*Schaaf et al.*, 2002]. The Albedo product is provided in three broadbands: visible (0.3-0.7 μm), near-infrared (0.7 – 5.0 μm) and shortwave (0.3 – 5.0 μm) using the spectral to broadband conversion approach developed by [*Liang et al.*, 2002]. The use of quality flags is necessary to ensure the albedo values have real meaning with high confidence as to the validity of the values. The confidence associated with the inversion results is provided through the use of data quality flags. The same

lat/lon box is used to obtain albedos over the Southeastern U.S. This study utilizes the shortwave broadband white sky (isotropic diffuse radiation) albedos where more than 80% of the albedos values are considered to be acceptable (data flag 2 or lower). Additionally, the 46 files are averaged on a monthly basis with each month having 3-4 retrievals.

TOA radiative forcing is computed using Eq. (5.1) given in the Introduction. The methodology is as follows. The area averaged variables described above are used in the in the timeseries analysis and as input into Eq. (5.1). The analysis of the TOA radiative forcing is broken into four portions: (1) assessments of individual impacts of AOD, cloud fraction and surface albedo; (2) a comparison between surface-cloud impacts versus aerosol effects, e.g., AOD and cloud fraction; (3) a combined assessment where AOD, cloud fraction, and surface albedo all change with time; (4) same as (3) with three different values for single scattering albedo that capture seasonal aerosol composition changes. For those analyses mean values of input variables are calculated to serve as constants from the data instead of using representative values. Unless otherwise stated, the constants identified in the Introduction are used as is in the calculations. The calculated mean AOD refers only to MODIS AOD. For the purposes of clarity, in this context maxima will refer to more negative values, and minima will refer to less negative values.

5.2.2 First Order Radiative Forcing Assessment Results

5.2.2.1 Temporal Variability of AOD, Cloud Fraction and Surface Albedo

Strong seasonality is a strong characteristic seen in the satellite AOD datasets of MODIS and MISR. Figure 5.1 shows the MODIS and MISR satellite monthly mean

AOD datasets as a timeseries from 2000 until 2009. Maxima occur during the warmer months with minima occurring during the cooler months. For most years the maxima occurs near 0.4, but in more recent years the maxima are around 0.3, whereas the minima hover between 0.05 – 0.1. For more detailed analysis see Chapter 4. Overall both datasets have decreasing trends with time. To determine trends without seasonal basis the same methodology from Alston et al. [2011b]. MODIS has a statistically significant decreasing linear trend (slope = -0.000415) in the monthly AOD anomalies using a t-test for $\alpha = 0.05$.

Cloud fraction behaves slightly different from the other two variables. As shown in Figure 5.2, cloud fraction appears to have a bimodal behavior in terms of maxima. The summer months generally have the highest maxima, but the winter months also have maxima albeit lower than the summer maxima. The largest minima occur during the fall with the spring having the other minima. Minima values vary around 0.2 – 0.45 while maxima values fluctuate between 0.5 – 0.8. Due to the dynamic nature of clouds the year-to-year behavior appears somewhat erratic. Additionally, the shorter time period considered in this study makes detecting a linear trend within the record challenging. As such, there is not a discernable trend in the monthly anomalies of cloud fraction.

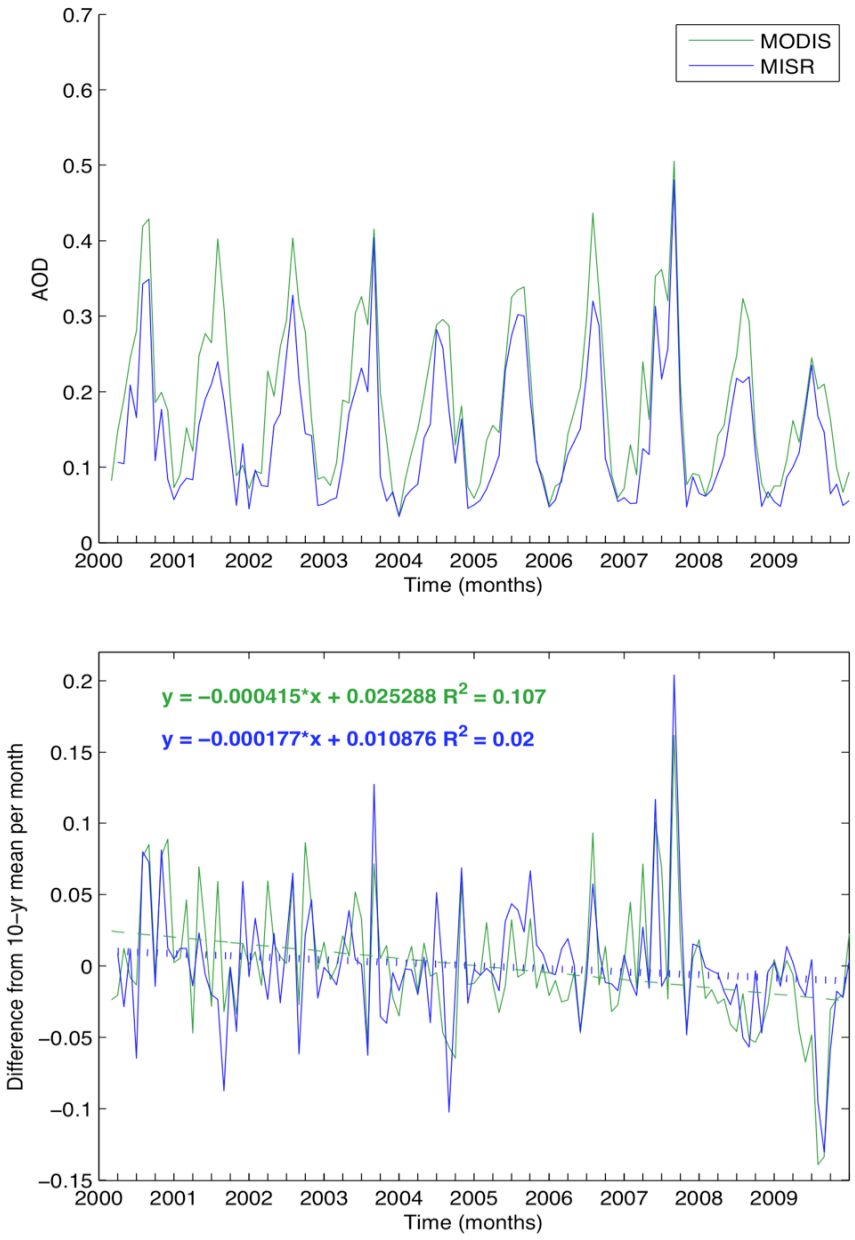

Figure 5.1: (top) Timeseries of monthly mean AOD from MODIS and MISR. (bottom) Timeseries of monthly mean AOD anomalies from MODIS and MISR. Linear regression information inset with figure.

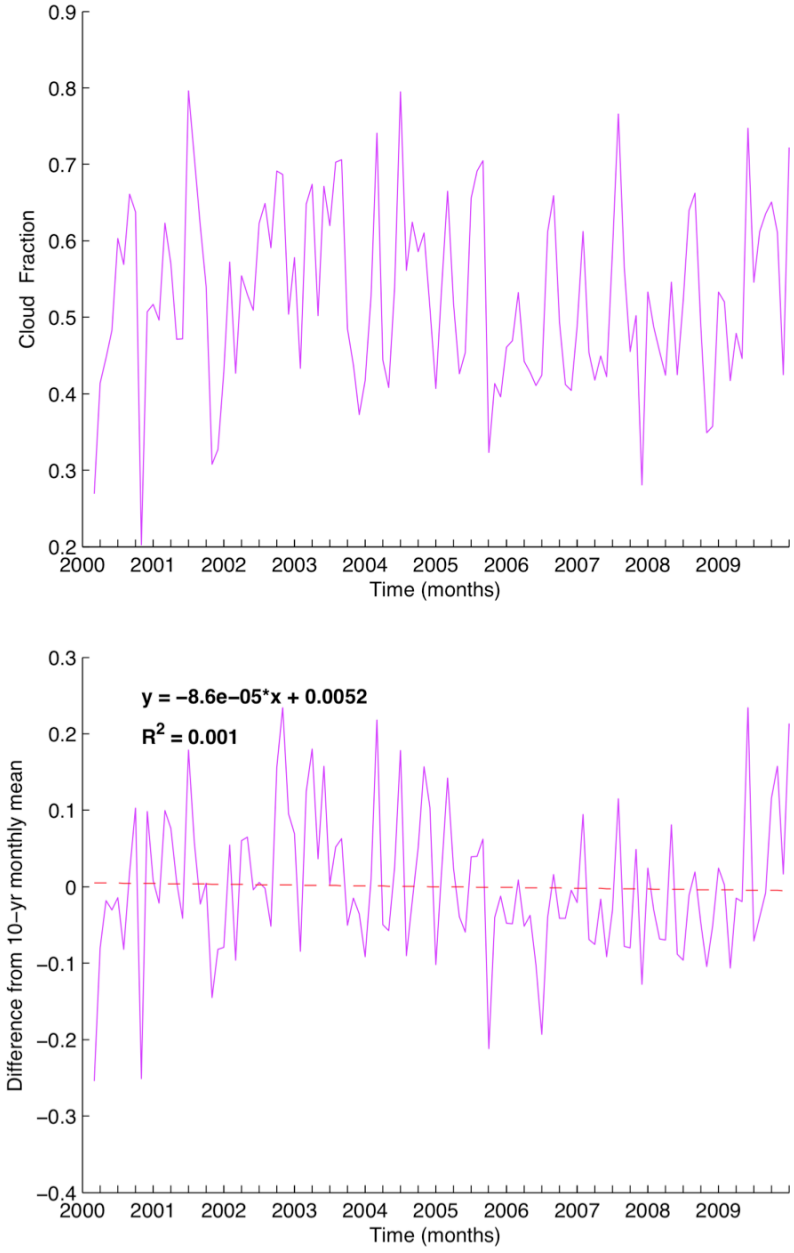

Figure 5.2: (top) Timeseries of monthly mean cloud fraction. (bottom) Timeseries of monthly mean cloud fraction anomalies. Linear regression information inset with figure.

The last variable considered is surface albedo. Surface albedo has strong seasonality as shown in Figure 5.3. As expected during the warmer seasons there are albedo changes associated with a green-up of vegetation that results in seasonal maxima.

While there is a seasonal cycle, the southeastern region of the U.S. is region that stays green throughout the year due to high concentration of evergreen trees. Thus surface albedos do not vary as much as other regions in U.S. Interestingly, during the first seven years of the timeseries, the maxima are almost 0.155, yet during the latter years, the maxima only occur between 0.145 and 0.15. *Barnes and Roy* [2010] found that this region experienced over a 20% change in land cover and land use from 1973-2008, though the associated albedo change during that time was negligible because the region retained a forested type of ecosystem. Subsequently, our area averaged albedo values compare well with those of *Barnes and Roy* [2010]. The minima occur between 0.1175 – 0.13, but the minima appear to be declining over time as well. After removing the seasonal component, surface albedo monthly anomalies have a decreasing linear trend (slope = -0.000052) for $\alpha = 0.05$.

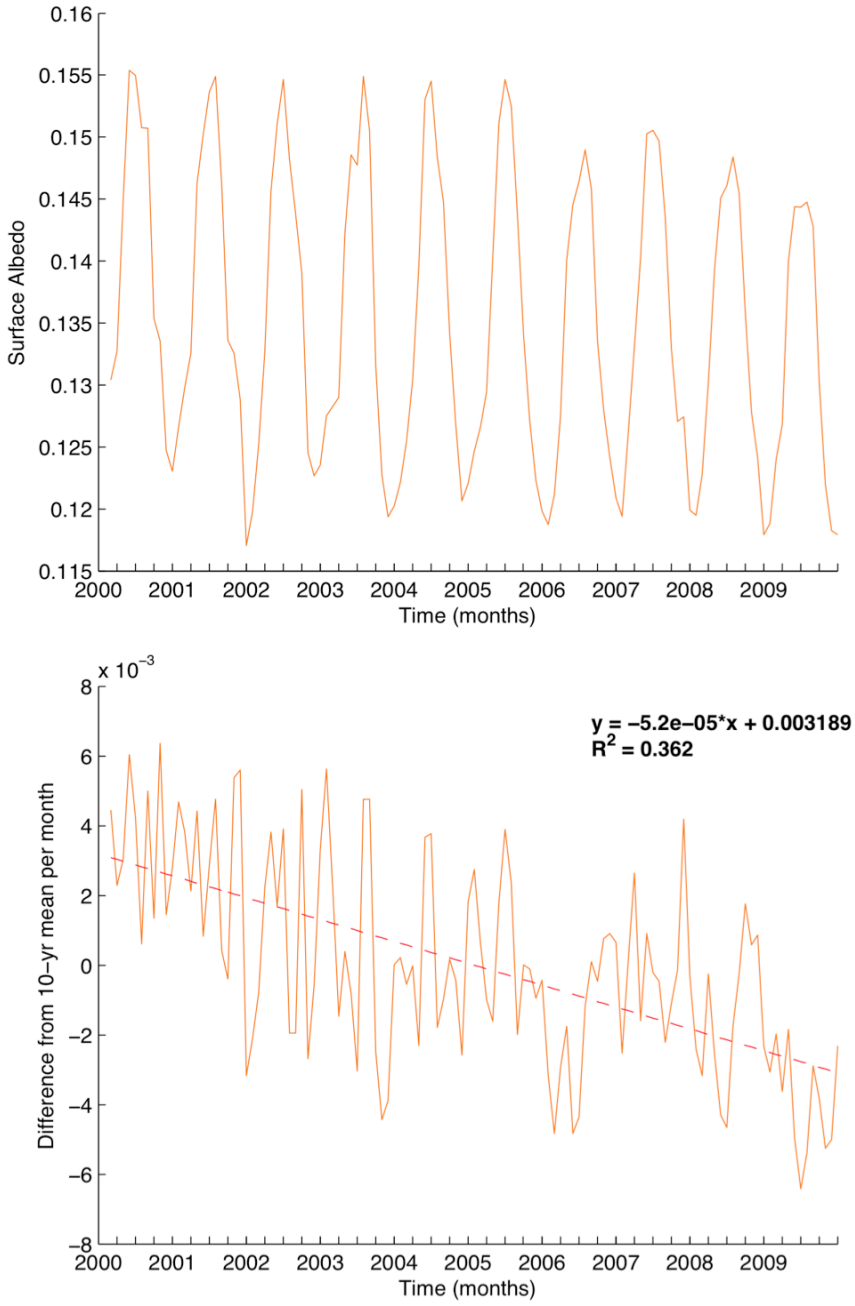

Figure 5.3: (top) Timeseries of monthly mean surface albedo. (bottom) Timeseries of monthly mean surface albedo anomalies. Linear regression information inset with figure.

5.2.2.2 Assessment of TOA Radiative Forcing Over the Past Decade

Independent Estimates of Radiative Forcing Due to AOD, Cloud Fraction and Surface Albedo

Functional analysis of Equation 5.1 provides some insight into the main drivers in the TOA radiative forcing calculations. Of the variables considered AOD would be the largest driver followed by cloud fraction then surface albedo. Yet the timeseries analysis revealed that cloud fraction varies the most with time, which could influence the behavior of the estimated TOA forcing. As discussed in Section 1.2.1, for these calculations of TOA radiative forcing, means of the variables are calculated for use in lieu of representative values along with the other equation constants, thus to assess the influence of each variable only this variable is allowed to vary with time.

Estimated TOA forcing only considering surface albedo and cloud fraction are shown in Figure 5.4, and the estimated TOA forcing only considering varying AOD (MODIS and MISR) are shown in Figure 5.5. Not surprisingly, the estimated forcing closely resembles the behavior of the input variables. Estimated TOA radiative forcing (ΔF = -8.14 to -7.68 W/m2) due only to surface albedo varied the least. ΔF varied between -8.9 and -4.5 W/m^2 due to cloud fraction. Only considering AOD yielded that largest variation in ΔF (-19 to -3.3 W/m^2) for MODIS. Using a timeseries of input data allows for understanding the dynamic nature of radiative forcing associated with changes in aerosol and other time-varying factors, instead of simplifying it down to a single value as was done in *Goldstein et al.* [2009] (ΔF = -3.9 W/m^2).

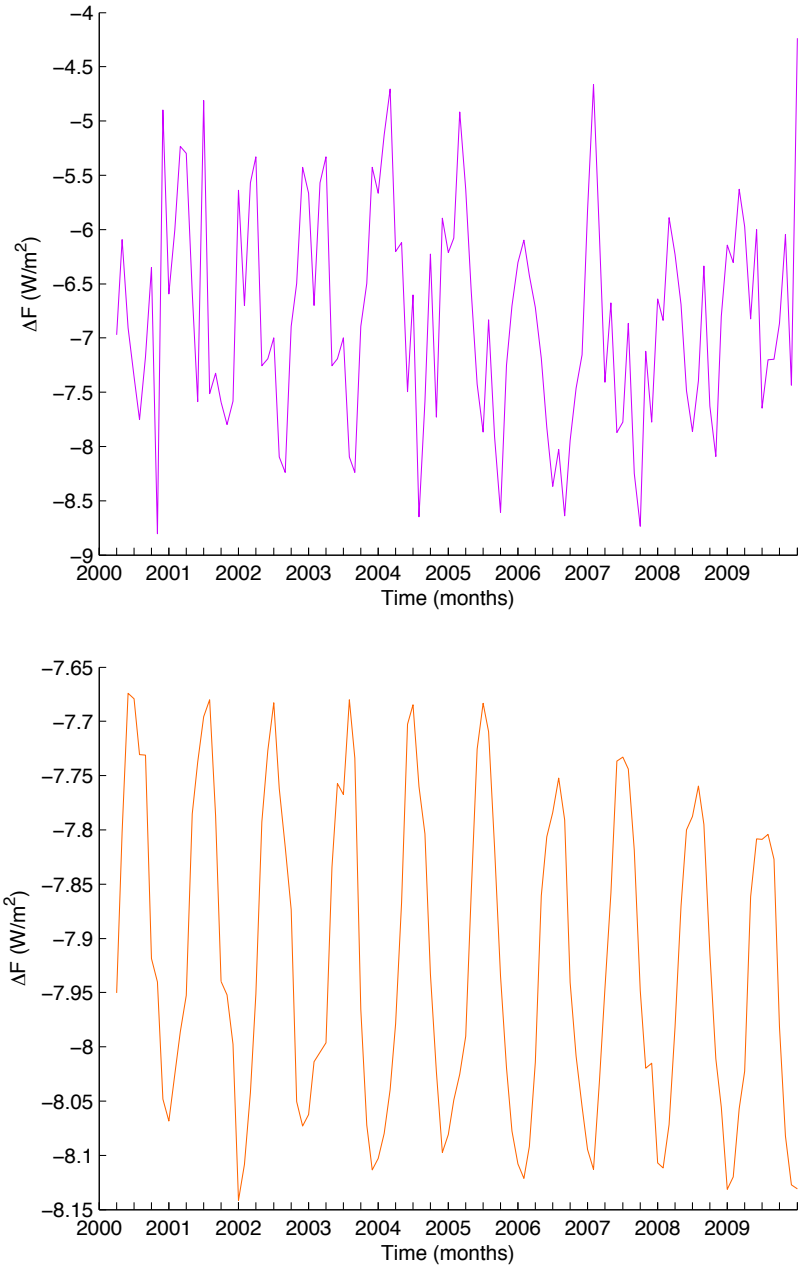

Figure 5.4: (top) Timeseries of estimated TOA radiative forcing due to only cloud fraction. (bottom) Timeseries of estimated TOA radiative forcing due to only surface albedo.

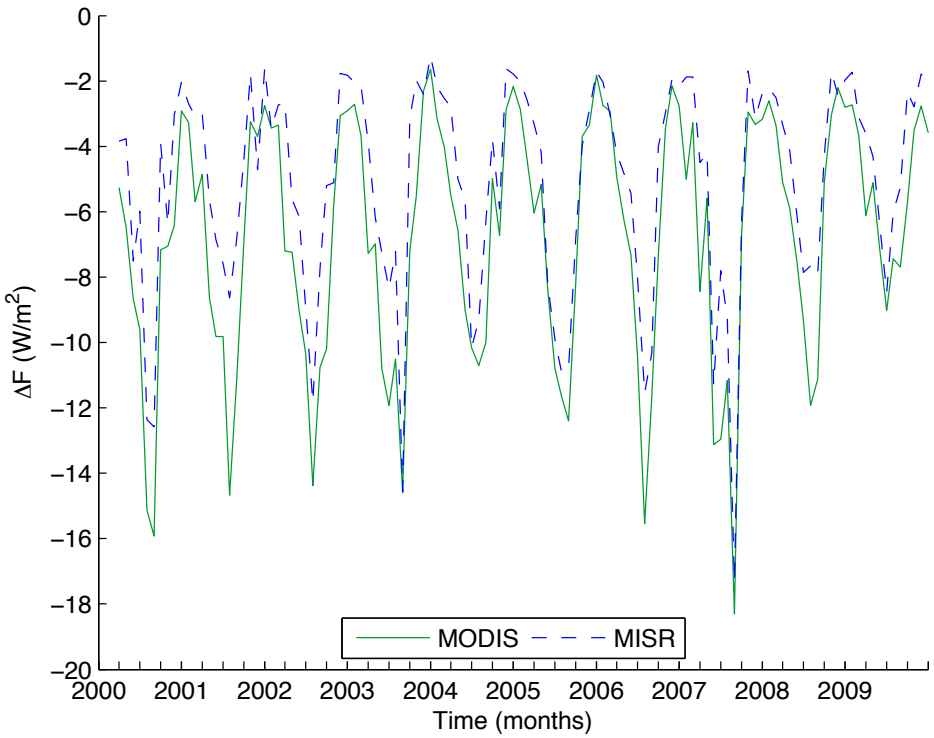

Figure 5.5: Timeseries of estimated TOA radiative forcing based on AOD from MODIS and MISR.

Surface-cloud and Aerosol Effects on Radiative Forcing

Estimates of TOA radiative forcing are modulated by the interaction between the different physical properties represented by variables and constants. How those estimates respond to only non-aerosol (non-AOD) variations are shown in Figure 5.6 (top). Figure 5.6 (bottom) shows how TOA radiative forcing responds to coupling MODIS AOD with either surface albedo or cloud fraction. Without time-varying aerosol effects, the radiative forcing resembles the timeseries of cloud fraction. It appears that surface albedo has a minor modulating effect that is most apparent in the minima shown in the teal line in Fig. 6(top). The addition of varying aerosol effects causes the radiative forcing to more closely resemble the MODIS AOD timeseries. However, cloud fraction does appear to

have an additive effect on radiative forcing more so than surface albedo as shown by the larger variation in the MODIS AOD and surface albedo timeseries (orange line, ΔF = -18.1 to -2.5 W/m^2) compared to the MODIS AOD and cloud fraction timeseries (purple line, ΔF = -23 to -2.4 W/m^2). Given the dynamics of cloud fraction, surface albedo and AOD our results seem to suggest that by using observations to estimate forcing instead of averaged values yields a more complete perspective of the climatic system.

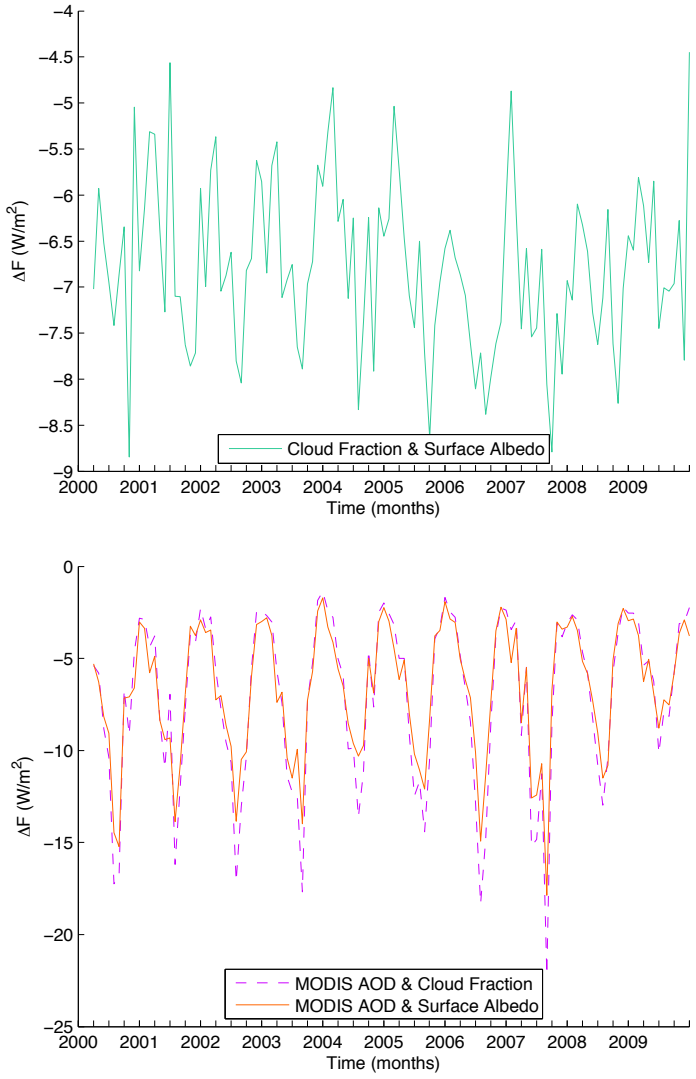

Figure 5.6: (top) Timeseries of estimated TOA radiative forcing due to cloud fraction and surface albedo. (bottom) Timeseries of estimated TOA radiative forcing due to aerosol effects. Orange line is the estimated forcing due to MODIS AOD and surface albedo. Purple line is the estimated forcing due to MODIS AOD and cloud fraction.

Sensitivity Analysis of SSA

Seasonal differences in aerosols not only affect concentration but also composition. A spatial analysis was performed using SSA from MISR averaged over 2000- 2009 is used to better understand the effect seasonality had on aerosol composition, see Figure 5.7. Both seasons appear to fairly uniform, though during the winter MISR had some retrieval errors. SSA range from lows of ~0.87 to highs of 0.96.

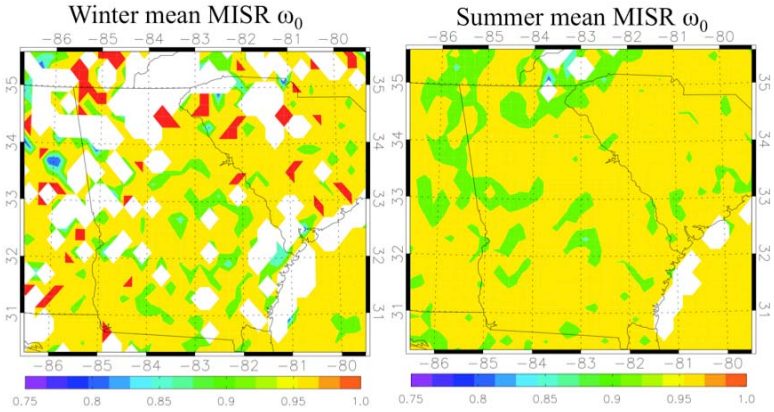

Figure 5.7: Maps of satellite derived winter and summer mean single scattering albedo from MISR onboard Terra.

The SSA used, 0.8, 0.85, and 0.9, are more consistent with measurements of SSA in the region [*Carrico et al.*, 2003], recalling that all previous estimates used a high SSA of 0.975, e.g., *Goldstein et al.* [2009]. We estimated TOA ΔF due to AOD, cloud fraction and surface albedo along with varying SSA (Figure 5.8). The lower the SSA results in less negative forcing most notable during the summer months. For instance, for SSA = 0.8 the largest maxima (most negative) of estimated forcing is approximately -19 W/m^2 for MODIS and -18 W/m^2 for MISR. Yet, for the cooler months when the forcing is at a minimum, varying SSA has little effect. If SSA fluctuated more (possibly due the influx

of different aerosols e.g., smoke) for this region then it is possible that it would have a more pronounced effect on the estimates of TOA radiative forcing.

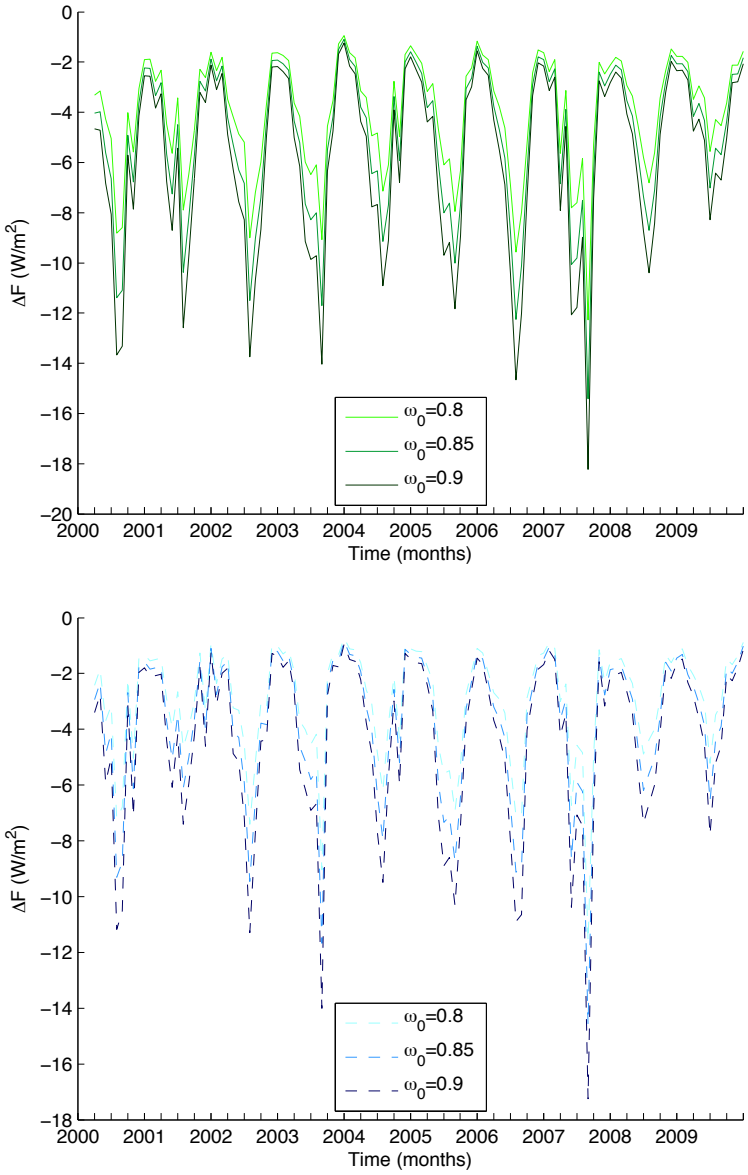

Figure 5.8: (top) Timeseries of estimated TOA radiative forcing based on MODIS AOD, cloud fraction and surface albedo for three different single scatting albedo (ω_0) values. (bottom) Timeseries of estimated TOA radiative forcing based on MISR AOD, cloud fraction and surface albedo for three different single scatting albedo (ω_0) values.

Combined AOD, Cloud Fraction and Surface Albedo Effects on Radiative Forcing

Allowing the AOD, cloud fraction and surface albedo to vary with time is a more reflective of actual variations in atmospheric and environmental conditions. We also allow the fractional day length (denoted D) in Eq. 5.1 to vary with time according to the latitude in Atlanta as a representative value of day length for the entire region. The behavior of the forcing estimates in Figure 5.9 appears similar to each other.

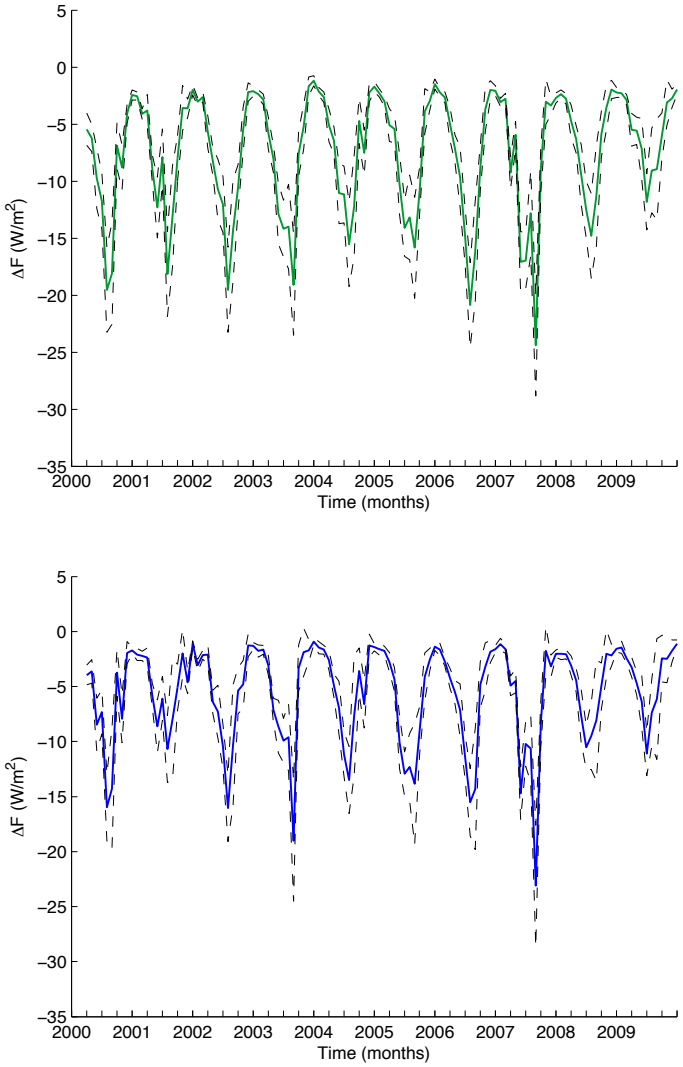

Figure 5.9: (top) Timeseries of estimated TOA radiative forcing based on MODIS AOD, cloud fraction and surface albedo. (bottom) Timeseries of estimated TOA radiative forcing based on MISR AOD, cloud fraction and surface albedo. The dashed black line represents +/- the standard deviation of the estimated radiative forcing.

Figure 5.9 resembles the behavior of the AOD and cloud fraction driven estimates of forcing in Figure 5.6. Closer examinations of the periods of increased negative forcing generally occur during periods of wildfire activity. The increased negative forcing around the summer of 2000 can be attributed to increases in AOD due to heavy wildfire activity (2000 and 2007) in the western portion of the U.S. (http://science.nasa.gov/science-news/science-at-nasa/2000/ast04aug_1m/). Also the increased negative forcing in 2007 is mainly due to two factors: 1) wildfire activity within the state of GA during May, and 2) events of aerosol transport into the region from wildfires in the western U.S. during late July and August. It is likely that these high AOD events as well as weather dynamics (e.g., high pressure systems that increase aerosol loading that take place during the summer) increase the standard deviation (STD) of the AOD and thus the estimated TOA forcing. Given the seasonality within the timeseries, we performed the standard deviation calculation on each respective month over all ten years e.g., all Januaries were combined to calculate the standard deviation of the estimated forcing for January and so on. The monthly mean (10-year mean of each respective month) of estimated forcing from MODIS during January is -2.47 +/- 0.351 W/m^2 and during July is -15.74+/-3.71 W/m^2. The January mean for MISR is -1.8 +/-0.55 W/m^2 and during July the mean is -12.11 +/-3.05 W/m^2.

During the cooler months, the minima (less negative) of radiative forcings vary between -6 to -3 W/m^2, and during the warmer months there is more variation with ΔF varying between -24 to -12.6 W/m^2 for MODIS and -22.5 to -11 W/m^2 for MISR. Yet if we take an average over time ΔF = -7.57 W/m^2 for MODIS and ΔF = -5.72 W/m^2 for MISR. The estimates of forcing presented here are more negative compared with the

results of *Carrico et al.* [2003] where they used the same first order approximation to estimate TOA radiative forcing (ΔF = -11.6 +/- 6 W/m^2) using instantaneous measurements of optical properties during six weeks in late summer 1999 in Atlanta. The estimates of direct TOA radiative forcing have a slightly increasing (less negative) linear trend, but it is not statistically significant. This result suggests that this region could be experiencing solar brightening. To determine if there is a true trend, we use a similar methodology here to calculate monthly radiative forcing anomalies by removing the seasonal signal from the timeseries as was used in Chapter 4. We then use the monthly anomalies to fit a linear regression, see Figure 5.10. Both anomaly timeseries show an increasing trend with time, which implies decreasing TOA forcing (less negative); however, only the anomalies for MODIS are statistically significant at the 95% confidence level where the slope is 0.012.

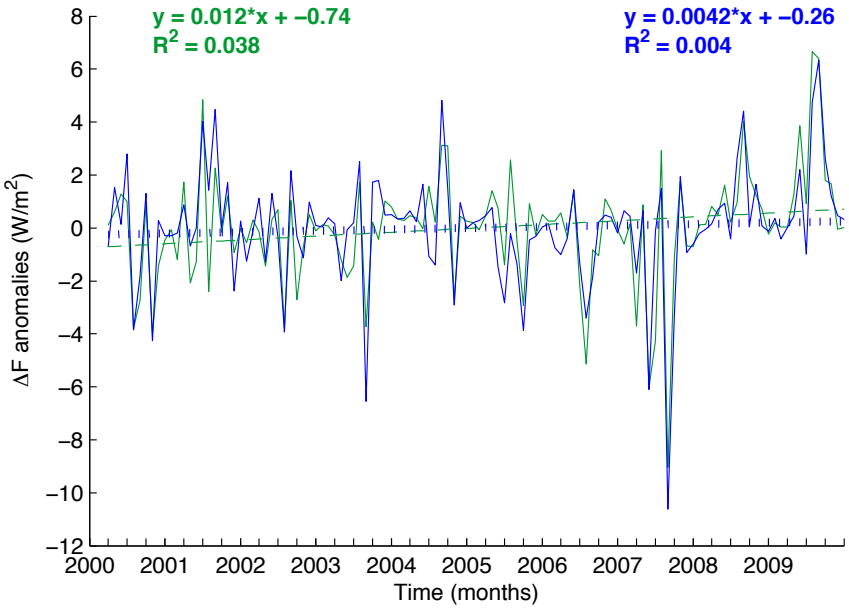

Figure 5.10 Timeseries of monthly anomalies of radiative forcing based on AOD for both MODIS (green) and MISR (blue).

To better visualize the differences between the estimated forcing considering only AOD from the forcing calculated using AOD, cloud fraction and surface albedo, we subtracted the AOD only estimates as shown in Figure 5.11.

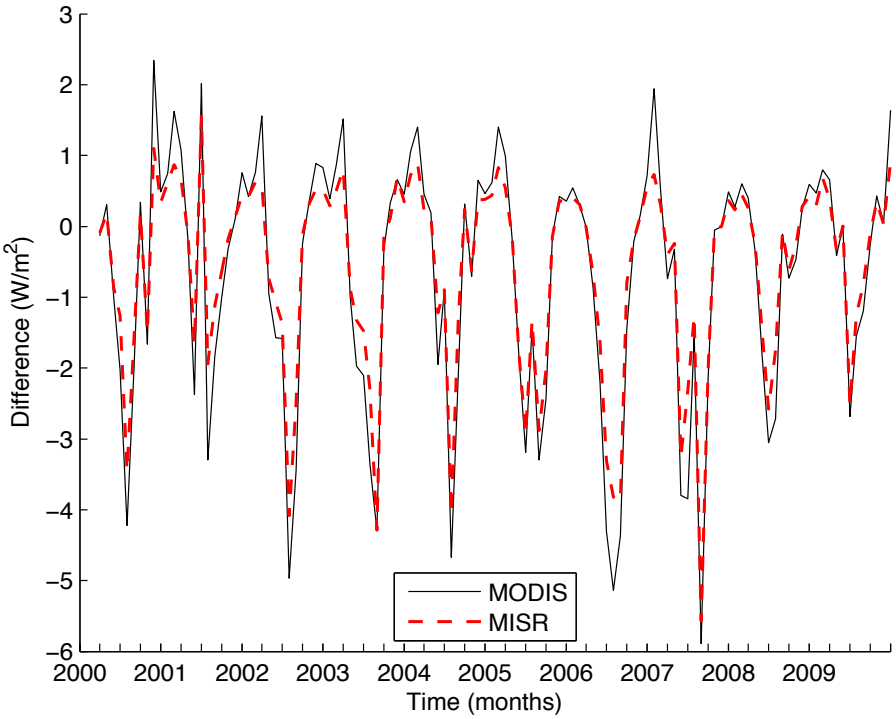

Figure 5.11: Timeseries of the difference in TOA radiative forcing where difference = TOA forcing due to AOD, cloud fraction and surface albedo – TOA forcing due to only AOD.

The convention is as follows: if the AOD only estimates are greater than the combined estimates then the difference is positive; however, if the AOD only estimates are less than the combined estimates then the difference is negative. During the cooler months the difference is between 1 and 2 W/m^2, which implies that the addition of surface-cloud effects reduces the estimated forcing during this time period. Not surprisingly, the largest difference was noted in the warmer months where the differences varied between -7 and -3 W/m^2. The aerosol-cloud effects appear to have an additive effect on the estimated forcing especially during periods of high AOD (increased negative forcing). For a first-

order approximation as shown here, the use of only AOD does provide information about the behavior of the TOA radiative forcing, yet by not including the aerosol-cloud effects your estimates are off by almost an amount equal to the standard deviation of the estimated forcing, which could introduce additional bias into the estimates.

To sum up major points of this analysis, first we have shown that using average values for either AOD, cloud fraction, surface albedo and SSA causes the seasonal characteristics to be lost in the TOA forcing estimates. Our analysis showed that by incorporating seasonal variations within the radiative forcing estimates leads to a more robust representation of forcings for this region. During the summer, TOA forcing can be as large as ~ 25 W/m^2 during biomass burning events and on average is ~ -11 to -15 W/m^2 using MODIS AOD and -10 to -12 W/m^2 using MISR AOD, which agrees well with results from *Carrico et al.* [2003], which found that TOA forcing was ~ 12 W/m^2. However, our results do not agree well with the estimated TOA forcing presented in *Goldstein et al*. [2009], which calculated TOA forcing due to summer aerosols around -4 W/m^2, yet our differences due to summer aerosols are almost double that. Nevertheless, recognizing the limitations of the first order assessment we perform more precise calculation of forcing through the use of a 1-D radiative transfer model that presented in Section 5.3.

5.3 Assessment of Aerosol Radiative Forcing with 1-D Radiative Transfer Modeling

5.3.1 Methodology for Optical and Radiative Transfer Modeling

To access the radiative impacts of aerosols many factors must be considered such as species, sources, concentrations, particle size distributions, atmospheric vertical structure, etc. In order to accurately represent regional Southeastern U. S. aerosols in both optical and radiative transfer models, we use information from both published literature and generic aerosol models. Based on this information we constructed cases that are representative of mixtures of aerosol species and concentrations for season (winter or summer), constituents (urban or background) and physical process (biomass burning and suspended organic aerosol layer). For each case the Mie optical modeling was performed to calculate the scattering and extinction coefficients, single scattering albedo (SSA or ω_0) and asymmetry parameter (g) for wavelengths encompassing the shortwave portion of the electromagnetic spectrum (0.3 – 2.0 μm). The AOD for each wavelength are calculated from computed extinction coefficients using satellite retrieved AOD at 550 nm or aerosol concentrations and the aerosol layer depth (see Section 5.3.1.1). The AOD, ω_0, and asymmetry parameter are used as input into the Santa Barbara Disort Atmospheric Radiative Transfer (SBDART) model (see Section 5.3.1.2) to calculate TOA and surface radiative fluxes and forcings. We examine daily mean forcings and their diurnal pattern.

5.3.1.1 Optical Modeling Using Mie Theory

The Mie code requires input of the microphysical properties of each respective assemblage of aerosols. We consider four aerosol species that make up most of the

measured $PM_{2.5}$: sulfates, organics, black carbon (BC) and nitrates [*Butler et al.*, 2003; *Edgerton et al.*, 2005]. Size distribution in terms of the parameters R_0 (the median radius) and σ (geometric standard deviation) of a log-normal function, and ρ (density) are taken from OPAC [*Hess et al, 1998*]. To account for hygroscopic effects on sulfates and nitrates, R_0 and the refractive indexes were calculated for each RH of interest, e.g., RH of 75% for the winter cases and 90% for the summer cases.

To address seasonality we compare the winter (W) with summer conditions (S) to create the four study cases: WB- Winter Background; WU-Winter Urban; SB-Summer Background, SU-Summer Urban. These cases were constructed based on aerosol composition data from the EPA's Air Quality System (http://www.epa.gov/airexplorer/). For sulfates we used ammoniated sulfates and for nitrates we used ammoniated nitrates based on EPA data. To construct representative compositional mixtures in terms of mass fraction of individual species, speciation concentrations were averaged for each season over all available data between years 2000 – 2009 (Figure 5.12).

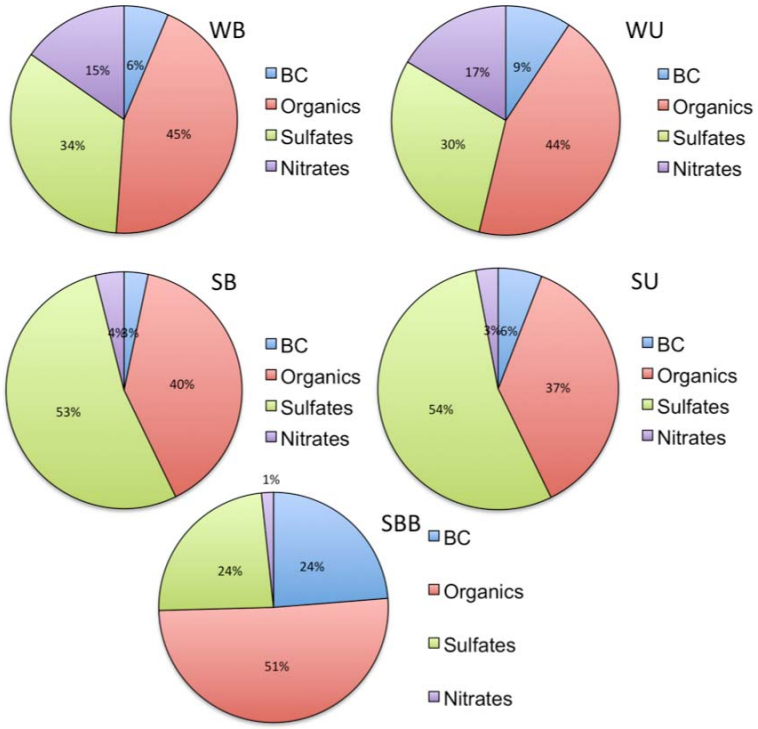

Figure 5.12: Mass fractions of BC, organics, sulfates and nitrates derived from EPA data and used in study cases (see also Table 5.1).

We consider the species to be externally mixed in keeping with satellite retrieval algorithms; however, there is observational evidence to support internal mixtures of BC with other aerosol species. For addressing this type of internal mixture, we follow a methodology similar to *Wang and Martin* [2007] and these cases will be denoted by WBi, WUi, SBi and SUi. We consider that all of the BC aerosols are covered by sulfate, and that internally mixed BC/Sulfate aerosols form an external mixture with Organics and Nitrates (at appropriate RH).

Table 5.1: Study case names and microphysical properties used in the optical modeling.

Model Cases								
	WB (Winter Background)				WU (Winter Urban)			
Microphysical Properties	BC	Organics	Sulfates 75%	Nitrates 75%	BC	Organics	Sulfates 75%	Nitrates 75%
R_0	0.01188	0.0296	0.0296	0.0296	0.0118	0.0296	0.0296	0.0296
ln σ	0.6931	0.8065	0.8065	0.8605	0.6931	0.8065	0.8065	0.8065
Density (ρ) (g/cm^3)	1.00	2.00	1.30	1.30	1.00	2.00	1.30	1.30
M*($\mu g/m^3$) /cm^{-3}	5.98E-05	2.81E-03	1.83E-03	1.83E-03	5.98E-05	2.81E-03	1.83E-03	1.83E-03
Mass Fraction	0.0636	0.4475	0.3359	0.1530	0.0933	0.4443	0.2976	0.1648
Number Fraction	0.7139	0.1067	0.1232	0.0561	0.7915	0.0801	0.0826	0.0457
	SB (Summer Background)				SU (Summer Urban)			
Microphysical Properties	BC	Organics	Sulfates 90%	Nitrates 90%	BC	Organics	Sulfates 90%	Nitrates 90%
R_0	0.0118	0.0348	0.0348	0.0348	0.0118	0.0348	0.0348	0.0348
ln σ	0.693	0.8065	0.8065	0.8065	0.6931	0.8065	0.8065	0.8065
Density (ρ) (g/cm^3)	1.00	2.00	1.18	1.18	1.00	2.00	1.18	1.18
M*($\mu g/m^3$) /cm^{-3}	5.98E-05	6.59E-03	4.28E-03	4.28E-03				
Mass Fraction	0.0330	0.3950	0.5329	0.0392	0.0590	0.3686	0.5426	0.0298
Number Fraction	0.7401	0.0805	0.1671	0.0123	0.8389	0.0475	0.1077	0.0059
	SBB (Summer Biomass Burning)							
R_0	0.011	0.0348	0.0348	0.0348				
ln σ	0.693	0.8065	0.8065	0.8065				
Density (ρ) (g/cm^3)	1.00	2.00	1.18	1.18				
M*($\mu g/m^3$) /cm^{-3}	5.98E-05	6.59E-03	4.28E-03	4.28E-03				
Mass Fraction	0.0217	0.6508	0.3037	0.0239				
Number Fraction	0.6743	0.1835	0.1319	0.0104				
	SALA (Summer Aerosol Layer Aloft) – Layer 1				SALA – Layer 2			
R_0	0.0118	0.0348	0.0348	0.0348		0.0348		
ln σ	0.693	0.8065	0.8065	0.8065		0.8065		
M*($\mu g/m^3$) /cm^{-3}	5.98E-05	6.59E-03	4.28E-03	4.28E-03		6.59E-03		
Density (ρ) (g/cm^3)	1.00	2.00	1.18	1.18		2.00		
Mass Fraction	0.0330	0.3950	0.5329	0.0392		1.00		
Number Fraction	0.7401	0.0805	0.1671	0.0123		1.00		

We calculate an effective refractive index based on the well-mixed sphere mixing rule [*Lesins et al.*, 2002] for a particle with the BC mass fraction presented in Table 5.1.

For the biomass burning case, $PM_{2.5}$ speciation mass measurements from the 2007 GA wildfire from the IMPROVE network are used [*Christopher et al.*, 2009]. Finally, for the aerosol layer aloft case, we use typical summertime aerosols for the first (lowest) layer, and the second layer is pure organics where measurements are provided by *Hennigan et al.* [2009]. CALIPSO is used to identify the frequency of this occurrence in the region, see Section 5.3.2.

The Mie model inputs and case names are summarized in Table 5.1. The parameter M* shown in Table 5.1 is the ratio of mass concentration and particle number concentration that was computed for each species to provide the conversion between mass concentration and particle number concentrations.

Mie optical model produces the normalized (per unit concentration) extinction, scattering and absorption coefficients, SSA, and asymmetry parameters for each species as a function of wavelength. The effective normalized coefficient of the external mixture is

$$k_{ext}^{eff}(\lambda) = \sum f_j k_j^{ext}(\lambda) \qquad (5.2)$$

where j represents each individual species, , and f_j is the number fraction. The effective normalized scattering coefficient is given by similar expression so that the effective SSA (ω_0) and the effective asymmetry parameter (g) are

$$\omega_0^{eff}(\lambda) = \frac{k_{sca}^{eff}(\lambda)}{k_{ext}^{eff}(\lambda)} \qquad (5.3)$$

$$g_{eff}(\lambda) = \frac{\sum f_j k_j^{sca}(\lambda) g_j(\lambda)}{k_{sca}^{eff}(\lambda)} \qquad (5.4)$$

From the calculations of the normalized effective extinction coefficient, the optical depth of a layer Δz with total particle number concentration N is

$$\tau(\lambda) = N k_{ext}^{eff}(\lambda)\Delta z \qquad (5.5)$$

Using satellite derived AOD at 550nm and layer depth (Δz) we can use Equation 5.4 to solve for the total number concentration per modeling case.

$$N = \frac{\tau(550)}{k_{ext}^{eff}(550)\Delta z} \qquad (5.6)$$

Multiplying $k_{ext}^{eff}(\lambda)$ by N gives the spectral AOD for each study case.

5.3.1.2 Radiative Transfer Modeling using SBDART

The Mie optical model output is used as input to SBDART in terms of considering boundary layer aerosols that are representative of southeastern U.S. Since this region is covered year round by evergreens, surface albedos do vary over seasons, but the magnitude of that variance is small, see Section 5.2.2.1, thus we use seasonal surface albedo values from MODIS. Since we are considering two seasons, we use the appropriate atmospheric profile (mid-latitude winter or mid-latitude summer). Table 5.2 summarizes the SBDART model inputs and Figure 5.13 presents a pictorial representation of the steps used for this modeling approach.

Table 5.2: SBDART model initialization for each study case

	Cases					
	WB	WU	SB	SU	SBB	SALA
Season	Mid-latitude Winter	Mid-latitude Winter	Mid-latitude Summer	Mid-latitude Summer	Mid-latitude Summer	Mid-latitude Summer
Wavelength min	0.3	0.3	0.3	0.3	0.3	0.3
Wavelength max	2	2	2	2	2	2
Albedo	0.12	0.12	0.15	0.15	0.15	0.15
SZA	50 - 85	50 - 85	10 – 84	10 – 84	10 - 84	10 – 84
AOD_{550nm}	0.04	0.09	0.28	0.34	0.7	L1= 0.04 L2= 0.24
Number of Layers	1	1	1	1	1	2
Layer Depth (km)	1	1	2	2	2	2 1

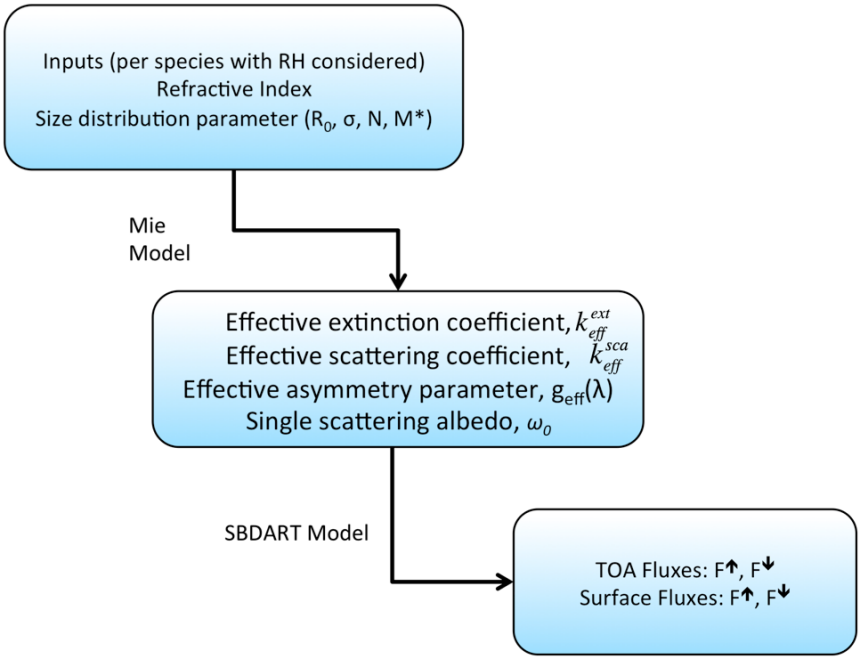

Figure 5.13: Schematic of general modeling approach

5.3.2 Vertical Profile Analysis of CALIPSO Data

Different aerosol layer depths or mixing layer thicknesses are considered also. To determine the thickness of the layer (shown in Table 5.2), one-year of CALIPSO browse images are used to determine "average" heights of those layers. We looked at winter overpasses (December 2008- February 2009) and summer overpasses (June 2009 – August 2009). We chose to use this year because we wanted a year with no problems with the laser and a year without any appreciable biomass burning in the region. Our analysis determined that during the winter, the aerosol layer was approximately 1km thick, and during the summer, the layer depth was about 2 km. Our analysis, which is summarized in Table 5.3and Table 5.4, revealed that during the winter, there are a number of days where there are no aerosols present or if there were some aerosols, they were not in sufficiently high enough concentration to have significant backscattering at 532nm. We also use this analysis to determine if there is a persistent organic aerosol layer aloft, and if there are two distinct layers, use the AOD and layer information from CALIPSO. Our analysis showed that there is no persistent aerosol layer aloft over this region, which is a tenet of the hypothesis from *Goldstein et al*. [2009]. Goldstein et al. offer different definitions of what "aloft" means, but they do not provide a clear single answer. Further casting doubt on this hypothesis is work by Heald et al. [2011] which concludes that data from 17 field experiments do not substantiate elevated SOA in the mid-troposphere where it is often predicted to be by models. It is possible that due to some of CALIPSO's limitations in the PBL and being able to discriminate between SOA and other aerosols, that there are aerosols present aloft so, we do consider a case where an

aerosol layer consisting of organics is aloft from a lower layer of typical summertime aerosols (SALA case).

Table 5.3: Aerosol layer analysis using CALIPSO browse images for winter 2008-2009. Attenuated= Signal attenuated; No Aerosols = No aerosols detected in the vertical feature mask; < = the 532nm total attenuated backscatter (km^{-1} sr^{-1}) is less than $2.0x10^{-2}$. Days without data that would have flown over area of interest: 1/11/09, 2/17/09, 2/19/09, 2/21/09, 2/24/09, 2/26/09, 2/28/09. Dashes denote missing data.

Winter			Layer 1		
Dates	Time (UTC)	# of layers	Layer Bottom (km)	Layer Top (km)	Layer Thickness
12/1/08	18:06	Attenuated	-	-	-
12/3/08	7:14	1	0.00	1.00	1.00
12/6/08	18:24	Attenuated	-	-	-
12/8/08	18:12	1	0.00	2.00	2.00
12/10/08	7:20	1	0.00	2.00	2.00
12/15/08	18:18	1	0.00	1.00	1.00
12/17/08	18:05	<	-	-	-
12/19/08	7:13	1	0.00	1.50	1.50
12/22/08	18:24	No Aerosols	-	-	-
12/24/08	18:12	1	0.00	1.00	1.00
12/26/08	7:20	1	0.00	1.00	1.00
12/31/08	18:18	No Aerosols	-	-	-
1/2/09	7:26	Attenuated	-	-	-
1/2/09	18:06	1	0.00	1.50	1.50
1/4/09	7:14	1	0.00	1.00	1.00
1/7/09	18:25	Attenuated	-	-	-
1/9/09	18:12	No Aerosols	-	-	-
1/16/09	18:19	Attenuated	-	-	-
1/18/09	7:41	<	-	-	-
1/20/09	7:15	Attenuated	0.00	1.50	1.50
1/23/09	18:26	1	-	-	-
1/25/09	18:14	No Aerosols	-	-	-
1/27/09	7:22	Attenuated	0.00	1.50	1.50
2/1/09	18:21		-	-	-
2/3/09	7:29	Attenuated	-	-	-
2/5/09	7:18	No Aerosols	0.00	1.00	1.00
2/8/09	18:28	1	0.00	1.00	-
2/10/09	18:16	1	0.00	1.50	-
2/12/09	7:24	1	0.00	1.00	1.00

Table 5.4: Aerosol layer analysis using CALIPSO browse images for summer 2009. Attenuated= Signal attenuated; < = the 532nm total attenuated backscatter (km^{-1} sr^{-1}) is less than $2.0x10^{-2}$. Dashes denote missing data.

Summer			Layer 1			Layer 2		
Dates	Time	# of layers	Layer	Layer	Layer	Layer	Layer	Layer
6/2/09	18:27	1	0.00	2.00	2.00	-	-	-
6/4/09	5:56	Attenuated	-	-	-	-	-	-
6/6/09	7:23	1	0.00	1.00	1.00	-	-	-
6/11/09	7:14	1	1.00	2.00	1.00	-	-	-
6/16/09	18:40	1	1.00	2.00	1.00	-	-	-
6/18/09	19:08	1	1.00	2.00	1.00	-	-	-
6/20/09	7:35	2	0.00	2.00	2.00	1.50	2.50	1.00
6/22/09	7:23	Attenuated	-	-	-	-	-	-
6/27/09	7:41	1	0.00	2.50	2.50	-	-	-
6/29/09	7:29	1	0.00	2.50	2.50	-	-	-
7/2/09	18:39	1	2.00	3.00	1.00	-	-	-
7/11/09	18:32	<				-	-	-
7/18/09	18:35	2	0.00	2.00	2.00	1.50	2.50	1.00
7/20/09	7:46	<	-	-	-	-	-	-
7/20/09	18:26	1	1.00	3.00	2.00	-	-	-
7/29/09	7:29	1	0.00	2.00	2.00	-	-	-
8/3/09	18:37	1	0.00	1.00	1.00	-	-	-
8/5/09	18:24	1	0.00	2.00	2.00	-	-	-
8/12/09	18:30	1	0.00	2.00	2.00	-	-	-
8/14/09	7:37	2	0.00	2.00	2.00	2.50	3.50	1.00
8/19/09	18:35	1	0.00	1.00	1.00	-	-	-
8/28/09	18:28	1	0.00	1.00	1.00	-	-	-

Our analysis revealed one date (August 14, 2009) where there were two distinct aerosol layers, see Figure 5.14. During this nighttime overpass, the lowest layer (0-2 km) is identified as polluted continental and has an AOD of 0.11, and the upper layer (2.5-3.5 km) is clean continental with an AOD of 0.03. Though CALIPSO's problem of misidentifying some polluted aerosols as polluted dust is still a minor issue, the majority of the aerosol typing was correct. While the CALIPSO derived AOD values are slightly on the low side, we have already established in Chapter 3 (Section 3.3.3.2) that problems with CALIPSO selecting the correct lidar ratio could be a possible reason why CALIPSO AOD is biased low against MODIS AOD [*Kittaka et al.*, 2011].We use our results from

the biomass burning case studies (see Chapter 3) to determine that for most of the biomass burning events there is only one layer of aerosols that is approximately 2 km thick (SBB case).

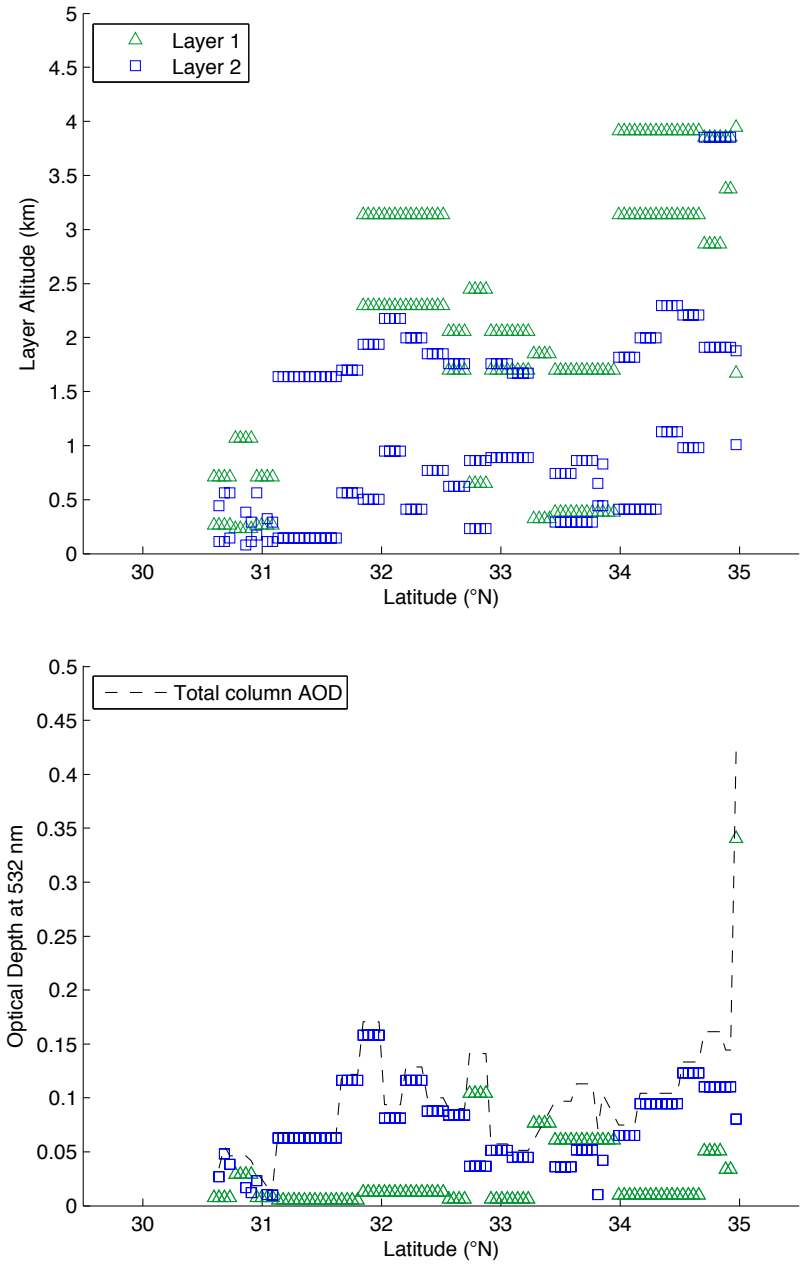

Figure 5.14: CALIPSO layer base and top (height), lidar ratio, and layer AOD for August 14, 2009 with an overpass time of 4:37am EDT.

5.3.3 Analysis of Optical Modeling Results of Southeastern U. S. Aerosols

Figure 5.15 shows the refractive indexes for sulfates and nitrates computed at multiple RH of 0% (dry salt), 50%, 75% (winter) and 90% (summer). As expected the only species with significant absorption as measured by the imaginary part of the refractive index is BC, Organics and the BC/Sulfate internal mixture. The other species can be called essentially light scattering. In the shorter wavelengths, sulfates and nitrates have different behaviors in their absorption spectra, but as wavelengths increase, the behavior of the two becomes similar. For nitrates, the dry salt has the strongest absorption relative to the other nitrate measurements at increasing RH. Sulfate behaves opposite of nitrate, where increases in RH lead to slightly more absorption. In the scattering spectra for sulfates and nitrates, the dry salts are the most scattering, while the uptake of water leads to decreases in scattering.

The Mie optical model requires each species be modeled individually and the external mixture of aerosols is done afterward for each study case outlined in Table 5.1. Figure 5.16 shows the normalized (per unit concentration) extinction coefficient and ω_0 for each species. The behaviors of the extinction and ω_0 curves are similar for sulfates and nitrates. The single scattering albedo (ω_0) provides additional information that can be used in interpreting the optical depth. The single scattering albedo is defined as the ratio between the scattering coefficient and the extinction coefficient. A high value of ω_0 implies that scattering is more dominant, vice versa small values imply absorption is more dominant. BC has the smallest extinction, but has the lowest ω_0, while ω_0 for organics falls in between the other species.

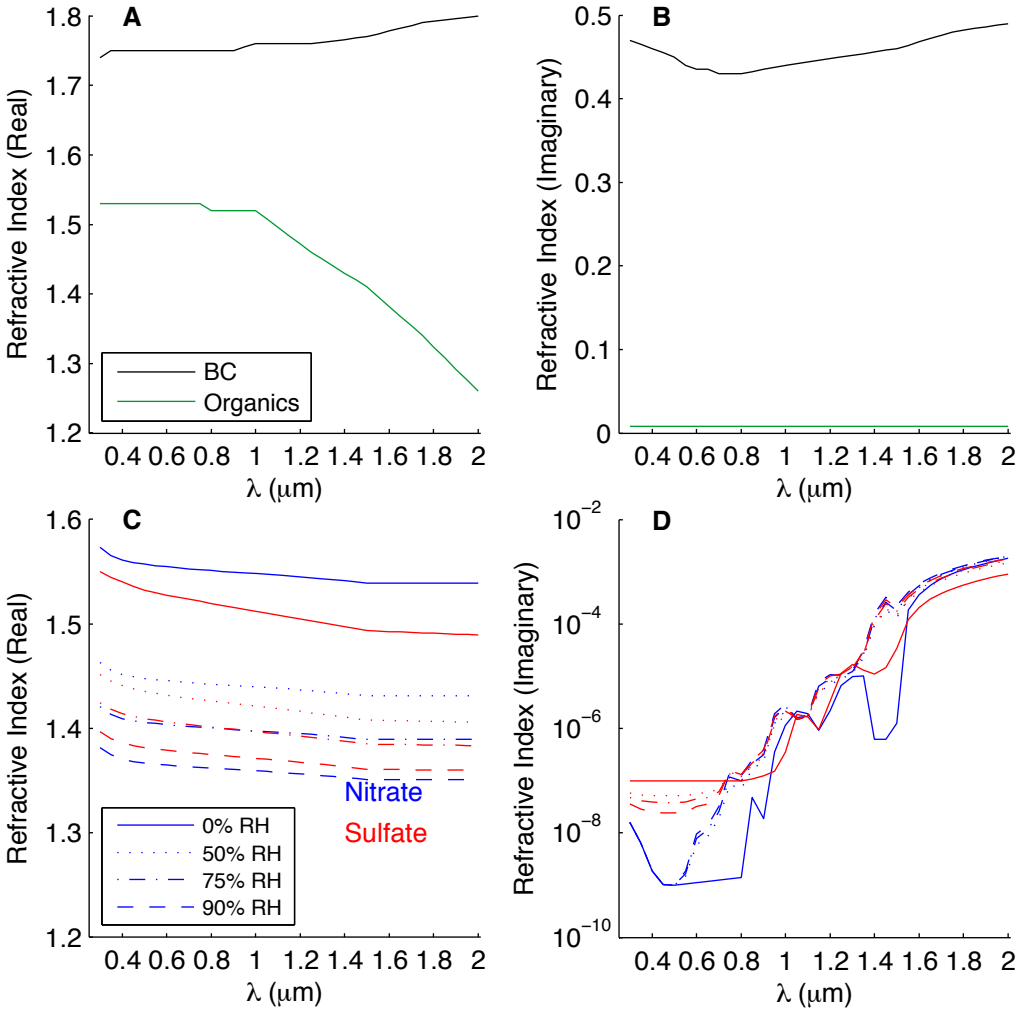

Figure 5.15: Real and imaginary parts of the refractive indexes for (A) BC, (B) organics, (C) nitrates, and (D) sulfates for wavelengths 0.3-2.0 μm. Nitrates and sulfates are shown for 0%, 50%, 75% and 90% RH.

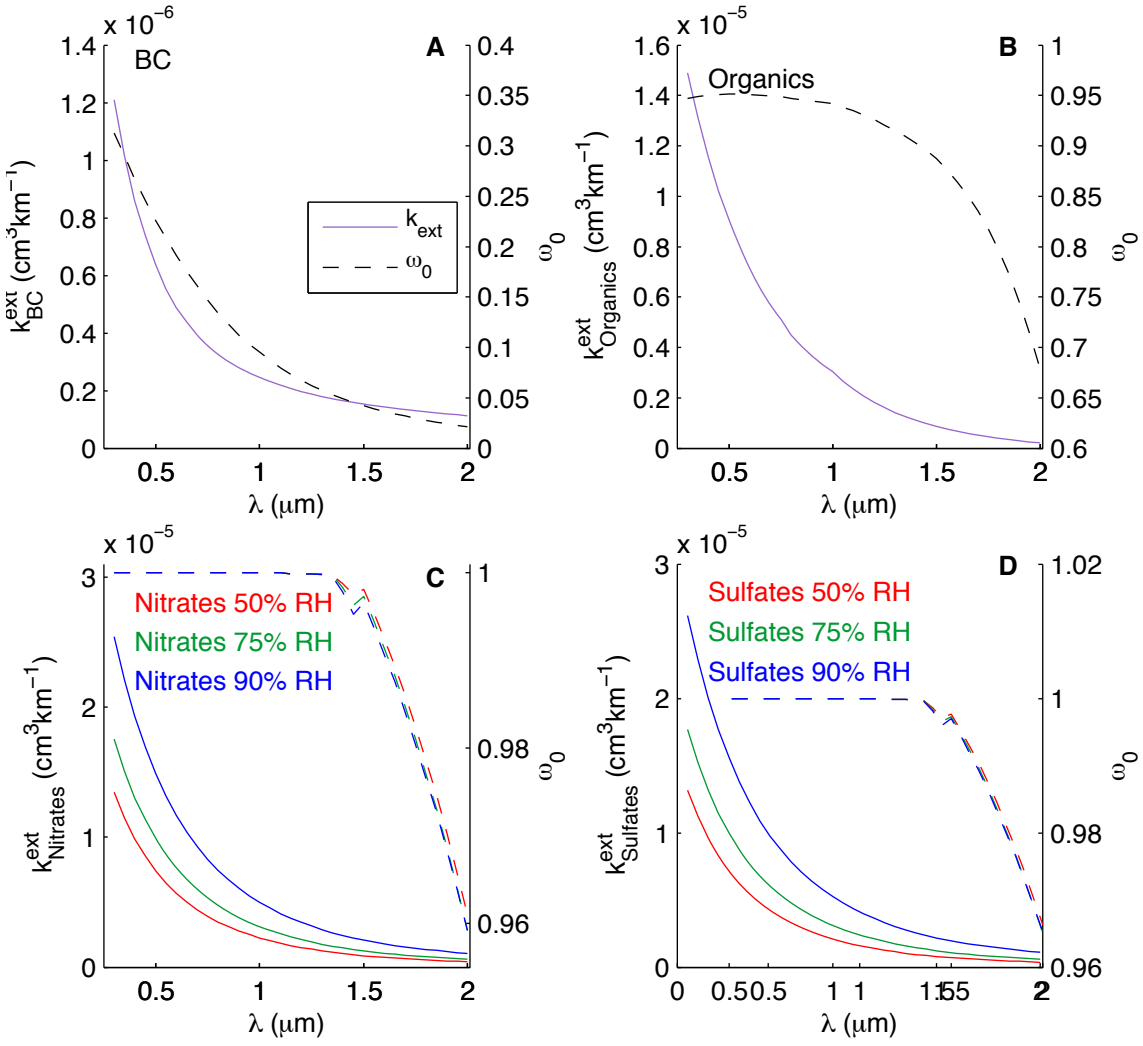

Figure 5.16: Normalized extinction coefficient (k_j^{eff}) and ω_0 for BC (A), organics (B), nitrates (C), and sulfates (D) for wavelengths 0.3 – 2.0 μm. For nitrates and sulfates at RH of 50%, 75% and 90%.

The outputs from the optical model are normalized properties and must be multiplied by the number concentrations per species for each case to obtain effective layer properties. Earlier MODIS AOD analyses from Chapters 2 and 4 were used to determine a representative AOD at 550 nm for each study case. Through Equations 5.2 and 5.6 we can then calculate the total number concentration, which can then be multiplied by the effective normalized extinction coefficient to determine the spectral

AOD for 0.2 – 2.0 μm. The spectral AOD (or τ) are shown in Figure 5.17. We used AOD from MODIS from earlier analyses in Chapter 2 and 4. The addition of a layer of organics above typical summer background conditions causes increased extinction. The biomass burning case (SBB) had the highest spectral AOD with values around 1.2 in the visible range, and the winter cases have the lowest AOD with values below 0.2. Though these effective properties are tuned to match satellite observed AOD, it would be useful to compare the spectral properties with those from AERONET; however, there are no AERONET stations in our region of interest. The effective asymmetry parameter (g) behaves similarly for all of the cases, with small differences between the cases (Figure 5.17). In fact, for the winter and summer cases, they are virtually the same. The urban cases have the lowest effective ω_0, followed by the background winter conditions. The cases with the highest ω_0 are the winter cases and the aerosol layer aloft (SALA). These effective ω_0 agree well with published literature data that show that scattering aerosols dominate this region [*Edgerton et al.*, 2005; *Tombach and Brewer*, 2005; *Blanchard et al.*, 2011; *Heald et al.*, 2011]. Also, these ω_0 agree well with satellite estimates of ω_0 from MISR, see Figure 5.7, though for the internal mixture SSA values are lower with ranges in the visible spectrum around 0.7 – 0.8. *Wang and Martin* [2007] found a similar result in SSA relating to external mixtures and internal mixtures.

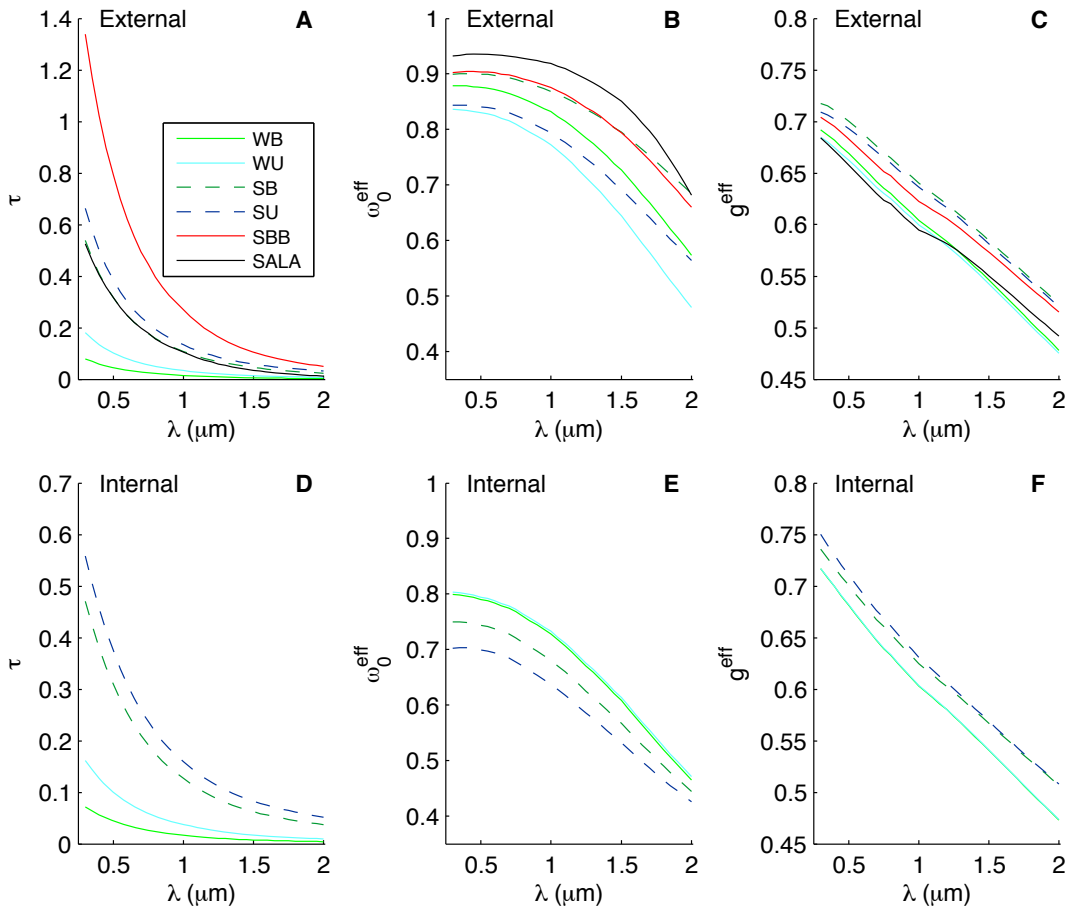

Figure 5.17: Effective AOD (τ), asymmetry parameter (g), and ω_0 for wavelengths 0.3 – 2.0 μm for each study case, considering the external aerosol mixtures (A, B, C) or internal mixtures (D, E, F).

5.3.4 Analysis of Modeled Radiative Forcing

Earlier in Section 5.2 we performed an estimate of TOA radiative forcing using the first order approximation where we used timeseries of surface albedo, cloud fraction and satellite AOD from both MODIS and MISR. However, that approximation is only applicable to TOA and cannot be used to determine the extent of surface forcing, not only for typical conditions (e.g., WB, SB) but for special cases such as biomass burning or deciphering the presence of an organic aerosol layer aloft. Thus we use the SBDART

radiative model to perform an assessment of TOA and surface forcing for our study cases (see Tables 5.1 and 5.2).

We define the radiative forcing as the difference in fluxes between clean atmosphere (refers to the model run without any aerosols) and aerosols (refers to the model run with aerosols as specified in Tables 5.1 and 5.2):

$$\Delta F_{TOA} = F_{TOA}^{\uparrow Clean} - F_{TOA}^{\uparrow Aerosols} \quad (5.7)$$

$$\Delta F_{Surface} = F_{Surface}^{\downarrow Aerosols} - F_{Surface}^{\downarrow Clean} \quad (5.8)$$

Equations 5.7 and 5.8 represent the direction of the fluxes: $\uparrow$ = upward flux and $\downarrow$ = downward flux. Using this convention negative values of ΔF are indicative of net aerosol cooling, and positive values are indicative if net aerosol warming.

Comparisons between the different cases are dependent upon aerosol speciation, concentration and RH, so we define the radiative forcing efficiency (RFE) as

$$RFE = \frac{\partial(\Delta F)}{\partial(\tau_{550nm})} \quad (5.9)$$

RFE is a useful metric because is removes aerosol load dependence. We use representative AOD at 550nm from MODIS for each study case (see Table 5.2). RFE is calculated for both the TOA and surface forcings. The units for RFE are $W/m^2\ \tau^{-1}$.

Figure 5.18 presents the results of daily mean TOA and surface forcing and RFE for the study cases considering the external mixture. All study cases result in negative TOA and surface forcing. The special summer cases SBB (biomass burning) and SALA (organic aerosol layer aloft) have the largest forcings in absolute terms. During the winter, modeled TOA forcing is -2.8 and -5 W/m^2 for the WB and WU cases, and these values generally agree with the estimated forcing given earlier in this chapter in Section

5.2.2.2. The modeled summer TOA forcings (SB = -13.3 W/m^2) also generally agree well with earlier estimates. Interestingly the study case that is representative of the Atlanta metropolitan area has less forcing (SU = -3.3 W/m^2) in absolute terms compared with background conditions that can be explained by relatively lower SSA as discussed below. All of the aerosol cases result in negative surface forcing (cooling). The SBB case had the largest degree of surface cooling, with the next highest being the summer cases. All of these estimates of forcing presented in this Chapter are significantly higher than those predicted by the IPCC (1.5 W/m^2) [*Forster et al*., 2007], though they consider global TOA forcing (~1.5 W/m2) as opposed to our regional study.

Figure 5.18 also shows that there is less variability in RFE at the TOA. We find that the urban cases have higher RFE at the TOA than background conditions at the surface, yet WB, WU, SB have RFE that vary between -40 to -70 W/m^2 τ^{-1}. The SU case is unexpected in terms of comparing its RFE from the surface with the TOA. The SU case has the lowest RFE for TOA forcing of -9.8 W/m^2 τ^{-1}, yet has the largest RFE for surface forcing of -406.7 W/m^2 τ^{-1}. As Figure 5.12 shows the SU case has slightly more BC than the SB case, it is likely this increase in BC lead to a less cooing, i.e., less negative TOA forcing. This suggests that the region experiences TOA cooling year around as opposed to just the summer as is implied in *Goldstein et al*. [2009]. Interestingly, the biomass burning case (SBB) has similar forcing efficiencies (-44 W/m^2 τ^{-1}) to that of summer background conditions (-47.6 W/m^2 τ^{-1}). This has an interesting implication for those situations where biomass burning aerosols are located aloft, our results suggest that in those cases the surface may experience increased surface level forcing.

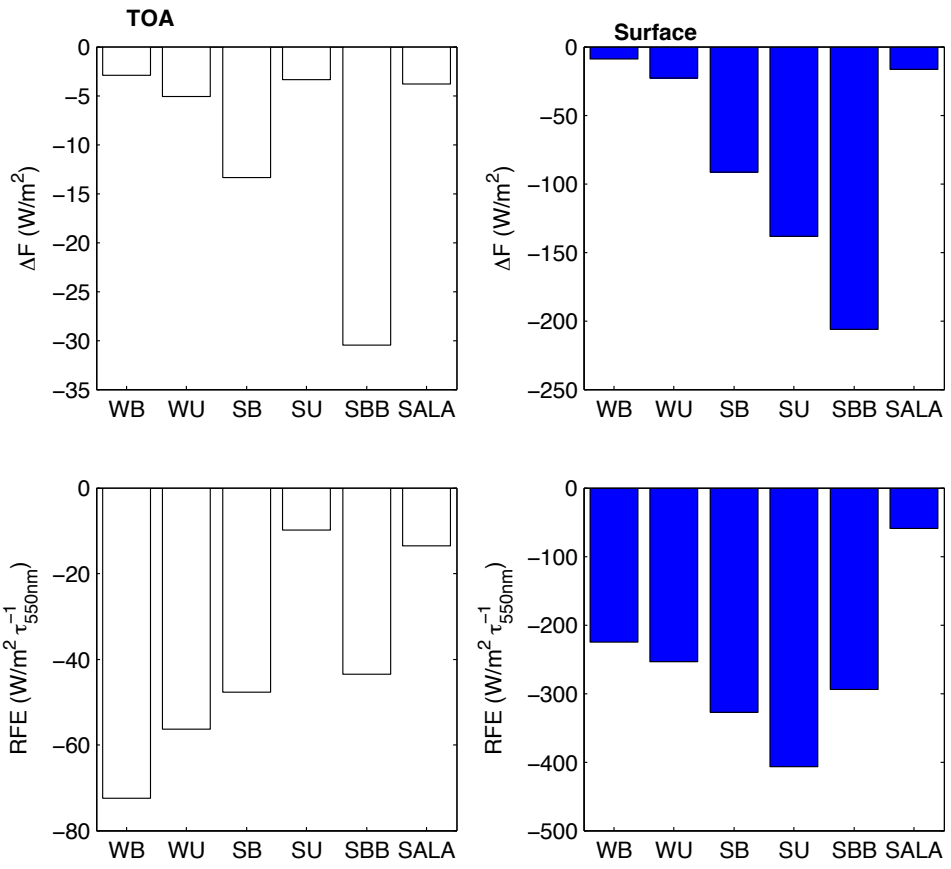

Figure 5.18: Modeled daily mean radiative forcing and its radiative forcing efficiency (RFE) at the TOA and surface for the study cases.

Previous studies demonstrated that the internal mixing of BC with other species leads to higher light absorption, i.e., lower SSA [*Lesins et al.*, 2002]. For a certain AOD and surface albedo, decreasing SSA will result in less negative TOA forcing, and even may cause a positive TOA forcing. Unfortunately, there are no measurements available to quantify the BC fraction internally mixed with other aerosol. The case of complete coating of BC by sulfates considered here is likely to give the lowest SSA, and thus helps to bracket the extent of the effect.

For the internally mixed cases, we show TOA forcing as a function of hour in Figure 5.19. Our analysis shows that for a majority of the day, TOA forcing is positive

for the summer cases. We believe that the lower SSA (i.e., different chemical composition: Sulfate coated BC) associated with these cases and high solar zenith angle leads to the sign change in TOA forcing. Thus when means are calculated of these internally mixed cases, the summer cases have positive mean TOA of 12.4 W/m^2 for SBi and 21.6 W/m^2 for SUi. The winter cases have negative mean TOA forcings of -1.4 W/m^2 for WBi and -3.6 W/m^2 for WUi, which are lower than the mean TOA for the externally mixed cases WB and WU. It should be noted, that the mean forcing for WUi agrees very well with the estimated forcing of *Goldstein et al.* [2009] of -3.9 W/m^2, which is interesting considering that in their study they considered a much larger region and did not consider different chemical speciation of aerosols.

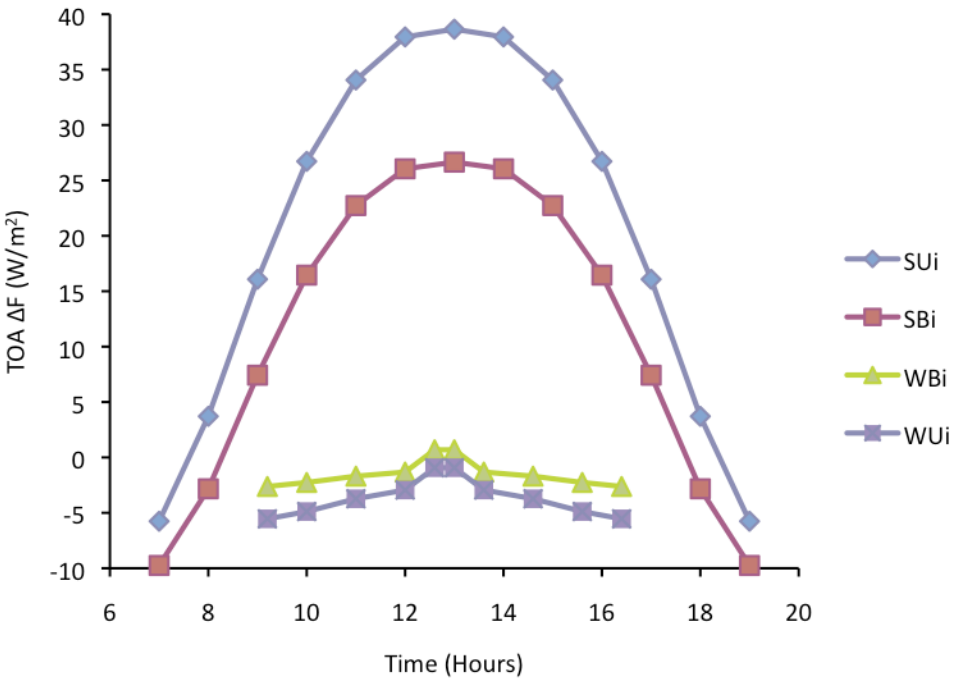

Figure 5.19: Diurnal pattern of TOA forcing as a function of time (SZA) for the internal study cases.

5.4 Chapter Summary

The primary goal of this research was to estimate the regional TOA aerosol direct radiative forcing and its dynamical nature over the past decade in the U. S. Southeast by accounting for changes in cloud cover, surface albedo and aerosol loading through AOD as measured by satellite. The use of ten year datasets allows for understanding how these variables and TOA direct radiative forcing change from a seasonal perspective. By exploring seasonality differences in aerosol composition and concentration can be taken into account. The AOD datasets from MODIS and MISR (both sensors onboard the Terra satellite) have decreasing linear trends. The MODIS AOD linear trend (slope = -0.000415) is statistically significant using a t-test statistic for $\alpha = 0.05$. Also, the surface albedo from MODIS shows a statistically significant decreasing linear trend (slope = -0.000052) for $\alpha = 0.05$, while cloud fraction from MODIS does not have an apparent trend.

Through varying AOD, cloud fraction and surface albedo one variable at a time while all other variables are kept constant allowed determination of the major drivers of direct TOA radiative forcing. AOD was a major driver of the estimated forcing calculations, while surface albedo and cloud fraction have modulating impacts on the influence of AOD on the estimated forcing. Allowing AOD, surface albedo, and cloud fraction to all vary gives a broad range of estimates of direct TOA radiative forcing from around -28 to -3 W/m^2. During the cooler months radiative forcing varies between –28 to -11 W/m^2, and during the warmer months the forcing varies between -28 to -12.6 W/m^2 for MODIS and -26 to -11 W/m^2 for MISR. In comparison, *Goldstein et al.* [2009] estimated the TOA radiative forcing was -3.9 W/m^2. The results of this study suggest that

this one value is overly simplistic and it does not provide any insight into the distinct seasonality of the aerosols in the U. S. Southeast. Additionally, these results expand the findings of *Alston et al*. [2011b] which suggests that this region is experiencing solar brightening as shown by a slightly increasing linear trend within the estimated direct TOA radiative forcing dataset.

The results from the SSA sensitivity analysis provide some interesting connections. SSA of 0.8, 0.85, and 0.9 were considered for all input variables varying, and during the warmer months the difference between the estimates based on SSA were pronounced. As expected, higher SSA yielded increased TOA radiative forcing (negative values). The timeseries of AOD revealed increased AOD associated with wildfires both locally and transported into the region. These smoke aerosols increase AOD, but they are more light absorbing than sulfate-based aerosols due to increased amounts of black carbon. Presently these wildfire impacts usually encompass one season. If the climate continues to change to a warmer equilibrium it is possible that the spatial extent and duration of the wildfires will increase, which will ultimately change the concentration and composition of aerosols in this region. We calculated monthly anomalies of estimated TOA forcing, and we found that with time there is a positive trend, which implies the region is experiencing less radiative cooling. The trend based on estimated TOA forcing for both satellites was positive; however, only the MODIS Terra trend was statistically significant at the 95% confidence interval. One implication from the result is that this region is experiencing solar brightening, though a longer timeseries will give statistical credence to this assertion.

The second part of this chapter focused on modeling radiative forcing at the TOA and surface through the use of an optical model and 1-D radiative transfer model (SBDART). We used representative microphysical properties to calculate optical properties of BC, organics, sulfates and nitrates as external mixtures. We also considered study cases where BC was coated with sulfate for an internal mixture. We used results from the Mie optical model of the effective aerosol layer properties to predict surface and TOA forcing using SBDART. We found that all of externally mixed aerosol cases considered resulted in negative TOA radiative forcing. The radiative forcing efficiency at the TOA varied from -9 to -72 W/m^2 τ^{-1}, while RFE at the surface varied from -50 to -410 W/m^2 τ^{-1}. Interestingly the RFE at the TOA was similar for the winter cases, and the modeled TOA forcing was more similar to the estimated forcing calculated by *Goldstein et al.* [2009]. The RFE of biomass burning both at the TOA and surface are similar to the RFE of summer background aerosol. This result has direct implications for biomass burning radiative effects in this region especially in the context of a potentially warming climate. The interpretation of the internally mixed cases are slightly more ambiguous, in that the diurnal TOA forcing for the SBi and SUi cases show positive values for most of the day. Since a majority of the day results in positive TOA forcing, the mean TOA forcing for these cases are 12.4 W/m^2 and 21.6 W/m^2. While the winter cases have negative mean TOA, their values (WBi = -1.4 W/m^2 and WUi = -3.6 W/m^2) are lower than those of the externally mixed cases.

CHAPTER 6

CONCLUSIONS

6.1 Dissertation Summary and Discussion

From their orbits high above, satellites have the unique ability to monitor life, weather and phenomena unlike earthly bound observers. As technology has advanced so has our understanding of science, especially atmospheric science. Today, there are multitudes of flying orbiters that provide an array of pertinent measurements to unlock the ever-changing state of our atmosphere. These satellites can be thought of as taking pictures with different types of lenses to glean different information, an apt description of using satellites for aerosol applications. Yet a satellite's operational life is short, thus we must plumb the depths of data they create. In that regard, this research developed and implemented methodologies for using satellite remotely sensed data in conjunction with ground based observations and modeling for characterization of regional aerosol variations with applications to air quality and climate studies in the Southeastern U. S.

This region is characterized by a sub-tropical climate, which includes humid wet summers and relatively mild winters. Though this region has a few large metropolitan areas, a significant portion of it remains covered in forests, which are natural source of biogenic emissions of volatile organic compounds, which thought to result in secondary organic aerosol (SOA) formation [*Lee et al.*, 2010; *Blanchard et al.*, 2011; *Heald et al.*, 2011]. It is this interplay between man and nature that creates a unique characteristics chemical composition of aerosol for this region. This region is scientifically interesting because of the intersection of a large source of biogenic aerosols with anthropogenic

influences, e.g., transportation, industry, etc. Some research has been done to quantify those influences from both ground and in-situ measurements [*Solomon et al.*, 2003; *Weber et al.*, 2007; *Hennigan et al.*, 2009]. Though much of the aerosol research has focused upon summer conditions, we strive to broaden and deepen those studies by building on the foundation previously laid through investigating different time and spatial scales and fusion of satellite data from an air quality and climatic perspective, examining the decade-long record of aerosol observations from space and ground.

The goals of this research presented in Chapter 1 were achieved through a combination of data analysis, data fusion, time series, and statistical analysis of multiple satellite sensors, e.g. MODIS, MISR, OMI and CALIPSO, and ground based measurements of aerosols, namely $PM_{2.5}$ and their composition. Data analysis was performed in conjunction with optical and radiative transfer modeling. This dissertation provides a framework for integrating satellite observations in ways that benefit societal health now (air quality) and in the future (climate).

We performed an assessment of air quality in the metropolitan Atlanta, GA area through the close integration of ground based measurements and satellites during the spring and summer season of 2004-2008 (Chapter 2). One of the first tasks was to create datasets of $PM_{2.5}$ that were close in time to MODIS Terra and MODIS Aqua overpass times of 10:30am and 1:30pm respectively. Comparison between $PM_{2.5}$ (Figure 2.2) and AOD (Figure 2.4) shows that MODIS AOD captures the seasonal and yearly variability reasonably well. Some information about diurnal behavior is retained, though as shown in Figure 2.3 the two datasets ($PM_{2.5,T}$ (for Terra overpass) and $PM_{2.5,A}$ (for Aqua overpass) correlated very well with R^2 varying between 0.78-0.85. Performing linear regressions of

MODIS Terra AOD vs. $PM_{2.5,24}$ and MODIS Aqua AOD vs. $PM_{2.5,24}$ further quantified how well AOD from both MODIS sensors encompassed the variability within the $PM_{2.5}$ datasets, see Table 2.4 and Table 2.5. Correlation coefficients with Aqua vary between 0.37 and 0.76, and Terra has r -values (correlation values) of 0.25–0.68. Information about aerosol composition was derived from the analysis of OMI AI. We found that mean AI for the Atlanta metropolitan area was around 0.3. This low value is due to the presence of relatively few absorbing aerosols among the majority of mildly UV-scattering aerosols that have lower AI. This means AI can be used as a background baseline for the area to identify transport of absorbing aerosols into the area, for instance, from biomass burning events or long-range transport of heavy pollution episodes. We also compared the two MODIS sensors and found that the two despite different overpass times agree well with each other with correlations greater than 0.78 (Figure 2.6).

With the robustness of the $PM_{2.5}$-AOD relationship established, we developed a probabilistic threshold approach to use AOD as proxy for $PM_{2.5}$ concentrations. This approach was novel in that it is not directly tied to a single linear regression, but rather is related to the linear regression statistics with time that allows for a more robust approximation between $PM_{2.5}$ and AOD. An example of the statistics associated with this method is that 80% of green AQI days have AOD below 0.3 (Figure 2.8). The threshold method predictions of Code Green and Code Yellow days based on AOD agree well with $PM_{2.5}$ based Code Green and Code Yellow days (Figure 2.9). With more years and exceptional events this method has the potential to improve upon its predictive capabilities with regards to Code Orange and Code Red days.

The following chapter (Chapter 3) delves into understanding the impact of wildfires on increases in AOD and $PM_{2.5}$. The large wildfire that occurred in the Southeastern part of GA in 2007 caused the increase in aerosol loading. This case study was done to examine the utility of using multi-satellite sensor data as a tool for characterizing biomass burning effects on the metropolitan Atlanta area. Using the methodology (developed in Chapter 2) of spatial and temporal averaging of the $PM_{2.5}$ datasets with the MODIS AOD datasets (Terra and Aqua), we determined that during the active burn period May 2007 there were 6 air quality exceedance days (5/4, 5/16, 5/22, 5/26, 5/27, 5/31) where $PM_{2.5}$ concentrations surpassed 35.5 $\mu g/m^3$ (Figure 3.2). Timeseries of AOD and $PM_{2.5}$ behaved similarly across all stations. Yet because the stations are located close together, we also explored the effect of AOD pixel proximity to the station by comparing timeseries of MODIS AOD with a radius of 0.5° and 0.25°. Making the radius small reduces the number of coincident matches between the station and AOD swath (Figure 3.3). Our results suggest that by using a smaller spatial radius around a station can improve the characterization of aerosol loading as measured by the station (r-values for Terra = 0.52 -0.9 and r-values for Aqua = 0.63 -0.89). The range of correlation coefficients underscores the variability seen across all the stations and highlights potential biases in selecting which stations to correlate with AOD. To compensate for this, the use of as many stations as possible could be beneficial.

The additional aerosol loading increased the linear correlations between AOD and $PM_{2.5}$ during the wildfire period (Table 3.1). We identified wildfire signatures using OMI AI data during the period May 25-30, 2007 (Figure 3.4). We allowed OMI AI to be negative to show the presence of UV-scattering aerosols throughout the region, and

against this background it was easy to discern the presence of the wildfire aerosols (AI > 0.7) during a poor air quality episode in late May. We also explored the benefits to using a space-based lidar (CALIPSO) for biomass burning applications (Figure 3.5 and Figure 3.6). CALIPSO provides information about the vertical structure of aerosols, which can be used to determine how far widespread the wildfire effects are relation to air quality (located near-surface) and aerosol transport (located aloft). CALIPSO measurements detect aerosol layers and then attempts to identify the aerosol type, e.g., dust, pollution. On May 7, CALIPSO retrieved backscattering was around 4.5 $km^{-1}sm^{-1}$ and on May 14 the backscattering was around 4.5 $km^{-1}sr^{-1}$ for the lowest layer and 2.0 $km^{-1}sr^{-1}$ for the second (higher) layer. Though the short time period reduced the number of CALIPSO overpasses, we were able to draw some conclusions from the analysis. First, we believe that CALIPSO miscategorizes biomass burning aerosols as polluted dust likely due the aerosols retrieved color ratio and backscattering coefficients. Second, there was at least one instance of two aerosol layers being present near the fire with one layer close to the ground likely impacting local air quality and the other layer being high enough for aerosol transport.

We highlight the advantages of data fusion with an in-depth analysis of MODIS Terra AOD, MODIS Aqua AOD, OMI AI and HYSPLIT backtrajectories to understand the dynamics that lead to poor air quality on May 22 and 31 (Figure 3.8 and Figure 3.9). For instance, on May 22 $PM_{2.5}$ monitors recorded very high concentrations of over 200 $\mu g/m^3$ and MODIS measured AOD values around 0.8. By fusing the data products together we can minimize the disadvantages associated with each individual satellite sensor. For instance, MODIS cannot directly provide information about aerosol

composition (scattering or absorbing), but OMI can. Yet OMI cannot provide visible confirmation of aerosol events as MODIS can, nor does OMI have a spatial resolution as fine scale as MODIS. Finally, we apply the methodology developed earlier to the recent fire of 2011. This fire occurred in the same location as the fire of 2007, and though it burned longer (April to September 2011) than the fire in 2007 less fuel was consumed. We compared the two fires with a non-burn year (2009) to ascertain the relative effects each fire had on aerosol loading in the region. Our analysis determined that the 2011 had a longer peak burn period compared to 2007, and these results verify that less peat was burned as shown by lower AOD values between 0.6 – 0.8 during the peak burn period (Figure 3.10).

Investigation of a decade-long perspective on aerosols in the region was presented in Chapter 4. We analyzed satellite AOD from MODIS Terra and MISR onboard Terra and $PM_{2.5}$ aerosol measurements from 2000-2009. The goal was to examine the temporal changes of $PM_{2.5}$ and AOD during the past decade. Both datasets show distinct seasonality. Our analysis shows that during the summer (JJA) mean AOD (~0.3 for both MODIS sensors and 0.28 for MISR) nearly tripled from winter (DJF) means (~0.85 for both MODIS and 0.6 for MISR). The $PM_{2.5}$ datasets behaved similarly. We used data from both the EPA's FRM network and GA Depart of Natural Resources continuous TEOM measurements that were split between three locales: Atlanta, All GA, and Outside Atlanta. The different $PM_{2.5}$ datasets allow for understanding how the urban area impacts the remainder of the region. Since we already established the agreement between MODIS sensors, we now want to ascertain the agreement among sensors onboard the Terra spacecraft. We found that the two sensors' agreement is a function of season (Figure 4.5)

with better agreement during the warmer seasons and less agreement during the cooler seasons.

We also explore the apparent seasonality from a spatial perspective (Figure 4.7). In keeping with earlier results, during the winter the region appears to have little variability in aerosol concentration inferred from MODIS Terra and MISR AOD (winter mean AOD for MODIS Terra is 0.03 and winter mean AOD for MISR is 0.05); yet in the summer there are distinct areas of high aerosol loading, e.g., metropolitan Atlanta, and the overall spatial pattern of AOD is highly variable. Our spatial analysis, however, did highlight areas of discontinuity in both satellite sensors' transition between land and ocean (see the increased AOD or missing AOD pixels near the coast). Finally, we conclude this chapter with timeseries analysis of both ground and satellite datasets (Figures 4.10 - 4.12). It was also important to understand a seasonal perspective, thus we calculated linear regressions with the seasonal component and without (anomalies). The $PM_{2.5}$ data record anomalies show a statistically significant ($\alpha = 0.05$) decrease. Despite the Atlanta area increasing the statewide average $PM_{2.5}$ concentrations, the decreases appear to be uniform. This suggests that air quality control policies have had reasonable success at reducing $PM_{2.5}$ concentrations in this region. The satellites anomalies timeseries generally have a negative trend though only MODIS Terra has a decreasing trend that is statistically significant. Our trend analysis agrees well with published trends on different geographical scales (broader regional definitions, e.g., Eastern U.S.) and surface types [*Mishchenko et al.*, 2007; *Zhang and Reid*, 2010].

Analyses of the decadal data records enable us to perform an assessment of the radiative impacts of regional aerosols (Chapter 5). We consider a first-order

approximation of TOA radiative forcing of aerosols [*Haywood and Shine*, 1995] as well as perform detailed radiative transfer modeling. Decadal TOA forcing (ΔF) (see Equation 5.1) was estimated by taking into account changes in AOD (MODIS onboard Terra and MISR), surface albedo (MODIS Terra), cloud fraction (MODIS Terra) and single scattering albedo (SSA or ω_0) from MISR during 2000-2009. We take advantage of the long dataset provided by Terra to understand the seasonal and interannual variability of the above variables. We also examined trends in AODs, surface albedo and cloud fraction datasets. Cloud fraction had not distinct seasonality and is highly variable with time (Figure 5.2) where minima values vary around 0.2 – 0.45 and maxima values fluctuate between 0.5 – 0.8; yet, surface albedo does have a decreasing trends and shows some seasonal pattern, the variance between winter (minima) and summer (maxima) are small in relative terms with the difference between the seasons around 0.4 (Figure 5.3).

To ascertain the individual effects of aerosols, clouds and surface variations, we estimated TOA forcing only considering changes in surface albedo and cloud fraction while holding AOD constant (using a 10-yr AOD mean). Our analysis shows that by themselves, these two constituents are not the main driver of forcing (Figure 5.5) as shown by ΔF only varying between -10 and -5 W/m^2 compared to the ΔF (-20 to -3 W/m^2) due to only AOD. Letting all three physical parameters vary with time, we estimated a complete TOA forcing over the past decade. During the cooler months, the minima (less negative) of radiative forcings vary between -6 to -3 W/m^2, and during the warmer months there is more variation with ΔF varying between -28 to -12.6 W/m^2 for MODIS and -26 to -11 W/m^2 for MISR. We also calculated the standard deviation of the estimates to provide some measure of the total variance within the TOA forcing.

Estimated TOA forcing due to MODIS Terra AOD and MISR AOD behaved similarly, but the absolute values were slightly different. To better understand the impact of the surface-cloud interactions have on TOA forcing, we subtracted the estimated forcing with all three variables from estimated forcing due to satellite AOD only (Figure 5.11). We found that the surface-cloud interactions have an additive effect on ΔF where the difference between AOD-only forcing and AOD, cloud fraction and surface albedo forcing caused an additional ~ 6 W/m^2 of forcing. The use of forcing anomalies determined that there has been less forcing with time, which suggests solar brightening. This analysis also address the effect of single scattering albedo We selected SSA (0.8, 0.85 and 0.9) from Figure (Figure 5.7) to assess the potential effects of changes in composition due to seasonality on TOA ΔF (Figure 5.7). Our results indicated that lower SSA resulted in less TOA forcing of about 5 W/m^2 in absolute terms, which has implications for biomass burning effects on the radiative budget.

Using more representative aerosol compositions and loading better estimate radiative forcing motivates the second half of Chapter 5, which investigates the changes in forcing at the surface and TOA due to Southeastern U. S. aerosols using a 1-D radiative transfer modeling analysis. We first used a Mie optical model to predict the properties of different aerosol study cases that we choose to be representative of the region. We used black carbon (BC), organics, nitrates and sulfates for our externally mixed cases. We also considered an internally mixed case where BC was coated with sulfate. In choosing test cases, care was taken to choose mixtures that were representative of different locales such as more urbanized vs. background (rural) and different seasons: winter and summer. We also wanted to model two special cases: the first is representative

of biomass burning events, and the second is testing the hypothesis that there is an organic aerosol layer aloft. Our results showed that the biomass burning case produced the highest spectral AOD with visible spectrum values around 1, which is consistent with the analysis from Chapters 2 and 3. . During the winter, modeled TOA forcing is -2.8 and -5 W/m^2 for the WB and WU cases, and the modeled summer TOA forcings (SB = -13.3 W/m^2) also generally agree with earlier estimates. While surface forcings varied from -3 to -210 W/m^2, see Figure 5.18. We introduced a metric to compare surface and TOA aerosol forcings: radiative forcing efficiency (RFE), where the units are W/m2 τ-1. RFE allows direct comparison between forcings as aerosol load is removed from consideration by dividing by AOD. RFE for the TOA produced less variation than at the surface. The radiative forcing efficiency at the TOA (amount of forcing per unit of AOD at 550 nm) varied from -9 to -72 W/m^2 τ^{-1}, and RFE at the surface varied from -50 to -410 W/m^2 τ^{-1} (Figure 5.18). It was found that the forcing efficiency for biomass burning aerosols are similar to the forcing efficiency of background aerosols during the summer that highlights the importance of possible increased biomass burning activity. The modeled forcings of the internally mixed case are more challenging to decipher because there is a sign change from negative to positive in the forcing (Figure 5.19).

6.2 Research Implications and Future Work

The threshold technique established in Chapter 2 could provide other areas of the U. S. and other countries a relatively quick way of understanding the potential air quality risks in a near-real time manner through the use of satellite data. Weber et al. [2010] suggest the use of seasonally averaged aerosol data from both the ground and satellites to improve quantification of the $PM_{2.5}$-AOD relationship through linear regressions. Related

research suggests using regionally averaged aerosol data improves $PM_{2.5}$-AOD linear regressions (their r-value for SE U. S was around 0.6) [*Zhang et al.*, 2009]. The research presented in this chapter combines both of these suggested approaches over a longer period of time, which could have broad applicability to operational tools such as the IDEA website (http://www.star.nesdis.noaa.gov/smcd/spb/aq/) currently run by NOAA [*Al-Saadi et al.*, 2005].

The data fusion methodology developed in Chapter 3 can be adapted to fit other regions where wildfires occur, which could be beneficial if climate-model prediction of warming increase the burn season, duration and frequency [*Park et al.*, 2007; *Spracklen et al.*, 2009]. One aspect of our research that is presented in Chapter 3 that separates our analysis from other published literature [*Bhoi et al.*, 2009; *Christopher et al.*, 2009]on the 2007 wildfire, is that first, we use more satellite sensors in our analysis. We use MODIS, OMI, and CALIPSO. The addition of OMI provides independent verification of wildfire aerosol impacts as well as indirect evidence for fire intensity (AI is related to concentration of aerosol in the UV channels). Additionally, we have identified an algorithm detection problem in the CALIPSO data, of which we have notified the CALIPSO science team. Additionally we use other products from CALIPSO (e.g., vertical feature mask, aerosol sub-typing, and layer AOD) to identify the vertical structure of the wildfire through multiple days during May 2007, and we estimate layer AOD using corrected lidar ratios, which we found compared more favorably with MODIS AOD.

The methodology developed in Chapter 4 has broad applicability to understanding aerosol behavior over longer time scales. While [*Mishchenko et al.*, 2007] detected a

decreasing trend in AOD, it was over ocean and the analysis was done for the entire globe. We are the first to publish results that related the decreasing trends in AOD to decreasing trends in surface $PM_{2.5}$ concentrations for this region. Streets et al. [2009] use GCM (global climate model) estimated AOD based upon aerosol emissions for their trend analysis. Though satellite AOD over land has more bias and uncertainties than it does over water, to our knowledge there have not been any studies that use satellite AOD to determine trends over any region of the U. S. Our analysis provides the critical first step in determining these aerosol trends from a climatic perspective.

Our analysis of ten years of satellite data to estimate TOA forcings as a function in time we are able to describe the decadal variability in TOA forcing. Our results indicate that over time there is less radiative forcing, which has implications for regional climate studies. Taken in totality our results suggest that aerosols alone cannot explain the climatic measures of surface temperature. It would appear that other climate controlling factors are playing an active role. Lastly, our finer spatial scale radiative transfer modeling revealed that aerosol compositions and solar zenith angle as a function of season play a large role in determining surface and TOA aerosol radiative effects and efficiencies. It is likely that future air control policies will need to target aerosol speciation as a way to balance the opposing effects of climate change mitigation and improvement of air quality.

We summarize possible avenues for future research below.

(1) Develop and apply AOD threshold technique to other regions in the U. S. and potentially abroad.

a. The system of EPA air quality monitors is sparse, especially in the central portion of the U. S., and other less densely populated areas. Using available satellite data to quickly disseminate air quality information could be of use for those states and areas.
b. Identification of aerosol transport events (biomass burning, dust storms, pollution).
c. Inclusion of newer satellite aerosol data products: VIIRS, GEOCAPE

(2) Extend climatology work to more regions with different aerosol compositions
a. Method to address efficacy of air quality control policies
b. Method to potentially address solar dimming/brightening

(3) Perform more detailed in-depth optical and radiative modeling
a. Incorporate more in-situ measurements for more realistic test cases and CERES satellite based radiation products.
b. Extend the test cases to cover more years – compare non-fire year to fire years over season as opposed to a single event
c. Extend CALIPSO analysis to more years to better characterize the vertical structure of aerosols and their associated concentrations

BIBLIOGRAPHY

Ahn, C., O. Torres, and P. K. Bhartia (2008), Comparison of Ozone Monitoring Instrument UV aerosol products with Aqua/Moderate Resolution Imaging Spectroradiometer and Multiangle Imaging Spectroradiometer observations in 2006, *J Geophys Res, 113*, D16S27, doi: 10.1029/2007JD008832.

Al-Saadi, J., et al. (2005), Improving national air quality forecasts with satellite aerosol observations, *Bull Amer Meteorol Soc, 86*(9), 1249-1261, doi: 10.1175/BAMS-86-9-1249.

Alpert, P., and P. Kishcha (2008), Quantification of the effect of urbanization on solar dimming, *Geophys Res Lett, 35*, L08801, doi: 10.1029/2007GL033012.

Alpert, P., P. Kishcha, Y. J. Kaufman, and R. Schwarzbard (2005), Global dimming or local dimming?: Effect of urbanization on sunlight availability, *Geophys Res Lett, 32*, L17802, doi: 10.1029/2005gl023320.

Alston, E. J., I. N. Sokolik, and B. G. Doddridge (2011a), Investigation into the use of satellite data in aiding characterization of particulate air quality in the Atlanta, Georgia metropolitan area *J Air & Waste Manage, 61*(2), 211-225, doi: 10.3155/1047-3289.61.2.211.

Alston, E. J., I. N. Sokolik, and O. V. Kalashnikova (2011b), Seasonal and interannual variability of atmospheric aerosols in the U. S. Southeast from ground and space based measurements over the past decade, *Atmos Meas Tech Discuss, 4*(6), 7559 - 7595, doi: 10.5194/amtd-4-7559-2011.

Andreae, M. O. (2009), A New Look at Aging Aerosols, *Science, 326*(5959), 1493-1494, doi: 10.1126/science.1183158.

Barnes, C. A., and D. P. Roy (2010), Radiative forcing over the conterminous United States due to contemporary land cover land use change and sensitivity to snow and interannual albedo variability, *J Geophys Res, 115*(G4), G04033, doi: 10.1029/2010jg001428.

Bhoi, S., J. J. Qu, and S. Dasgupta (2009), Multi-sensor study of aerosols from 2007 Okefenokee forest fire, *J Appl Remote Sens, 3*(031501), doi: 10.1117/1.3078070.

Blanchard, C. L., G. M. Hidy, S. Tanenbaum, and E. S. Edgerton (2011), NMOC, ozone, and organic aerosol in the southeastern United States, 1999-2007: 3. Origins of organic aerosol in Atlanta, Georgia, and surrounding areas, *Atmos Environ, 45*(6), 1291-1302, doi: 10.1016/j.atmosenv.2010.12.004.

Butler, A. J., M. S. Andrew, and A. G. Russell (2003), Daily sampling of PM 2.5 in Atlanta: Results of the first year of the Assessment of Spatial Aerosol Composition in Atlanta study, *J Geophys Res, 108*(8415), doi: 10.1029/2002JD002234.

Cardelino, C., M. Chang, J. St. John, B. Murphey, J. Cordle, R. Ballagas, L. Patterson, K. Powell, J. Stogner, and S. Zimmer-Dauphinee (2001), Ozone predictions in Atlanta, Georgia: Analysis of the 1999 ozone season, *J Air & Waste Manage, 51*(8), 1227-1236.

Carrico, C. M., M. H. Bergin, J. Xu, K. Baumann, and H. Maring (2003), Urban aerosol radiative properties: Measurements during the 1999 Atlanta Supersite Experiment, *J Geophys Res, 108*(D7), 8422, doi: 10.1029/2001JD001222.

Chameides, W. L., et al. (1992), Ozone precursor relationship in the ambient atmosphere, *J Geophys Res, 97*(D5), 6037-6055, doi: 10.1029/91JD03014

Christopher, S. A., and P. Gupta (2010), Satellite remote sensing of particulate matter air quality: The cloud-cover problem, *J Air & Waste Manage, 60*(5), 596-602, doi: 10.3155/1047-3289.60.5.596.

Christopher, S. A., P. Gupta, U. Nair, T. J. Jones, S. Kondragunta, Y. L. Wu, J. L. Hand, and X. Zhang (2009), Satellite remote sensing and mesoscale modeling of the 2007 Georgia/Florida fires *IEEE J Sel Top App Rem Sens, 2*(3), 163 - 175, doi: 10.1109/JSTARS.2009.2026626.

Chu, D. A., Y. J. Kaufman, C. Ichoku, L. A. Remer, D. Tanré, and B. N. Holben (2002), Validation of MODIS aerosol optical depth retrieval over land, *Geophys Res Lett, 29*(12), 1617, doi: 10.1029/2001GL013205.

Confalonieri, U., B., R. A. Menne, K. L. Ebi, M. Hauengue, R. S. Kovats, B. Revich, and A. Woodward (2007), Human health. In: Climate change 2007: Impacts, Adaptation and Vulnerability. Contribution of working group II to the Fourth Assessment Report of the Intergovernmental Panel on Climate Change*Rep.*, Cambridge, UK and New York, NY, USA.

de Graaf, M., P. Stammes, O. Torres, and R. B. A. Koelemeijer (2005), Absorbing Aerosol Index: Sensitivity analysis, application to GOME and comparison with TOMS, *J Geophys Res, 110*(D01201), doi: 10.1029/2004jd005178.

Diem, J. E., M. A. Hursey, I. R. Morris, A. C. Murray, and R. A. Rodriguez (2010), Upper-level atmospheric circulation patterns and ground-level ozone in the Atlanta metropolitan area, *J Appl Meteorol Clim, 49*(11), 2185-2196, doi: 10.1175/2010jamc2454.1.

Diner, D. J., J. C. Beckert, G. W. Bothwell, and J. I. Rodriguez (2002), Performance of the MISR instrument during its first 20 months in Earth orbit, *Geoscience and Remote Sensing, IEEE Transactions on, 40*(7), 1449-1466.

Dirksen, R. J., K. F. Boersma, J. de Laat, P. Stammes, G. R. van der Werf, M. V. Martin, and H. M. Kelder (2009), An aerosol boomerang: rapid around-the-world transport of smoke from the December 2006 Australian forest fires observed from space, *J Geophys Res, 114*(D21201), doi: 10.1029/2009JD012360.

Draxler, R. R. (2006), The Use of Global and Mesoscale Meteorological Model Data to Predict the Transport and Dispersion of Tracer Plumes over Washington, D.C, *Weather Forcast, 21*(3), 383-394, doi: 10.1175/WAF926.1.

Dutton, E. G., D. W. Nelson, R. S. Stone, D. Longenecker, G. Carbaugh, J. M. Harris, and J. Wendell (2006), Decadal variations in surface solar irradiance as observed in a globally remote network, *J Geophys Res, 111*(D19), D19101, doi: 10.1029/2005jd006901.

Eatough, D. J., R. W. Long, W. K. Modey, and N. L. Eatough (2003), Semi-volatile secondary organic aerosol in urban atmospheres: meeting a measurement challenge, *Atmos Environ, 37*(9-10), 1277-1292, doi: 10.1016/S1352-2310(02)01020-8.

Edgerton, E. S., B. E. Hartsell, R. D. Saylor, J. J. Jansen, D. A. Hansen, and G. M. Hidy (2005), The Southeastern Aerosol Research and Characterization Study: Part II. Filter-based measurements of fine and coarse particulate matter mass and composition, *J Air & Waste Manage, 55*(10), 1527 - 1341.

Edgerton, E. S., B. E. Hartsell, R. D. Saylor, J. J. Jansen, D. A. Hansen, and G. M. Hidy (2006), The Southeastern Aerosol Research and Characterization Study, Part 3: Continuous measurements of fine particulate matter mass and composition, *J Air & Waste Manage, 56*(9), 1325-1341.

Edgerton, E. S., G. S. Casuccio, R. D. Saylor, T. L. Lersch, B. E. Hartsell, J. J. Jansen, and D. A. Hansen (2009), Measurements of OC and EC in coarse particulate matter in the southeastern United States, *J Air & Waste Manage, 59*(1), 78-90, doi: 10.3155/1047-3289.59.1.78.

Engel-Cox, J. A., G. S. Young, and R. M. Hoff (2005), Application of satellite remote-sensing data for a source analysis of fine particulate matter transport events, *J Air & Waste Manage, 55*(9), 1389-1397.

Engel-Cox, J. A., C. H. Holloman, B. W. Coutant, and R. M. Hoff (2004), Qualitative and quantitative evaluation of MODIS satellite sensor data for regional and urban scale air quality, *Atmos Environ, 38*(16), 2495-2509, doi: 10.1016/j.atmosenv.2004.01.039.

Fairlie, T. D., et al. (2009), Lagrangian sampling of 3-D air quality model results for regional transport contributions to sulfate aerosol concentrations at Baltimore, MD, in summer 2004, *Atmos Environ, 43*(20), 3275-3288, doi: 10.1016/j.atmosenv.2009.02.026.

Forster, P., et al. (2007), Changes in atmospheric constituents and in radiative forcing, in *Climate Change 2007: The Physical Science Basis. Contribution of Working Group I to the Fourth Assessment Report of the Intergovernmental Panel on Climate Change*, edited by S. Solomon, D. Qin, M. Manning, Z. Chen, M. Marquis, K. B. Averyt, M.Tignor and H. L. Miller, Cambridge University Press, Cambridge, UK and New York, NY, USA.

Fromm, M., R. Bevilacqua, R. Servranckx, J. Rosen, J. P. Thayer, J. Herman, and D. Larko (2005), Pyro-cumulonimbus injection of smoke to the stratosphere: Observations and impact of a super blowup in northwestern Canada on 3 - 4 August 1998, *J Geophys Res, 110*(D08205), doi: 10.1029/2004jd005350.

Gilgen, H., A. Roesch, M. Wild, and A. Ohmura (2009), Decadal changes in shortwave irradiance at the surface in the period from 1960 to 2000 estimated from Global Energy Balance Archive Data, *J Geophys Res, 114*, D00D08, doi: 10.1029/2008jd011383.

Goldstein, A. H., C. D. Koven, C. L. Heald, and I. Y. Fung (2009), Biogenic carbon and anthropogenic pollutants combine to form a cooling haze over the southeastern United States, *Proc Natl Acad Sci USA, 106*, 8835-8840, doi: 10.1073/pnas.0904128106.

Gupta, P., and S. A. Christopher (2008a), An evaluation of Terra-MODIS sampling for monthly and annual particulate matter air quality assessment over the Southeastern United States, *Atmos Environ, 42*(26), 6465-6471, doi: 10.1016/j.atmosenv.2008.04.044.

Gupta, P., and S. Christopher (2008b), Seven year particulate matter air quality assessment from surface and satellite measurements, *Atmos Chem Phys, 8*(12), 3311-3324, doi: 10.5194/acp-8-3311-2008.

Gupta, P., and S. A. Christopher (2009), Particulate matter air quality assessment using integrated surface, satellite, and meteorological products: Multiple regression approach, *J Geophys Res, 114*(D14205), doi: 10.1029/2008JD011496.

Gupta, P., S. A. Christopher, J. Wang, R. Gehrig, Y. Lee, and N. Kumar (2006), Satellite remote sensing of particulate matter and air quality assessment over global cities, *Atmos Environ, 40*(30), 5880-5892, doi: 10.1016/j.atmosenv.2006.03.016.

Hansen, J., R. Ruedy, J. Glascoe, and M. Sato (1999), GISS analysis of surface temperature change, *J Geophys Res, 104*(D24), 30997-31022, doi: 10.1029/1999jd900835.

Haywood, J. M., and K. P. Shine (1995), The effect of anthropogenic sulfate and soot aerosol on the clear sky planetary radiation budget, *Geophys Res Lett, 22*(5), 603-606, doi: 10.1029/95gl00075.

Heald, C. L., et al. (2011), Exploring the vertical profile of atmospheric organic aerosol: comparing 17 aircraft field campaigns with a global model, *Atmos Chem Phys Discuss, 11*(9), 25371-25425, doi: 10.5194/acpd-11-25371-2011.

Hennigan, C. J., M. H. Bergin, A. G. Russell, A. Nenes, and R. J. Weber (2009), Gas/particle partitioning of water-soluble organic aerosol in Atlanta, *Atmos Chem Phys, 9*(11), 3613-3628, doi: 10.5194/acp-9-3613-2009.

Herman, J. R., P. K. Bhartia, O. Torres, C. Hsu, C. Seftor, and E. Celarier (1997), Global distribution of UV-absorbing aerosols from Numbus 7/TOMS data, *J Geophys Res, 102*(D14), 16,911-916,922, doi: 10.1029/96JD03680.

Hinkelman, L. M., P. W. Stackhouse, Jr., B. A. Wielicki, T. Zhang, and S. R. Wilson (2009), Surface insolation trends from satellite and ground measurements: Comparisons and challenges, *J Geophys Res, 114*, D00D20, doi: 10.1029/2008jd011004.

Hoff, R. M., and S. A. Christopher (2009), Remote sensing of particulate pollution from space: Have we reached the promised land?, *J Air & Waste Manage, 59*(6), 645-675, doi: 10.3155/1047-3289.59.6.645.

Jacob, D. J., and D. A. Winner (2009), Effect of climate change on air quality, *Atmos Environ, 43*(1), 51-63, doi: 10.1016/j.atmosenv.2008.09.051.

Jimenez, J. L., et al. (2009), Evolution of Organic Aerosols in the Atmosphere, *Science, 326*(5959), 1525-1529, doi: 10.1126/science.1180353.

Ju, J., D. P. Roy, Y. Shuai, and C. Schaaf (2010), Development of an approach for generation of temporally complete daily nadir MODIS reflectance time series, *Remote Sens Environ, 114*(1), 1-20, doi: 10.1016/j.rse.2009.05.022.

Kahn, R. A., B. J. Gaitley, M. J. Garay, D. J. Diner, T. F. Eck, A. Smirnov, and B. N. Holben (2010), Multiangle Imaging SpectroRadiometer global aerosol product assessment by comparison with the Aerosol Robotic Network, *J Geophys Res, 115*, D23209, doi: 10.1029/2010jd014601.

Kahn, R. A., M. J. Garay, D. L. Nelson, K. K. Yau, M. A. Bull, B. J. Gaitley, J. V. Martonchik, and R. C. Levy (2007), Satellite-derived aerosol optical depth over dark water from MISR and MODIS: Comparisons with AERONET and implications for climatological studies, *J Geophys Res, 112*(D18), D18205, doi: 10.1029/2006jd008175.

Kahn, R. A., D. L. Nelson, M. J. Garay, R. C. Levy, D. J. Diner, J. V. Martonchik, S. R. Paradise, E. G. Hansen, and L. A. Remer (2009), MISR Aerosol product attributes and statistical comparisons with MODIS, *IEEE Trans Geosci Rem Sens, 47*(12), 4095 - 4114, doi: 10.1109/TGRS.2009.2023115.

Kahn, R. A., M. J. Garay, D. L. Nelson, R. C. Levy, M. A. Bull, D. J. Diner, J. V. Martonchik, E. G. Hansen, L. A. Remer, and D. Tanrè (2011), Response to "Toward unified satellite climatology of aerosol properties. 3. MODIS versus MISR versus AERONET", *J Quant Spectrosc Ra, 112*(5), 901-909, doi: 10.1016/j.jqsrt.2010.11.001.

Kittaka, C., D. M. Winker, M. A. Vaughan, A. Omar, and L. A. Remer (2011), Intercomparison of column aerosol optical depths from CALIPSO and MODIS-Aqua, *Atmos Meas Tech, 4*(2), 131-141, doi: 10.5194/amt-4-131-2011.

Koren, I., L. A. Remer, Y. J. Kaufman, Y. Rudich, and J. V. Martins (2007), On the twilight zone between clouds and aerosols, *Geophys Res Lett, 34*, L08805, doi: 10.1029/2007gl029253.

Langmann, B., B. Duncan, C. Textor, J. Trentmann, and G. R. van der Werf (2009), Vegetation fire emissions and their impact on air pollution and climate, *Atmos Environ, 43*(1), 107-116, doi: 10.1016/j.atmosenv.2008.09.047.

Lee, S., A. G. Russell, and K. Baumann (2007), Source apportionment of fine particulate matter in the Southeastern United States, *J Air & Waste Manage, 57*(9), 1123 - 1135, doi: 10.3155/1047-3289.57.9.1123.

Lee, S., Y. Wang, and A. G. Russell (2010), Assessment of secondary organic carbon in the Southeastern United States: A review, *J Air & Waste Manage, 60*(11), 1282-1292, doi: 10.3155/1047-3289.60.11.1282.

Lee, T. F., S. D. Miller, C. Schueler, and S. Miller (2006), NASA MODIS previews NPOESS VIIRS capabilities, *Weather Forcast, 21*(4), 649-655, doi: 10.1175/WAF935.1.

Lesins, G., P. Chylek, and U. Lohmann (2002), A study of internal and external mixing scenarios and its effect on aerosol optical properties and direct radiative forcing, *J Geophys Res, 107*(D10), 4094, doi: 10.1029/2001jd000973.

Levy, R. C., L. A. Remer, S. Mattoo, E. F. Vermote, and Y. J. Kaufman (2007), Second-generation operational algorithm: Retrieval of aerosol properties over land from inversion of Moderate Resolution Imaging Spectroradiometer spectral reflectance, *J Geophys Res, 112*, D13211, doi: 10.1029/2006JD007811.

Levy, R. C., L. A. Remer, J. V. Martins, Y. J. Kaufman, A. Plana-Fattori, J. Redemann, and B. Wenny (2005), Evaluation of the MODIS Aerosol Retrievals over Ocean and Land during CLAMS, *J Atmos Sci, 62*(4), 974-992, doi: 10.1175/jas3391.1.

Levy, R. C., L. A. Remer, R. G. Kleidman, S. Mattoo, C. Ichoku, R. Kahn, and T. F. Eck (2010), Global evaluation of the Collection 5 MODIS dark-target aerosol products over land, *Atmos Chem Phys*, *10*(21), 10399-10420, doi: 10.5194/acp-10-10399-2010.

Liang, S., H. Fang, M. Chen, C. J. Shuey, C. Walthall, C. Daughtry, J. Morisette, C. Schaaf, and A. Strahler (2002), Validating MODIS land surface reflectance and albedo products: methods and preliminary results, *Remote Sens Environ*, *83*(1-2), 149-162, doi: 10.1016/S0034-4257(02)00092-5.

Liu, L., and M. I. Mishchenko (2008), Toward unified satellite climatology of aerosol properties: Direct comparisons of advanced level 2 aerosol products, *J Quant Spectrosc Ra*, *109*(14), 2376-2385, doi: 10.1016/j.jqsrt.2008.05.003.

Liu, Y., R. A. Kahn, A. Chaloulakou, and P. Koutrakis (2009a), Analysis of the impact of the forest fires in August 2007 on air quality of Athens using multi-sensor aerosol remote sensing data, meteorology and surface observations, *Atmos Environ*, *43*(21), 3310 - 3318, doi: 10.1016/j.atmosevn.2009.04.010.

Liu, Z., M. Vaughan, D. Winker, C. Kittaka, B. Getzewich, R. Kuehn, A. Omar, K. Powell, C. Trepte, and C. Hostetler (2009b), The CALIPSO lidar cloud and aerosol discrimination: Version 2 algorithm and initial assessment of performance, *J Atmos Oceanic Techol*, *26*(7), 1198-1213, doi: 10.1175/2009JTECHA1229.1.

Livingston, J. M., et al. (2009), Comparison of aerosol optical depths from the Ozone Monitoring Instrument (OMI) on Aura with results from airborne sunphotometry, other space and ground measurements during MILAGRO/INTEX-B, *Atmos Chem Phys*, *9*(18), 6743 - 6765, doi: 10.5194/acp-9-6743-2009.

Long, C. N., E. G. Dutton, J. A. Augustine, W. Wiscombe, M. Wild, S. A. McFarlane, and C. J. Flynn (2009), Significant decadal brightening of downwelling shortwave in the continental United States, *J Geophys Res*, *114*, D00D06, doi: 10.1029/2008jd011263.

Martonchik, J. V., R. A. Kahn, and D. J. Diner (2009), Retrieval of aerosol properties over alnd using MISR observations, in *Satellite Aerosol Remote Sensing Over Land*, edited by A. A. Kokhanovsky and G. de Leeuw, Springer, Berlin.

Martonchik, J. V., D. J. Diner, K. A. Crean, and M. A. Bull (2002), Regional aerosol retrieval results from MISR, *IEEE Trans Geosci Rem Sens*, *40*(7), 1520-1531.

Menne, M. J., C. N. Williams, and R. S. Vose (2009), The U.S. historical climatology network monthly temperature data, Version 2, *Bull Amer Meteorol Soc*, *90*(7), 993-1007, doi: 10.1175/2008BAMS2613.1.

Metzger, K., P. Tolbert, M. Klein, J. Peel, W. Flanders, K. Todd, J. Mulholland, P. Ryan, and H. Frumkin (2004), Ambient air pollution and cardiovascular emergency department visits, *Epidemiology*, *15*(1), 46, doi: 10.1097/01.EDE.0000101748.28283.97.

Mishchenko, M., I. Geogdzhayev, W. Rossow, B. Cairns, B. Carlson, A. Lacis, L. Liu, and L. Travis (2007), Long-term satellite record reveals likely recent aerosol trend, *Science*, *315*(5818), 1543, doi: 10.1126/science.1136709.

National Research Council (2005), *Radiative Forcing of Climate Change: Expanding the Concept and Addressing Uncertainties*, 180 pp., The National Academies Press, Washington, DC.

Omar, A. H., et al. (2009), The CALIPSO automated aerosol classification and lidar ratio selection algorithm, *J Atmos Oceanic Techol*, *26*(10), 1994 - 2014, doi: 10.1175/2009JTECHA1231.1.

Panicker, A. S., G. Pandithurai, P. D. Safai, S. Dipu, and D.-I. Lee (2010), On the contribution of black carbon to the composite aerosol radiative forcing over an urban environment, *Atmos Environ*, *44*(25), 3066-3070, doi: 10.1016/j.atmosenv.2010.04.047.

Park, R. J., D. J. Jacob, and J. A. Logan (2007), Fire and biofuel contributions to annual mean aerosol mass concentrations in the United States, *Atmos Environ*, *41*(35), 7389-7400, doi: 10.1016/j.atmosenv.2007.05.061.

Peel, J. L., K. B. Metzger, M. Klein, W. D. Flanders, J. A. Mulholland, and P. E. Tolbert (2007), Ambient air pollution and cardiovascular emergency department visits in potentially sensitive groups, *Am J Epid*, *165*(6), 625-633, doi: 10.1093/aje/kwk051.

Penning de Vries, M. J. M., S. Beirle, and T. Wagner (2009), UV Aerosol Indices from SCIAMACHY: introducing the SCattering Index (SCI), *Atmos Chem Phys*, *9*(24), 9555-9567, doi: 10.5194/acp-9-9555-2009.

Platnick, S., M. D. King, S. A. Ackerman, W. P. Menzel, B. A. Baum, J. C. Riedi, and R. A. Frey (2003), The MODIS cloud products: algorithms and examples from Terra, *Geoscience and Remote Sensing, IEEE Transactions on, 41*(2), 459-473, doi: 10.1109/TGRS.2002.808301

Prados, A. I., S. Kondragunta, P. Ciren, and K. R. Knapp (2007), GOES Aerosol/Smoke Product (GASP) over North America: Comparisons to AERONET and MODIS observations, *J Geophys Res, 112*(D15201), doi: 10.1029/2006jd007968.

Remer, L. A., et al. (2008), Global aerosol climatology from the MODIS satellite sensors, *J Geophys Res, 113*, D14S07, doi: 10.1029/2007jd009661.

Schaaf, C. B., et al. (2002), First operational BRDF, albedo nadir reflectance products from MODIS, *Remote Sens Environ, 83*(1-2), 135-148, doi: 10.1016/S0034-4257(02)00091-3.

Schwartz, S. E., R. J. Charlson, R. A. Kahn, J. A. Ogren, and H. Rodhe (2010), Why hasn't Earth warmed as much as expected?, *Journal of Climate, 23*(10), 2453-2464, doi: 10.1175/2009JCLI3461.1.

Slaughter, J. C., T. Lumley, L. Sheppard, J. Q. Koenig, and G. G. Shapiro (2003), Effects of ambient air pollution on symptom severity and medication use in children with asthma, *Ann Allergy Asthma Immunol, 91*(4), 346-353.

Solomon, P. A., et al. (2003), Overview of the 1999 Atlanta Supersite Project, *J Geophys Res, 108*, doi: 10.1029/2001JD001458.

Spracklen, D. V., L. J. Mickley, J. A. Logan, R. C. Hudman, R. Yevich, M. D. Flannigan, and A. L. Westerling (2009), Impacts of climate change from 2000 to 2050 on wildfire activity and carbonaceous aerosol concentrations in the western United States, *J Geophys Res, 114*(D20301), doi: 10.1029/2008JD010966.

Streets, D. G., F. Yan, M. Chin, T. Diehl, N. Mahowald, M. Schultz, M. Wild, Y. Wu, and C. Yu (2009), Anthropogenic and natural contributions to regional trends in aerosol optical depth, 1980 - 2006, *J Geophys Res, 114*(D00D18), doi: 10.1029/2008jd011624.

Tian, D., Y. Hu, Y. Wang, J. Boylan, and A. G. Russell (2009), Assessment of biomass burning emissions and their impacts on urban and regional $PM_{2.5}$: A Georgia case study, *Environ Sci Technol, 43*(2), 299-305, doi: 10.1021/es801827s.

Tolbert, P. E., J. A. Mulholland, D. L. Macintosh, F. Xu, D. Daniels, O. J. Devine, B. P. Carlin, M. Klein, A. J. Butler, and D. F. Nordenberg (2000), Air quality and pediatric emergency room visits for asthma and Atlanta, Georgia, *Am J Epid*, *151*(8), 798-810.

Tombach, I., and P. Brewer (2005), Natural background visibility and regional haze goals in the Southeastern United States, *J Air & Waste Manage*, *55*(11), 1600 - 1620.

Torres, O., A. Tanskanen, B. Veihelmann, C. Ahn, R. Braak, P. K. Bhartia, P. Veefkind, and P. Levelt (2007), Aerosols and surface UV products from Ozone Monitoring Instrument observations: An overview, *J Geophys Res, 112*(D24S47), doi: 10.1029/2007JD008809.

U.S. Environmental Protection Agency (2006), National Ambient Air Quality Standards for particulate matter: Final rule 40 CFR part 50, edited, pp. 61444 - 61233, Federal Register.

U.S. EPA (2009), Air quality designations for the 2006 24-Hour fine particle ($PM_{2.5}$) National Ambeint Air Quality Standards, under review, Title 40, Part 81, edited by U. S. E. P. Agency, Federal Register, Washington, DC.

Vaughan, M. A., K. A. Powell, R. E. Kuehn, S. A. Young, D. M. Winker, C. A. Hostetler, W. H. Hunt, Z. Liu, M. J. McGill, and B. J. Getzewich (2009), Fully automated detection of cloud and aerosol layers in the CALIPSO lidar measurements, *J Atmos Oceanic Techol*, *26*(10), 2034-2050, doi: 10.1175/2009JTECHA1228.1.

Wang, J., and S. A. Christopher (2003), Intercomparison between satellite-derived aerosol optical thickness and $PM_{2.5}$ mass: Implications for air quality studies, *Geophys Res Lett, 30*(21), 2095, doi: 10.1029/2003GL018174.

Wang, J., and S. T. Martin (2007), Satellite characterization of urban aerosols: Importance of including hygroscopicity and mixing state in the retrieval algorithms, *J Geophys Res*, *112*, D17203, doi: 10.1029/2006JD008078.

Weber, R., et al. (2007), A study of secondary organic aerosol formation in the anthropogenic-influenced southeastern United States, *J Geophys Res, 112*, D13302, doi: 10.1029/2007JD008408.

Weber, S. A., J. A. Engel-Cox, R. M. Hoff, A. I. Prados, and H. Zhang (2010), An improved method for estimating surface fine particle concentrations using seasonally adjusted satellite aerosol optical depth, *J Air & Waste Manage, 60*(5), 574-585, doi: 10.3155/1047-3289.60.5.574.

Wen, G., A. Marshak, R. F. Cahalan, L. A. Remer, and R. G. Kleidman (2007), 3-D aerosol-cloud radiative interaction observed in collocated MODIS and ASTER images of cumulus cloud fields, *J Geophys Res, 112*, D13204, doi: 10.1029/2006jd008267.

Wild, M. (2009), Global dimming and brightening: A review, *J Geophys Res, 114*(D00D16), doi: 10.1029/2008JD011470.

Wild, M., B. Trüssel, A. Ohmura, C. N. Long, G. König-Langlo, E. G. Dutton, and A. Tsvetkov (2009), Global dimming and brightening: An update beyond 2000, *J Geophys Res, 114*(D00D13), doi: 10.1029/2008jd011382.

Winker, D. M., M. A. Vaughan, A. H. Omar, Y. Hu, K. A. Powell, Z. Liu, W. H. Hunt, and S. A. Young (2009), Overview of the CALIPSO mission and CALIOP data processing algorithms, *J Atmos Oceanic Techol, 26*, 2310-2323, doi: 10.1175/2009JTECHA1281.1.

Wu, J., A. M. Winer, and R. J. Delfino (2006), Exposure assessment of particulate matter air pollution before, during, and after the 2003 Southern California wildfires, *Atmos Environ, 40*(18), 3333-3348, doi: 10.1016/j.atmosenv.2006.01.056.

Zhang, H., R. Hoff, and J. A. Engel-Cox (2009), The relation between Moderate Resolution Imaging Spectroradiometer (MODIS) aerosol optical depth and $PM_{2.5}$ over the United States: A geographical comparison by U.S. Environmental Protection Agency regions, *J Air & Waste Manage, 59*(11), 1358-1369, doi: 10.3155-1047-3289.59.11.1358.

Zhang, J., and J. S. Reid (2010), A decadal regional and global trend analysis of the aerosol optical depth using a data-assimilation grade over-water MODIS and Level 2 MISR aerosol products, *Atmos Chem Phys, 10*(22), 10949-10963, doi: 10.5194/acp-10-10949-2010.

Zhang, J., J. S. Reid, and B. N. Holben (2005), An analysis of potential cloud artifacts in MODIS over ocean aerosol optical thickness products, *Geophys Res Lett, 32*, L15803, doi: 10.1029/2005GL023254.

VITA

Erica J. Alston was born in North Carolina in 1981. She grew up in rural Eastern N. C., where she participated in variety of activities such as football, track and field, cheerleading and quiz bowl. She also held elected offices in the student body government. She graduated Louisburg High School June 1999, and enrolled at Clark Atlanta University in Fall 1999. Ms. Alston graduated in May 2004 with a B.S. in Mathematical Science and a M. S. in Applied Mathematics. While interning with the National Oceanic and Atmospheric Administration she developed her master's thesis research, which focused upon developing a migrational model for predicting the number of juvenile salmon that would make to the sea in the Pacific Northwest. Since 2004 Ms. Alston has been employed with the National Aeronautical and Space Administration at Langley Research Center where her work has focused on data fusion of multiple satellite sensors, which led to her pursuing a Ph.D in the School of Earth and Atmospheric Sciences at the Georgia Institute of Technology in Atlanta, GA. While a student Ms. Alston published two peer-reviewed manuscripts related to her dissertation research. During her matriculation she was co-advised by Drs. Irina Sokolik (primary) and Judith Curry. Ms. Alston will graduate in May 2012 with a Ph.D in Atmospheric Sciences with a concentration in Remote Sensing.